Side Population Cells in the Adult Heart

A Dissertation
SUBMITTED TO THE FACULTY OF
UNIVERSITY OF MINNESOTA
BY

Amritha Yellamilli

IN PARTIAL FULFILLMENT OF THE REQUIREMENTS
FOR THE DEGREE OF
DOCTOR OF PHILOSOPHY

Dr. Jop H. van Berlo – Adviser

Dr. Daniel J. Garry – Co-Advisor

June 2018

Acknowledgements

First, I would like to thank my advisor, Jop H. van Berlo. He took a chance on me in a way that most people wouldn't have and introduced me to the exciting field of cardiac regeneration. I would also like to thank the van Berlo lab for providing a happy research environment.

There are several people at the University of Minnesota whom I would like to thank for their unwavering support and kindness they have shown me over the past five years. I would like to thank Lisa Schimmenti, Pete Bitterman, Linda McLoon, Susan Shurson, Nick Berg and Dr. Post. I would also like to specifically thank Yoji Shimizu. He has always been there for me. Each one of these people has helped me become a better person and hopefully a better physician-scientist. I will never be able to thank them enough.

Next, I would like to thank all the people who inspired me to pursue my dreams in science and medicine. I would like to thank Mrs. Debbie Frazier, my computer programming, AP Biology and Robotics high school teacher. It all started with her. Her joy and passion for all sciences were infectious, and her faith in me propelled me through all four years of high school and beyond.

I would also like to thank Mehrdad Arjomandi and Robert M. Tombes for giving me such incredible research opportunities while I was an undergraduate student. They helped build me from the ground up as a scientist and always challenged me to do and be better.

I would especially like to thank Sarah, Lu, Jamie, and Jana. I am so lucky that I had the amazing opportunity to work with these incredibly talented, driven, and passionate former Ph.D. students and postdocs. They have truly shaped who I am as a scientist and a person. I am lucky enough to count them all as my friends and I hope that someday I will grow up to be just like them. ☺

I would also like to thank all of my friends, especially Ruchi and Michelle. They have been through it all with me and inspired me in so many ways inside and outside of lab. They made this journey one I will not forget.

And finally, I would like to thank my family for their endless and unconditional love and support.

Dedication

I dedicate this thesis to my family.
To my parents, Krishna and Champa, and my brothers, Shiva and Abhi,
I've come this far because of you.

Abstract

The clinical outcomes for heart failure remain poor because current therapies do not address a critical feature of heart failure – loss of functional cardiomyocytes. To decrease the morbidity and mortality of patients with heart failure, multiple strategies are being developed to replace dead cardiomyocytes with new, functional ones. Adult stem cell transplantation studies have had modest clinical benefits primarily attributed to paracrine effects on several endogenous processes including cardiac regeneration. Many cardiac progenitor cell populations have been isolated from the adult mammalian heart and studied in cell culture or after transplantation; however, their roles in endogenous cardiac regeneration are highly contested. In the thesis work presented here, we used the side population phenotype as an unbiased approach to determine whether an endogenous progenitor cell population exists in the adult mammalian heart. We generated a new Abcg2-driven, lineage-tracing mouse model that efficiently labels side population cells in multiple tissues throughout the body, including the heart. With this mouse model, we first showed that the side population phenotype enriches for endogenous stem cells in the bone marrow and small intestine under homeostatic conditions. In the adult heart, we showed that cardiac side population cells contribute to 21% of newly formed cardiomyocytes either through direct differentiation or fusion. Moreover, cardiac side population cells are responsive to different forms of cardiac injury. Further characterization of cardiac side population cells will help us understand how they can be targeted *in vivo* for

the development of new heart failure therapies.

Table of Contents

Acknowledgements i
Dedication iii
Abstract iv
Table of Contents vi
List of Tables vii
List of Figures viii

Background and Significance 1
Materials and Methods 64
Results 77
Discussion and Future Directions 132
References 142

List of Tables

Table 1	GFP-labeling of bmSPCs, LSK and bone marrow lineages in Mhy7-CreER $R26^{Tom/+}$ $Abcg2^{MCM/+}$ $R26^{GFP/+}$ bone marrow chimeric mice.	128
Table 2	GFP-labeling of bmSPCs, LSK and bone marrow lineages in VE-Cadherin-CreERT2 $R26^{GFP/+}$ mice.	129
Supplementary Table 1.	Antibody details for immunofluorescence staining of histological sections.	130
Supplementary Table 2.	Antibody details for immunofluorescence staining of fixed, isolated adult cardiomyocytes.	131

List of Figures

Figure 1	Efficient labeling of ABCG2-expressing cells in tamoxifen-injected Abcg2$^{MCM/+}$ R26$^{GFP/+}$ mice.	91
Figure 2	BMSPCs and LSK cells are extensively labeled in tamoxifen-injected Abcg2$^{MCM/+}$ R26$^{GFP/+}$ mice.	93
Figure 3	Endogenous, lineage-traced bmSPCs give rise to differentiated bone marrow cells *in vivo.*	95
Figure 4	Short-term lineage-tracing of endogenous intestinal stem cells give rise to differentiated intestinal cells *in vivo.*	97
Figure 5	Long-term lineage-tracing of endogenous intestinal stem cells give rise to differentiated intestinal cells *in vivo.*	99
Figure 6	cSPCs are extensively labeled in tamoxifen-injected Abcg2$^{MCM/+}$ R26$^{GFP/+}$ mice.	100
Figure 7	Endogenous, lineage-traced cSPCs give rise to cardiac endothelial cells.	101
Figure 8	Endogenous, lineage-traced cSPCs give rise to cardiomyocytes.	104
Figure 9	Cardiomyocytes do not express ABCG2.	106
Figure 10	Cytosolic calcium dynamics of lineage-traced cardiomyocytes are comparable to non-lineage- traced cardiomyocytes.	108
Figure 11	Lineage-traced bone marrow cells do not significantly contribute to lineage-traced cardiomyocytes.	110
Figure 12	Labeled endothelial cells do not contribute to lineage trace-cardiomyocytes.	112
Figure 13	CSPC contribution to cardiomyocytes increases following MI.	113
Figure 14	Noncardiomyocyte labeling in the remote region, border zone and infarct following MI.	115

Figure 15	CSPC contribution to cardiomyocytes increases following acute adrenergic cardiac injury.	116
Figure 16	CSPCs give rise to cardiomyocyte through fusion and differentiation into cardiomyocytes.	118
Figure 17	CSPCs give rise to newly-formed noncardiomyocytes and cardiomyocytes.	120
Figure 18	Nucleation of lineage-traced and non-lineage-traced cardiomyocytes is the same.	122
Figure 19	Lineage-traced cSPCs give rise to 21% of newly-formed cardiomyocytes in the adult heart.	124
Supplementary Figure 1	Labeling in other organs in $Abcg2^{MCM/+}$ $R26^{GFP/+}$ mice.	126
Supplementary Figure 2	Quantification of newly-formed cardiomyocytes using the EdU and Tamoxifen co-injection strategy.	127

Background and Significance:

Regenerating the Failing Heart

HEART FAILURE

Definition and Classification

Heart failure is a clinical syndrome characterized by symptoms resulting from impaired ventricular pumping and/or filling. Three systems are used to classify types and stages of heart failure[1,2]. These classification systems are essential to understand because they help clinicians decide which therapeutic strategies to pursue to improve clinical outcome and quality of life for heart failure patients.

The first system of categorizing heart failure is based on how well the left ventricle functions, which is measured by left ventricular ejection fraction (LVEF). The 2013 American College of Cardiology Foundation (ACCF)/American Heart Association (AHA) and 2016 European Society of Cardiology (ESC) guidelines both categorize heart failure with LVEF less than 40% as heart failure with reduced ejection fraction (HFrEF) and heart failure with LVEF greater than or equal to 50% as heart failure with preserved ejection fraction (HFpEF)[1,2]. The 2016 ESC guidelines further specify that HFpEF patients must also present with elevated natriuretic peptides along with structural heart disease or diastolic dysfunction[1]. It is important to distinguish between HFpEF and HFrEF because the pathophysiology underlying HFpEF is distinct from the pathophysiology of HFrEF. In general, HFrEF is caused by primary cardiac disease or injury; whereas, HFpEF is caused by systemic conditions that result in progressive cardiac injury. Moreover, pharmacological therapies that slow disease

progression and improve quality of life for patients with HFrEF have limited effectiveness in patients with HFpEF[3].

The 2016 ESC and 2013 ACCF/AHA guidelines also describe other categories of heart failure based on LVEF[1,2]. Heart failure with LVEF between 40% and 49% is categorized as heart failure with moderately reduced ejection fraction (HFmrEF) and borderline HFpEF by the 2016 ESC and 2013 ACCF/AHA guidelines, respectively. This category of heart failure is more similar in presentation, treatment, and outcomes to HFpEF than HFrEF[2]. The 2013 ACCF/AHA guideline includes a fourth category of heart failure for HFrEF patients whose LVEF improved to greater than 40%. These heart failure patients are categorized as improved HFpEF and are clinically distinct from HFrEF and HFpEF patients[2].

The New York Heart Association (NYHA) classification system is the second system used to classify heart failure based on the impact of heart failure on physical activity and symptom provocation[1,2]. Clinicians commonly use that NYHA classification system in conjunction with the LVEF classification system in most clinical trials for heart failure. Patients with NYHA Class I heart failure can participate in any physical activity without eliciting heart failure symptoms, while patients with NYHA Class II and III experience symptoms with slight and moderate physical activity, respectively. Finally, patients with NYHA Class IV heart failure have symptoms at rest.

The third classification system outlined in the 2013 ACCF/AHA guideline is unique from the other two systems because it highlights a category for patients who are at high risk of developing heart failure but do not have any heart failure symptoms or structural heart disease (Stage A)[2]. Stage A heart failure patients are important to recognize because optimal management of risk factors at this stage can help prevent the development of heart failure in these patients. The other stages of heart failure in the ACCF/AHA classification system correspond with NYHA classes. Stage B describes heart failure with structural heart disease without symptoms and corresponds to NYHA Class I heart failure. Stage C describes heart failure with structural heart disease and symptoms and encompasses NYHA Class I, II, and III heart failure. The final category, Stage D, describes heart failure that no longer responds to pharmacological therapies and corresponds with NYHA Class IV.

Epidemiology

Over the past several decades, the epidemiology of heart failure has changed as new therapies have been developed and implemented to manage heart failure as well as associated risk factors and comorbidities. Despite these improvements, the projected clinical and financial burden of heart failure is expected to increase significantly in the future.

From 1979 to 2000, the incidence of heart failure has remained unchanged in both men and women[4.] However, the incidence of HFpEF

increased during this period in time[5]. More recently, the incidence of heart failure declined 37.5% from 315.8 per 100,000 to 219.3 per 100,000 from 2000 to 2010. There was a more significant decline in the incidence of heart failure in women compared to men and in the incidence of HFrEF compared to HFpEF[6]. The overall decrease in heart failure incidence is likely due to improved management of comorbidities and risk factors associated with heart failure[6].

Despite the decreasing incidence of heart failure, the prevalence of heart failure is projected to increase 23% from 2.42%in 2012 to 2.97% in 2030[7]. As the population in the US continues to increase and the overall population ages, the number of people with heart failure is projected to increase by 46% from 5.7 million people in 2012 to over 8 million people by 2030[7].

As the prevalence of heart failure increases, the financial burden placed on countries throughout the world continues to grow. From 2012 to 2030, the medical cost of heart failure in the US is projected to increase 2.5-fold from $20.9 billion to $53.1 billion annually with approximately 80% of this cost attributed to hospitalizations[7]. During this same period of time, the total cost of heart failure, which includes both direct and indirect costs, is projected to increase from $30.7 billion to $69.8 billion annually[7]. Globally, the total cost of heart failure in 2012 was $108 billion with more money spent per capita in high-GDP countries like the US[8].

More concerning than the growing financial burden of heart failure, is the poor clinical outcomes heart failure patients face. Heart failure mortality improved

from the 1980s to early 2000s. From 1979 – 1984, the 5-year mortality was 57% which decreased to 48% from 1996 – 2000[4]. This improvement was attributed to the improved use of pharmacological therapies for the treatment of HFrEF[6.] HFrEF patient survival improved during this time while HFpEF survival remained unchanged[5]. Since then, however, the mortality rates for all forms of heart failure have remained the same with 52.6% of heart failure patients dying within five years of diagnosis[6].

Pathophysiology

The pathophysiology underlying heart failure is complex and multifactorial; however, there are key pathways that have been well-established in the context of heart failure and are targeted by current pharmacological therapies.

Neurohormonal Activation:

Two neurohormonal pathways are central to the progression of heart failure and are targets for pharmacological therapies: the sympathetic nervous system and the renin-angiotensin-aldosterone (RAA) system. These pathways have synergistic effects that work to maintain perfusion of vital organs following cardiac injury. While activation of these pathways may initially be beneficial, chronic activation has a deleterious impact on the heart and contributes significantly to the progression of heart failure.

During the initial stages of cardiac injury, activation of the sympathetic

nervous system maintains adequate perfusion to the body by increasing cardiac output, cardiac preload and total peripheral resistance. Baroreceptors in the carotid sinus and aortic arch sense a fall in cardiac output leading to activation of the sympathetic nervous system. As a result, postganglionic sympathetic neurons release norepinephrine and chromaffin cells in the adrenal medulla release epinephrine. These catecholamines bind to adrenergic receptors throughout the body. In the heart, norepinephrine and epinephrine bind to β1-receptors on pacemakers cells and cardiomyocytes to increase heart rate, contractility, and relaxation, which results in increased cardiac output[9,10]. Throughout the body, norepinephrine and epinephrine bind to α1-receptors on smooth muscle cells causing vasoconstriction of arterial vessels to maintain blood pressure, and thereby perfusion, to vital organs as well as vasoconstriction of venous vessels to increase cardiac preload thereby increasing cardiac output.

Despite the initial beneficial effects of sympathetic nervous system activation, chronic activation contributes to the deterioration in cardiac function over time. Chronic activation of the sympathetic nervous system causes cardiac remodeling, alters cardiomyocyte excitation-contraction coupling, induces cardiomyocyte hypertrophy and apoptosis, and increases the risk of arrhythmias. Over time, it also leads to desensitization of β–adrenergic signaling caused by decreased β–adrenergic receptor density at the sarcolemma and uncoupling of β–adrenergic receptors and intracellular signaling pathways. Higher levels of norepinephrine also correlate with poor heart failure outcomes. In a clinical trial

with over 4,000 patients with HFrEF, higher plasma norepinephrine levels directly correlated with higher mortality and poorer clinical outcomes[11]. β-blockers, which bind to β–adrenergic receptors, prevent norepinephrine and epinephrine signaling and are used to treat chronic heart failure patients. They have been shown to prevent, and sometimes reverse, adverse effects of chronic sympathetic nervous system activation and improve clinical outcomes for patients with HFrEF[9]. In clinical trials, β-blockers have not been shown to improve clinical outcomes for HFpEF patients[3].

Like the sympathetic nervous system, the RAA system also maintains perfusion to vital organs during the initial phase of cardiac injury. The first step of RAA system activation is the release of renin from juxtaglomerular cells located in the renal afferent arterioles. Renin release occurs in response to decreased blood pressure sensed directly by juxtaglomerular cells, reduced sodium and chloride concentrations in renal tubular fluid detected by macula densa cells in the distal nephron, and sympathetic nervous system activation with norepinephrine and epinephrine binding to β1-adrenergic receptors on juxtaglomerular cells. Renin converts angiotensinogen to angiotensin I, which is subsequently cleaved to angiotensin II by angiotensin-converting enzyme (ACE). Angiotensin II is that central effector molecule of the RAA system. It also stimulates the sympathetic nervous system, the release of aldosterone from the adrenal cortex and the release of antidiuretic hormone (ADH) from the posterior pituitary. In the kidney, angiotensin II, ADH, and aldosterone bind to their

respective receptors in renal epithelial cells located throughout the nephron to increase renal reabsorption of sodium and water thereby increasing total blood volume. Angiotensin II also acts in the central nervous system to increase thirst. Systemically, it also causes arterial and venous vasoconstriction. In the heart, angiotensin II causes cardiomyocyte hypertrophy, cardiomyocyte apoptosis, and extracellular matrix deposition. To block that effect of chronic RAA activation, ACE inhibitors, angiotensin receptor blockers and mineralocorticoid receptor blockers are used.

Cardiomyocyte Apoptosis and Necrosis:

During the progression of heart failure, there is a continuous loss of cardiomyocytes arising from cardiomyocyte apoptosis and necrosis. Several studies evaluated cardiomyocyte death in patients with HFrEF caused by ischemic heart disease and dilated cardiomyopathy. These studies demonstrated that the percent of apoptotic cardiomyocytes in explanted failing hearts was 0.08% – 0.25% of all cardiomyocytes, which was at least forty times higher than in healthy controls[12–18]. While this level of cardiomyocyte apoptosis may seem low, a transgenic mouse model, which overexpressed FKBP-caspase-8 fusion protein in cardiomyocytes, illustrated that low levels of cardiomyocyte apoptosis (0.023%) cause mice with normal cardiac function at three weeks-of-age to develop dilated cardiomyopathy with significant mortality by nine weeks-of-age[19]. Moreover, disease progression in HFrEF patients correlates with the level of

cardiomyocyte apoptosis. HFrEF with rapidly progressing heart failure had two-fold and eight-fold higher levels of cardiomyocyte apoptosis than HFrEF with intermediate and slowly progressing heart failure[15]. The level of cardiomyocyte apoptosis did not differ between failing hearts with ischemic heart disease or dilated cardiomyopathy[15]. Along with cardiomyocyte apoptosis, cardiomyocyte necrosis has been shown to occur in HFrEF caused by ischemic heart disease or dilated cardiomyopathy[16,17]. Interestingly, a study attributed gender differences observed in the clinical progression of heart failure to differing levels of cardiomyocyte necrosis. They found that cardiomyocyte apoptosis occurred at similar levels in male and female explanted hearts but that there were higher levels of cardiomyocyte necrosis in male hearts compared to female hearts[16].

Because cardiomyocyte death plays an essential role in the progression of heart failure, it is imperative that we develop new therapies to address this clinical problem. Sympathetic nervous system and RAA system activation can cause cardiomyocyte apoptosis through direct and indirect mechanisms[20–22]. Therapies that block these pathways have been shown to decrease levels of cardiomyocyte apoptosis; however, there is still a need to develop treatments that directly target cardiomyocyte death[20–22]. Two general strategies are being pursued to address this clinical problem. The first strategy is to prevent cardiomyocytes from undergoing apoptosis[23]. The second strategy is to generate new cardiomyocytes to replace ones that have undergone apoptosis and necrosis. Transplantation of cells into the failing heart is one of the main

approaches clinically tested with the goal of generating new cardiomyocytes in the failing heart.

CELL THERAPIES FOR HEART FAILURE

Several cell types have been tested in clinical trials to replace dead cardiomyocytes within the failing heart. Most animal studies and a significant number of clinical trials evaluated cell therapies within the setting of acute myocardial ischemic injury. Here, I will focus our discussion on cell therapies that have been tested in clinical trials for chronic heart failure patients.

Skeletal Myoblasts

Skeletal myoblasts were the first adult stem cells transplanted into the failing human heart[24]. Researchers believed that skeletal myoblasts would work well to replace nonviable, akinetic myocardium because skeletal myoblasts are contractile, lineage-committed, autologous, and convenient to obtain and expand in culture[25]. Some even believed that skeletal myoblasts might also differentiate into cardiomyocytes *in vivo*. Initial studies demonstrated that transplantation of cultured C2C12 myoblasts into uninjured, syngeneic mice resulted in engraftment and differentiation of myoblasts into myofibers that did not induce arrhythmias or injure the heart regardless of the route of delivery[26,27]. In subsequent studies in mice, rats, rabbits, pigs, and sheep; autologous skeletal myoblasts isolated from skeletal muscle biopsies were injected directly into the area of injury in

cryoinjured and ischemic-injured hearts[28–34]. The transplanted myoblasts formed islands of myotubes that expressed skeletal muscle myosin heavy chain, reduced fibrosis, and improved cardiac function. When ventricular arrhythmias were assessed in porcine studies, no significant difference was observed between transplantation of myoblasts or media[32,33]. While it has been demonstrated that skeletal myoblasts and myotubes can form gap junctions and electrochemically couple with neonatal and adult cardiomyocytes in co-culture, engrafted myoblasts and myotubes did not electrochemically couple with the surrounding myocardium in all transplantation studies[28–34].

In 2001, the first study of skeletal myoblast transplantation was published in a 72-year-old man with refractory ischemic heart failure (New York Heart Association Class III with an ejection fraction of 21%) undergoing coronary artery bypass grafting (CABG)[24]. Two weeks before surgery, cells were isolated from a biopsy of the patient's vastus lateralis and expanded in a myogenic cell culture media. CD56+ cells were then sorted and injected epicardially into the posterior wall of the left ventricle after completion of the CABG surgery. The patient recovered without any complications. Five months later, segmental contractility of the posterior wall of the left ventricle measured by echocardiography increased from 0% before transplantation to 40%, and viable tissue was detected with positron emission tomography (PET) scan at the myoblast injection site. Importantly, left ventricular ejection fraction (LVEF) increased to 30% and no

arrhythmias were reported. This study provided evidence that myoblast transplantation in humans was feasible[24].

After this initial study, two Phase I trials were carried out by separate groups in Europe and the US with ischemic heart failure patients[35,36]. In the US trial, autologous skeletal myoblasts (mononuclear, CD56+) were injected epicardially into the infarct or border zones following implantation of left ventricular assist devices (LVADs). When LVADs were explanted either at the time of heart transplantation or after death, the myocardia where myoblasts were injected were harvested for histological analysis. Transplanted cells were identified by trichrome staining and immunohistochemical staining for skeletal muscle myosin heavy chain. The engraftment rate was calculated to be less than 1% of the approximately 300 million transplanted myoblasts regardless of whether the cells were transplanted into non-viable myocardium in the infarct or into viable myocardium in the border zone. Additionally, the study authors also reported increased vessel density surrounding engrafted cells compared to non-transplanted areas. In the European trial, autologous myoblasts (CD56+ and Desmin+) were injected epicardially into multiple regions in the infarcted areas at the time of CABG surgery in ten patients with ischemic heart failure[36]. LVEF increased significantly from 23.8 % to 32.1% with improvement in NYHA classification. A third Phase I trial evaluated the safety and therapeutic potential of injecting autologous skeletal myoblasts into the endocardium of infarcted tissue, instead of the epicardium like the previous trials, using the NOGA

catheter-based system in an in-patient setting[37]. In this study, systolic and diastolic dimensions improved without any difference in heart failure symptoms or global cardiac function between myoblast- and vehicle-injected hearts. The incidence of arrhythmias was also the same in both groups[37].

Because of these promising findings; a multi-center, double-blind, randomized, controlled Phase II trial in Europe, the Myoblast Autologous Grafting in Ischemic Cardiomyopathy (MAGIC) trial, was carried out to investigate the therapeutic benefits of skeletal myoblast[38]. This study had 97 participants randomized to three groups: placebo, low dose (400 million CD56+ cells), and high dose (800 million CD56+ cells). In this study, they did not find any improvement in regional or global cardiac function after transplantation of autologous skeletal myoblast in conjunction with CABG surgery versus CABG surgery with placebo[38]. Over time, the enthusiasm for transplantation of autologous skeletal myoblasts for the treatment of heart failure diminished because of the lack of integration with surrounding myocardium, increased risk of cardiac arrhythmias, inconsistent effects on cardiac function and development of other cell therapies for the treatment of heart failure[39].

Bone Marrow-Derived Cells

Bone marrow-derived cells are the most extensively studied cells for transplantation into the injured heart. In 1999, a study was published that evaluated the ability of different populations of bone marrow-derived cells to

regenerate the injured heart[40]. Three weeks after cryoinjury, rats received one of the following four injection: freshly isolated bone marrow mononuclear cells (BMMCs), which contain both mesenchymal stem cells (MSCs) and hematopoietic stem cells; MSCs; MSCs cultured with 10μM 5-azacytidine, which researchers showed induces expression of cardiac troponin I and myosin heavy chain in MSCs; and culturing media as a control. One million cells suspended in 50 μls of culturing media were injected directly into the middle of the scar area. Five weeks later, histological analysis of injured myocardium was carried out. Transplanted cells that stained positively for Troponin I were found in the three groups of rats that had been transplanted with BMMCs, MSCs, MSCs cultured with 5-azacytidine but not in rats injected with culture media alone. Furthermore, infarcts injected with either of the three different types of bone marrow cells had a significantly higher capillary density compared to the media control. Most of the endothelial cells did not originate from the transplanted cells indicating that transplanted cells stimulated angiogenesis instead of transdifferentiating into endothelial cells. Importantly, only MSCs treated with 5-azacytidine resulted in a statistically significant decrease in infarct size and left ventricular chamber size as well as improved systolic function of the heart. These findings suggested that MSCs cultured under cardiogenic conditions improved cardiac function following cardiac injury by enhancing angiogenesis and transdifferentiating into cardiomyocytes[40].

In the following years, other populations of bone marrow cells were also studied in animal models. Hematopoietic stem cells (HSCs), defined by their expression of c-kit and lack of expression of differentiated bone marrow lineage markers (Lin^- $c\text{-}kit^+$), were studied in animal models of myocardial ischemic injury. In initial studies, two 2.5 ml injections of $24x10^4$ – $1x10^5$ GFP-expressing $Lin^-c\text{-}kit^+$ bone marrow cells were administered directly into the border zone 5 hours after permanent ligation of the left anterior descending artery. Nine days later, 12 out of 30 mice still had GFP-labeled cells identifiable in the infarcted myocardium [41,42]. The 12 mice with successful engraftment of Lin^- $c\text{-}kit^+$ bone marrow cells had improved systolic and diastolic function compared to uninjected and $Lin^-c\text{-}kit^+$ injected controls. The authors claimed that this improvement in cardiac function arose from transdifferentiation of transplanted cells into cardiomyocytes, endothelial cells, and smooth muscle cells. Most transplanted Lin^- $c\text{-}kit^+$ bone marrow cells differentiated into cardiomyocytes in the infarct region based on expression of GATA4, MEF2, Nkx2.5, Connexin 43, cardiac myosin and Ki67 and BrdU incorporation.

The regenerative capacity of transplanted Lin^- kit^+ bone marrow cells reported in these initial studies was remarkable; however, subsequent investigations by two independent groups were not able to reproduce these findings in their entirety. These groups also observed a vast number of transplanted cells in the infarct 9-10 days after transplantation; however, all of these cells expressed hematopoietic markers and none of the cardiomyocyte

markers described in the original studies[43,44]. Transplanted cells were also largely gone from the heart by 28-30 days post-transplantation[43,44]. These groups repeated these transplantation experiments with whole bone marrow, $Lin^{-}c\text{-}kit^{+}Sca^{-}1^{+}CD45^{+}$ bone marrow cells and long-term reconstituting HSCs ($c\text{-}kit^{+}$ $Thy1.1^{lo}$ Lin^{-} $Sca^{-}1^{+}$) and found the same negative results[43,45].

Despite these contradictory findings, the race to use different populations of bone marrow cells to regenerate the damaged heart had taken off. The two types of cells studied in clinical trials are BMMCs, which are a heterogeneous mixture of bone marrow cells purified using Ficoll gradient centrifugation and MSCs, which are a subpopulation of BMMCs that become adherent when cultured for several days. Most clinical trials with BMMCs and MSCs have tested them in the acute setting following myocardial infarction (MI). Here, I will highlight the pre-clinical and clinical trials that have studied these cells in the context of heart failure.

Bone Marrow Mononuclear Cells (BMMCs):

In humans, BMMCs are made up of 2.4% hematopoietic progenitor cells ($CD45^{lo}CD34^{+}$), 0.1% early hematopoietic progenitor cells ($CD45^{lo}CD34^{+}HLA\text{-}DR^{-}$), 28.4% CD4+ T cells ($CD45^{+}CD3^{+}CD4^{+}$), 14.9% CD8+ T cells ($CD45^{+}CD3^{+}CD8^{+}$), 1.9% B cells ($CD45^{+}CD19^{+}$), 10% Monocytes ($CD45^{+}$ $CD14^{+}$), and 1.2 % NK cells ($CD45^{+}$ $CD56^{+}$)[46]. BMMCs have been transplanted in clinical trials using two primary strategies. The first strategy is injecting BMMCs

directly into the heart like in the animal studies described above. This is primarily done using the NOGA catheter-based system so, unlike animal studies were cells were injected into the epicardium, cells in these trials are injected into the endocardium. The second approach used to transplant BMMCs is infusing them into coronary vessels supplying areas of ischemic injury. A study in 2002 demonstrated that, when human MSCs are injected systemically into the left ventricular lumen of uninjured immunodeficient mice, human MSCs can traverse vessel walls to engraft throughout the heart at a rate similar to that of other transplantation approaches[47].

Initial studies of autologous BMMCs injected directly into the endocardium of failing hearts demonstrated improved clinical and functional outcomes. In 2003, the first nonrandomized trial injecting BMMCs using the NOGA system was carried out with 21 chronic ischemic heart failure patients (HFrEF with an average NYHA staging of 2.5)[46]. The first fourteen patients received BMMC transplantation while the last seven served as non-transplanted controls. Between the two groups, there was no significant difference between stage of heart failure, risk factors, comorbidities, pharmacological therapies or gender. Patients in the transplantation group received on average 15 injections of 2 million freshly isolated BMMCs per injection into segments of viable myocardium with low mechanical activity. No significant complications like arrhythmias resulted from injection of BMMCs. At the two-month follow-up, BMMC-treated participants had significant improvements in heart failure symptoms and a 4%

increase in LVEF compared to control participants. Contractile function at the site of injection also improved from baseline and persisted for four months. A follow-up clinical trial using the same approach with BMMC transplantation in chronic ischemic heart failure patients (HFrEF with an average NYHA staging of 3.5) showed a similar 4% improvement in LVEF compared to baseline. Although global glucose metabolism and perfusion did not improve; regional glucose metabolism and perfusion of injected areas were significantly enhanced compared to non-injected controls[48]. Despite the promising findings published in these studies, the FOCUS-HF trial (phase I, controlled, randomized, single-blinded) and the FOCUS-CCTRN trial (phase II, controlled, randomized and double-blinded) both found that endocardial injection of autologous BMMCs with the NOGA system did not significantly improve clinical or functional outcomes in ischemic heart failure patients in 6-month period of time[49,50].

The other approach that has been used to transplant autologous BMMCs is intracoronary infusion into vessels supplying injured myocardium. The phase I/II controlled, randomized TOPCARE-CHD clinical trial tested intracoronary transplantation of BMMCs and circulating peripheral blood progenitor cells. BMMC intracoronary fusion improved LVEF by 3% compared to baseline, but this improvement was not statistically different from the control group[51]. This increase in LVEF did not translate to improvements in overall survival; however, participants with lower baseline N-terminal pro-brain natriuretic peptide (NT-proBNP) levels who were transplanted with BMMCs with higher colony formation

units had significantly better survival[51,52]. There was no difference in functional or clinical outcomes in participants transplanted with circulating peripheral blood progenitor cell from baseline or three-month followup[51]. Shortly after the findings of these studies were published, another group reported that they did not observe any improvements in systolic function between BMMC infused and saline-infused controls using the same approach, although they did find a significant improvement in diastolic function[53]. Because of these mixed results, the first group that published the initial study hypothesized that the discrepancies might arise from differing retention rates of infused cells. To increase homing of transplanted cells, they used shock-wave therapy before infusion of BMMCs into the coronary vessels[54]. It was thought that shock wave therapy, which has been shown to increase expression of chemokines expressed after acute myocardial injury, may increase BMMC-retention and, therefore, improve the consistency of published studies. Participants were randomized to low-dose shock wave with or without BMMCs, high dose shock waves with or without BMMCs or placebo shock waves with BMMCs. High-dose and low-dose shock wave both improved LVEF from baseline and compared to shock-wave with placebo infusion and placebo shock-wave with BMMCs. Of note, the improvement in baseline LVEF after BMMC intracoronary infusion reported in the first study was not observed in this study.

BMMC intracoronary infusion in patients with chronic heart failure caused by dilated cardiomyopathy also improved systolic function and clinical

presentation long-term; however, these benefits did not translate into improvements in overall mortality[55,56]. Histological evaluation of endomyocardial biopsies obtained before and three months after infusion of BMMCs showed trending increase in the ratio of capillaries to cardiomyocytes. The authors also noted Ki67 staining but did not identify which cells were stained or provide quantifications in either the cell therapy or control group. There was a 5% improvement in LVEF compared to baseline which was observable at the one-month follow-up and persisted throughout the 3-year follow-up. This improvement was not observed in the control arm where the participants' ejection fraction remained stable at 21%. NYHA classification in the therapy group improved relative to both baseline and control group classifications. These observed changes did not translate into improvements in mortality, which were the same between the two groups.

Mesenchymal Stem Cells (MSCs):

Pre-clinical studies of MSCs in a porcine model tested the efficacy of transplanting MSCs in the context of acute myocardial ischemia-reperfusion injury[57,58]. Three days after myocardial ischemia-reperfusion injury was performed in female pigs, MSCs harvested and expanded in cell culture from male pigs were injected into the endocardial area of damage. MRI and histological analysis showed that transplanted MSCs engrafted in the heart with no detectable engraftment elsewhere in the body[57,58]. Fourteen percent of

engrafted MSCs expressed GATA-4 or Nkx2.5 providing evidence of cardiomyocyte commitment; however, most engrafted MSCs did not stain for any cardiomyocyte or noncardiomyocytes markers indicating that they remained undifferentiated up to three months after transplantation[58]. Eight weeks after transplantation, pigs injected with MSCs had smaller infarcts and less myocardial fibrosis. In control pigs, infarcts were transmural; whereas infarcts in MSC treated pigs were limited to the midmyocardium with sparing of endocardial and epicardial layers[57]. There was also improved cardiac energy utilization in MSC-treated pigs[57]. All of these factors resulted in a 15% improvement in cardiac function in MSC treated pigs from the time of transplantation with no observable change in control animals. The effect of MSC transplantation on mortality was not determined. These studies provided mechanistic data demonstrating the beneficial effects of transplanted MSCs on cardiac remodeling, metabolism, and function[57,58].

After the promising results of these porcine studies, clinical trials were initiated to evaluate the therapeutic benefits of MSCs in patients with HFrEF caused by ischemic heart disease or dilated cardiomyopathy. The MSC-HF trial was a placebo-controlled, randomized, double-blinded study that evaluated the clinical benefits of endocardial injections of autologous MSCs compared to saline injections in sixty participants with ischemic heart failure (average LVEF of 26% and NYHA Class II-III[59,60]. Although there was a 6% improvement in LVEF with no major adverse side effects, clinical presentation, assessed by NYHA class

and 6-minute walking test, was not significantly different between MSC and saline-injected participants over the six-month follow-up period. Another study, the C-CURE trial, assessed the safety and therapeutic benefits of culturing MSCs in a cardiopoietic cocktail before endocardial injection using the NOGA system[61]. Transplantation of cardiopoietic MSCs significantly improved LVEF by 7% from baseline and distance covered during the 6-minute walking test compared to baseline. No changes were observed in the standard of care controls. NYHA class, overall mortality and LVEF were not significantly different between the two groups. Importantly, these findings were not compared to classic MSCs so it is difficult to assess whether the 7% improvement in LVEF observed can be directly attributed to culturing MSCs in a cardiopoietic cocktail[61].

While these studies demonstrated the beneficial effects of injecting autologous MSCs for the treatment of ischemic heart failure, two clinical trials compared allogeneic and autologous MSC transplantation in ischemic and dilated cardiomyopathy heart failure patients[62,63]. Allogeneic MSCs pose an advantage over autologous MSCs because allogeneic MSCs can be generated ahead of time and stored until they are needed. The use of autologous MSCs requires more planning and time since bone marrow must be harvested and expanded in cell culture for several weeks before they are ready for transplantation. The POSEIDON and POSEIDON-DCM trials compared the therapeutic effects of allogeneic MSCs to autologous MSCs in ischemic and dilated cardiomyopathy respectively[62,63]. In ischemic heart failure (average LVEF

26.5 and NYHA class I-III), autologous MSCs improved quality of life and exercise capacity assessed by the 6-minute walk test in the fifteen patients studied[62]. Allogeneic MSCs did not have significant beneficial effects but was shown to be safe with minimal crossreactivity occurring. Interestingly, in participants with heart failure caused by dilated cardiomyopathy (average LVEF 26.5 and NYHA class I-III), the opposite was found. Allogeneic MSCs improved LVEF by 8%, 6-minute walking test, clinical presentation, and quality of life during the six-month follow-up, while autologous MSCs improved LVEF by 5% but did not improve other measures like allogeneic MSCs did. The greater beneficial effects of allogeneic MSCs in this patient population was attributed to immune modulatory effects, improved endothelial cells dysfunction and younger age of allogeneic donors[63].

Based on clinical trials of bone marrow-derived cells, both BMMCs and MSCs appeared to have similar beneficial effects. The phase I/II TAC-HFT trial directly compared BMMCs and MSCs to each other in 65 participants with ischemic heart failure, average LVEF of 35.5% and NYHA class I-III[64,65]. While both BMMCs and MSCs improved clinical presentation compared to placebo, only MSCs resulted in decreased infarct size, improved regional function at the site of injection and improvement in the 6-minute walk test. In this study, neither BMMCs and MSCs significantly improved LV dimensions or ejection fraction compared to the placebo control.

Despite the mixed results regarding the efficacy of transplanted bone marrow-derived cells, there is cumulative evidence that these cells provide clinical benefits over standard of care[66].

Cardiac Derived Cells

In addition to bone marrow cells, cells isolated from the heart have been tested in clinical trials. Cardiosphere-derived cells (CDCs) and c-kit+ cells and are the two main cardiac cell types transplanted in human patients; however, the therapeutic effects of CDCs have not been studied within the context of chronic heart failure.

Cardiosphere-derived cells (CDCs):

Cardiospheres were first described in 2004[67]. When researchers cultured lightly digested pieces of human myocardial biopsies, they found that the loosely adherent cells growing out of these samples could be harvested and cultured on Poly-D-lysine to generate balls of cells about 200 microns in diameter, which they called cardiospheres. A subsequent study found that if cardiospheres were plated on fibronectin, they formed a monolayer of cells that could be expanded and passaged up to three times. These cells were called cardiosphere-derived cells (CDCs)[68]. Researchers were able to generate cardiospheres and CDCs from mouse, rat and pig cardiac tissue in addition to human biopsies[69]. Transplantation of either cardiospheres or CDCs were shown to improve cardiac

function following MI in mice, rats, and pigs[67,70,71]. In a follow-up study that directly compared cardiospheres and CDCs, researchers found that cardiospheres engrafted at a higher rate and had a greater therapeutic effect than CDCs following MI[72]. Another study also showed that CDCs were more beneficial than BMMCs and bone marrow MSCs[73]. The CADUCEUS trial is the only clinical trial that has assessed the safety and potential therapeutic benefits of intracoronary infusion of CDCs in the acute setting for MI patients with ejection fractions between 25% – 45%[74,75]. At baseline, the seventeen patients transplanted with CDCs had an average ejection fraction of 42.2 ± 8.9 and the eight control patients had an average ejection fraction of 42.5 ± 11.1. These patients did not meet the definition of heart failure outline by both the ESC and ACCF/AHA guidelines for heart failure. Intracoronary infusion of CDCs 1.5 to 3 months after MI, did not pose any significant safety concerns and resulted in decreased infarct size and improve regional cardiac function without any significant change in the function of the entire heart[74,75]. Since this study assessed the therapeutic benefits of intracoronary infusion of CDCs in the acute setting following MI, it is difficult to conclude whether CDCs would have beneficial effects in heart failure patients.

C-kit$^+$ cells:

The c-kit protein is a tyrosine kinase receptor that is commonly used as a marker to identify hematopoietic stem cells. Researchers inadvertently identified

residential cardiac c-kit$^+$ cells and published their findings in 2002[76]. They were studying gender-mismatched transplanted hearts to see whether bone marrow c-kit$^+$ cells from male recipients infiltrated into female donor hearts. Using fluorescent *in situ* hybridization (FISH) to identify cells with Y chromosomes, they found that most of the c-kit$^+$ cells did not contain a Y chromosome or express hematological markers indicating that they originated from the female donor heart[76].

Since then, clusters of cardiac c-kit$^+$CD34$^-$CD45$^-$cells have been identified in mice, rats, dogs, pigs, and humans[76–78]. Isolated c-kit$^+$ cells from the heart have been shown to be multipotent and self-renewing. A small fraction of c-kit$^+$ cells (7-10%) express cardiac transcription factors GATA-4, MEF2C, and Nkx2.5; while less than 0.5% express cardiac sarcomeric proteins indicating that c-kit$^+$ cells may be committed to the cardiomyocyte lineage. Moreover, c-kit$^+$ cells can differentiate into several different cardiac lineages. When c-kit$^+$ cells were cultured in differentiation media, 29-40% expressed cardiac myosin and α-sarcomeric actin, 18-23% expressed alpha-smooth muscle, and 18-23% expressed von Willebrand factor; however, these cells did not morphologically or structurally resemble mature cardiomyocytes, endothelial cells, and smooth muscle cells[77,78]. Isolated c-kit$^+$ cells can also be expanded and passaged in cell culture for over a year and single c-kit$^+$ cells can give rise to clones with an efficiency of 3.5%[77].

Animal studies have shown that transplantation of cultured c-kit$^+$ cells either immediately following MI injury or in chronic ischemic injury improve survival through differentiation. In the initial study that characterized residential c-kit$^+$ cells, researchers injected 100,000 cultured c-kit cells into the border zone five hours after MI[77]. After twenty days, LVEF was over 10% higher in rats treated with c-kit$^+$ cells than untreated rats. Overall, systolic and diastolic function improved compared to untreated MI rats. Interestingly, c-kit$^+$ cell-treated hearts had larger infarcts than control rats (70% versus 55%), which the authors attributed to improved survival because untreated rats with the same size infarcts died within twenty days following MI. The improvements in survival and cardiac function were ascribed to the generation of new cardiomyocytes, endothelial cells, and smooth muscle cells. EGFP-labeled clones derived from c-kit$^+$ cells injected into the border zone following MI engrafted and differentiated into cardiomyocytes, smooth muscle cells, and endothelial cells[77]. In a follow-up study, the same group evaluated the therapeutic benefits of systemic delivery of clonogenic GFP-labeled c-kit$^+$ cells four hours after ischemia-reperfusion injury in rats. They found similar improvements as intramyocardial injection of c-kit+ cells with increased systolic and diastolic function compared to control ischemic-reperfusion injured rats. GFP-labeled c-kit+ cells traversed the vessel wall to engraft and differentiate into cardiomyocytes[79]. Since c-kit$^+$ cells need to be expanded in cell culture to get sufficient numbers of cells for transplantation, another study evaluated intracoronary infusion of GFP-labeled c-kit$^+$ cells thirty

days after inducing MI to simulate a more clinically relevant timeline for the administration of c-kit$^+$ cells[80]. A month later, c-kit$^+$ transplanted hearts had improved cardiac function, smaller infarct size, and decreased myocardial fibrosis compared to vehicle-infused MI hearts. However, in these studies, only 7 of the 17 rats transplanted with c-kit$^+$ cells had identifiable GFP-labeled cells.

Not all groups who have studied c-kit$^+$ cell transplantation in mice have observed beneficial effects on cardiac function[81,82]. After demonstrating their ability to successfully isolate, culture, and differentiate c-kit$^+$ cells; a group of researchers showed that transplantation 500,000 luciferase-expressing c-kit$^+$ cells into the border zone following MI led to minimal engraftment assessed using in vivo imaging and histological analysis. There was no measurable improvement in cardiac function compared to control-injected mice[81]**.** These findings were replicated by another group that transplanted c-kit$^+$ cells from transgenic ACT-GFP/MHC-nLAC mice into wild type mice following MI and found some GFP-labeled c-kit$^+$ cells that engrafted in the heart but did not differentiate into cardiomyocytes assessed by expression of α-actinin or β-galactosidase[82].

In heart failure patients, there is only one Phase I clinical trial that has been published regarding the therapeutic potential of c-kit$^+$ cells to date[83,84]. The SCIPIO trial was a controlled, randomized clinical trial that evaluated the safety and effects of transplanting c-kit$^+$ cells into patients with ischemic heart failure (average LVEF of 30% and average NYHA Class II). Right atrial appendages were harvested at the time of CABG and c-kit$^+$ cells were isolated and expanded

in cell culture until there were sufficient numbers of cultured c-kit^{+} cells. Most patients had 1,000,000 cells infused into coronary arteries supplying areas of injury[84]. Over the following 12 months, there were impressive improvements in clinical and functional outcomes with a 12% increase in LVEF from baseline,10% decrease in infarct size, and significant improvements in NYHA class and quality of life scores[85]. There was some concern about the data published in the supplementary figures of this paper that curbed the enthusiasm for the findings[86]. A phase II CONCERT-HF trial is currently recruiting participants to evaluate the safety and therapeutic effect of bone marrow MSCs, cardiac c-kit^{+} cells or a combination of both on outcomes for ischemic heart failure patients[87].

Paracrine Effects of Adult Cell Therapies

Although initial cell therapy studies in animals proposed that the long-term beneficial effects of cell therapies arose from differentiation of transplanted cells into mature cardiac cells, subsequent studies demonstrating the lack of long-term engraftment have prompted researchers to explore other mechanisms to account for the beneficial effects. There is a growing consensus that the paracrine effects of transplanted cells on residential cells in recipients underlies the clinical improvements reported. There are several ways that paracrine factors from transplanted cells have been proposed to exert beneficial effects on the failing heart: increasing cytoprotection, modulating the immune system, preventing

cardiac remodeling, increasing angiogenesis and stimulating endogenous cardiac regeneration.

Several studies proposed that cell therapies exert their beneficial effects by activating endogenous cardiac regeneration, the process by which the adult heart generates new cardiomyocytes. Endogenous cardiac regeneration has been proposed to occur through either proliferation of existing cardiomyocytes or differentiation from a cardiac progenitor cell population. Published data demonstrated that transplantation of bone marrow and cardiac cell therapies enhances endogenous cardiac regeneration by targeting both proposed processes. Two of these studies utilized the double transgenic *Myh6*-MerCreMer-ZEG mouse model to test the effects of transplanted bone marrow-derived c-kit^{+} cells, MSCs, and CDCs on endogenous cardiac regeneration. In *Myh6*-MerCreMer-ZEG mice, β-galactosidase is expressed in all cells before Cre-mediated recombination while GFP is only expressed in cardiomyocytes upon Cre-mediated excision of a stop sequence[88]. Following 4-OH-tamoxifen or tamoxifen injections, cardiomyocytes are labeled with GFP while all noncardiomyocytes are labeled with β-galactosidase. If new cardiomyocytes arise from proliferation of pre-existing cardiomyocytes, they will express GFP, but if they originate from differentiation of an endogenous cardiac progenitor cell population, new cardiomyocytes will be labeled with β-galactosidase. By quantifying the changes in GFP and β-galactosidase labeling of cardiomyocytes after cell transplantation, researchers determined the effects of bone marrow c-

kit^{+} cells, bone marrow MSCs, and CDC transplantation on endogenous cardiac regeneration following MI[89,90]. Epicardial transplantation of bone marrow c-kit^{+} cells into the border zone immediately after permanent ligation of the left coronary artery increased the percentage of total cardiomyocytes labeled with β-galactosidase and decreased the percentage of GFP labeled cardiomyocytes compared to control MI mice[89]. This finding provided evidence that transplantation of bone marrow c-kit^{+} cells activates endogenous cardiac progenitor cells to give rise to new cardiomyocytes following MI. Epicardial transplantation of bone marrow MSC, on the other hand, did not alter β-galactosidase and GFP labeling of cardiomyocytes indicating that, if bone marrow MSCs stimulate endogenous cardiac regeneration, newly-formed cardiomyocytes arise from proliferating cardiomyocytes[89]. Contrary to this finding, studies in mice and pigs showed that intramyocardial injections of MSCs enhance proliferation and cardiomyocyte commitment of c-kit^{+} cells[91,92]. Another study combined the *Myh6*-MerCreMer-ZEG mouse model with 5-Bromo-2'-deoxyuridine (BrdU) injections to quantify GFP and β-galactosidase labeling of newly formed cardiomyocytes following MI with or without epicardial CDC injections at the time of surgery[90]. Five weeks after MI, CDC-treated mice had higher levels of BrdU incorporation in GFP^{+} and GFP^{-} cardiomyocytes compared to untreated MI controls with about four-fold more cardiomyocytes arising from progenitor cell population than proliferating cardiomyocytes in CDC treated mice[90].

With evidence that transplanted cells may exert their beneficial effects through activation of endogenous cardiac regeneration, there is a growing interest in understanding the mechanisms underlying endogenous cardiac regeneration with the goal of finding more direct methods of activating this process for the treatment of heart failure. One question that has plagued the field of cardiac regeneration is the relative contributions of endogenous cardiac progenitor cells and proliferating cardiomyocytes.

ENDOGENOUS CARDIAC REGENERATION

Endogenous cardiac regeneration is the ability of the postnatal heart to generate new cardiomyocytes. In the past, scientists believed that new cardiomyocytes did not form after birth; however, a seminal study published in 2009 provided convincing evidence that adult human hearts generate new cardiomyocytes at low levels throughout their lifetimes[93,94]. In this study, researchers developed a carbon-dating method to approximate the age of cardiomyocyte nuclei harvested from postmortem hearts. From 1945 to 1961, above-ground atomic bomb testing resulted in a spike in the amount of atmospheric, radioactive ^{14}C, which made its way up the food chain to become incorporated into humans within 1-2 years. This group quantified the amount of ^{14}C present in genomic DNA isolated from cardiomyocyte nuclei and compared it to the amount of atmospheric ^{14}C present at the time of birth. Even when they accounted for polyploidization that occurs earlier in life, they found that ^{14}C levels

in cardiomyocyte genomic DNA corresponded to atmospheric ^{14}C levels at time points after birth, indicating postnatal generation of new cardiomyocytes. The researchers then tested different mathematical models and identified the one that fits best with the measured ^{14}C content of cardiomyocyte genomic DNA. Based on this model, they approximated an annual renewal rate of 0.8% at twenty years of age which declines to about 0.3% at seventy-five years of age[93,94].

While this study provided groundbreaking evidence that continuous, low-level generation of new cardiomyocytes occurs in humans, the strategy employed in this study could not be used to identify the cellular source of new cardiomyocytes. Over the past two decades, a combination of animal and human studies have been used to evaluate the contribution of different sources to the endogenous generation of new cardiomyocytes in the adult mammalian heart.

Extracardiac Progenitor Cells

Analysis of gender-mismatched cardiac transplantations suggested that there may be an extracardiac source of new cardiomyocytes in humans. Three studies assessed cardiomyocyte chimerism in female hearts transplanted into male recipients with FISH to identify cardiomyocyte nuclei with Y-chromosomes. In one study, eight of the thirteen patients biopsied had Y chromosome^{+} cardiomyocytes that accounted for 0.16% of the 31,000 cardiomyocytes analyzed[95]. The other studies, however, found that all autopsy samples contained Y chromosome^{+} cardiomyocytes, although the exact percentages

varied widely between each report from 0.04% to 9%[76,96]. Interestingly, 17% of Y chromosome$^+$ cardiomyocytes also expressed Ki67 compared to only 1% of all other cardiomyocytes, suggesting that Y chromosome+ cardiomyocytes were more proliferative[76]. A follow-up study assessed how MI effects chimerism of cardiomyocytes by quantifying the percent of Y chromosome$^+$ cardiomyocytes in donor hearts that suffered MI following transplantation. Although there appeared to a slightly higher percentage of Y chromosome$^+$ cardiomyocytes in MI-injured transplanted hearts (0.07%) compared to non-MI hearts (0.02%), the difference was not significant[97]. Although there were inconsistencies regarding the extent of cardiomyocyte chimerism reported, these studies provided evidence that an extracardiac source of new cardiomyocytes exists in humans.

Studies in mice further explored the possibility of a circulating extracardiac progenitor cell source by connecting the circulatory systems of two mice through a procedure called parabiosis. In the first study, wild-type mice were joined to transgenic GFP mice following permanent ligation of the LAD artery in wild-type mice[44]. Eight weeks after the surgery, GFP$^+$ cells could be identified throughout the heart, but they were all hematopoietic in origin. No GFP$^+$ cells expressing cardiac markers and smooth muscle markers could be identified. While this study suggested that extracardiac cells do not contribute to cardiomyocytes following MI, another group hypothesized that the lack of cardiomyocyte labeling observed in this experiment resulted from the mice undergoing parabiosis immediately after MI. Therefore, this group performed parabiosis one month before ligating

the LAD artery. They connected one group of transgenic α-MCM mice to transgenic GFP mice and another group of transgenic α-MCM mice to ZEG mice. One month later, α-MCM mice underwent LAD ligation. After two weeks, transdifferentiation and fusion of extracardiac circulating cells were assessed by quantifying the percent of cardiomyocytes that were $GFP^{+}Cre^{-}/GFP^{-}\beta$-galactosidase^{+} and $GFP^{+}Cre^{+}/GFP^{+}\beta$-galactosidase^{-}, respectively. In both experiments, 0.17% of cardiomyocytes arose from fusion while only 0.0016% of cardiomyocytes arose from transdifferentiation[98]. These findings provide evidence that a small number of extracardiac cells fuse with cardiomyocytes following injury and an even lower percentage transdifferentiate into cardiomyocytes.

Although the exact identity of the circulating extracardiac sources of cardiomyocytes could not be discerned in these studies, the literature at the time suggested that these cells may originate from the bone marrow compartment. A study evaluating cardiomyocyte chimerism in female patients who had undergone gender-mismatched bone marrow transplantations for the treatment of hematological malignancies demonstrated that 0.23% of all cardiomyocyte analyzed were Y-chromosome^{+}, which was in line with the three of the four gender-mismatched cardiac transplantation studies[99]. The women in these studies had an average LVEF of 67.5%.

Studies with bone marrow chimeric mice where almost all bone marrow cells were labeled demonstrated their negligible contribution to cardiomyocyte

formation that likely arose from fusion of bone marrow cells with pre-existing cardiomyocytes[43,45,100]. Two groups transplanted unfractionated bone marrow from transgenic GFP mice into wild-type mice and ligated the left coronary artery one or two months after bone marrow transplantation[43,45]. When cardiomyocyte labeling was assessed up to two months later, 0.003% of cardiomyocytes expressed GFP[45]. In these studies, the contribution of fusion and transdifferentiation could not be assessed; however, there is evidence that endogenous bone marrow cells primarily undergo fusion with pre-existing cardiomyocytes and do not transdifferentiate into cardiomyocytes. When LacZ Cre-inducible reporter mice were transplanted with bone marrow from transgenic mice with ubiquitously expressed Cre and GFP driven by a b-actin promoter, all GFP-labeled cardiomyocytes were β-galactosidase^{+}, and none were β-galactosidase^{-} indicating that they all arose from fusion. Taken together, these studies show that extracardiac circulating cells can fuse with pre-existing cardiomyocytes, but do not significantly contribute to new cardiomyocyte formation in the adult mammalian heart.

Proliferating Cardiomyocytes

The newt, zebrafish, and neonatal mouse hearts have all been shown to regenerate following cardiac injury through the proliferation of pre-existing cardiomyocytes. To determine whether cardiomyocyte proliferation is the source of cardiomyocytes in the adult mouse heart, a group of researchers used multi-

isotope imaging mass spectrometry (MIMS) to identify newly-formed cardiomyocytes in *Myh6*-MerCreMer-ZEG mice[101,102]. In a previous publication using only the *Myh6*-MerCreMer-ZEG mouse model, it was reported that pre-existing cardiomyocytes give rise to new cardiomyocytes under homeostatic conditions since the percent of GFP^+ and β-galactosidase$^+$ cardiomyocytes did not change over time[88]. However, following MI, the percent of GFP^+ cardiomyocytes decreased and the percent of β-galactosidase$^+$ cardiomyocytes increased suggesting that β-galactosidase expressing cardiac progenitor cells gave rise to cardiomyocytes[88]. In a seminal follow-up study, the same group used MIMS to analyze cardiac sections from *Myh6*-MerCreMer-ZEG mice continuously given ^{15}N thymidine to identify newly-formed cardiomyocytes. The relative amount of naturally occurring ^{15}N is much lower than ^{14}N isotope. Using MIMS to generate pseudocolored images of the ratio of ^{15}N to ^{14}N, researchers identified cardiomyocyte nuclei that had undergone DNA synthesis on cardiac sections and evaluated their GFP expression. During normal aging, 77% of $^{15}N^+$ cardiomyocytes expressed GFP compared to 84% of $^{15}N^-$ cardiomyocytes. Following MI, 67% of all cardiomyocytes expressed GFP while 71% of $^{15}N^+$ cardiomyocytes expressed GFP. In the sham hearts, 83% of $^{15}N^+$ cardiomyocytes expressed GFP. They estimated that the annual rates of cardiomyocytes renewal were 0.76% and, that in the two months following MI, 3.2% of cardiomyocytes undergo cell division. While these results are often cited to suggest that cardiomyocyte proliferation is the sole source of new

cardiomyocytes, the lower level of GFP-labeling in MI hearts (71%) versus sham hearts (83%) would suggest that a progenitor cell population may still contribute to endogenous cardiac regeneration.

Another group used a different approach to assess the contribution of cardiomyocyte proliferation in endogenous cardiac regeneration. In the MADM reporter mouse model, only Cre-expressing cells that are actively undergoing karyokinesis will be labeled with fluorophores. Cells that undergo karyokinesis alone without subsequent cytokinesis will express both red fluorescent protein (RFP) and GFP, while daughter cells that arise from karyokinesis followed by cytokinesis will be labeled with either RFP or GFP. When they used the *Myh6*-CreERT2-MADM$^{GT/TG}$ mice to study cardiomyocyte proliferation at after MI, they found the same low levels of labeling between sham and MI hearts. In one-month-old mice that were treated with tamoxifen from birth, they observed labeling of less than 0.05% of cardiomyocytes. When they analyzed the distance between daughter cardiomyocytes over 65% of them were between 250 -1000 microns away from each other. The data presented in this study does not fit well with other studies which may arise from limitations in the MADM reporter model. When they performed LAD ligation in β-actin CreER MADM$^{GT/TG}$ mice where Cre is expressed in all cells, they did not see any difference in labeling between sham and MI hearts four weeks after MI contrary to what would be expected and there was only sparse labeling of RFP or GFP expressing cells.

While these studies along with others provide evidence that proliferating cardiomyocytes play an essential role in endogenous cardiac regeneration, none of them convincingly rule out the contribution of an endogenous cardiac progenitor cell population[103,104].

Endogenous Cardiac Progenitor Cells

C-kit$^+$ Cells:

C-kit$^+$ cells have been isolated from the adult heart and shown to be multipotent and self-renewing cells in cell culture and after transplantation. As the consensus grew that transplanted cells largely exert their beneficial effects through paracrine factors that target endogenous cells in the body, researchers began to wonder whether residential c-kit$^+$ cells were responding to these therapies. Transplantation studies in *Myh6*-MerCreMer-ZEG showed that injection of bone marrow c-kit$^+$ cells and CDCs increased the contribution of endogenous cardiac progenitor cells. Additionally, MSC transplantation increased the proliferation and cardiomyocyte differentiation of residential cardiac c-kit$^+$ cells.

Early studies evaluated the role of endogenous c-kit$^+$ cells in the adult mammalian heart following MI. Immunohistochemical analysis of residential c-kit$^+$ cells in human myocardial samples showed an increase in the total number of c-kit$^+$ cells and the percentage of c-kit$^+$ cells undergoing mitosis in patients that had

died acutely after MI. In explanted chronic ischemic heart failure myocardium, these measurements were also elevated but not to the same extent. Co-expression of c-kit with cardiomyocyte, smooth muscle and endothelial cell markers was also increased in both types of samples[105]. These findings suggested that c-kit$^+$ cells are activated immediately following MI with sustained, but lower, levels of activation thereafter. Using *Kit*-GFP transgenic mice, another group also found that the numbers of endogenous c-kit$^+$ cells in the heart increases immediately following MI and peaks at day ten post-MI before starting to decrease[106]. They also showed that these c-kit$^+$ cells co-express cardiomyocyte transcription factors as well as smooth muscle and endothelial cell markers.

Endogenous c-kit$^+$ cells are also activated in response to acute adrenergic injury. In rats injected with a single dose of 5mg/kg isoproterenol, a β-adrenergic receptor agonist; 8% of cardiomyocytes underwent apoptosis with complete recovery of cardiac function in 6 days[107]. In this study, they noted that endogenous c-kit$^+$ cells, which they had shown were resistant to isoproterenol-induced apoptosis *in vitro*, were more proliferative. Researchers found that 88% of c-kit$^+$ cells were undergoing proliferation leading to an 8% increase in the total number of c-kit$^+$ cells[108]. In a feline model of acute adrenergic injury, another group did not observe an overall change in the number of ventricular c-kit$^+$ cells, although they did report increased BrdU incorporation in c-kit$^+$ cells[109]. Three days after acute isoproterenol injury in rats, newly formed cardiomyocytes were

observed in the subendocardium and apex with 0.18% of cardiomyocytes labeled with BrdU[108]. To assess the source of these newly formed cardiomyocytes, they injected *Myh6*-MerCreMer-ZEG mice with tamoxifen and BrdU and quantified GFP and β-galactosidase labeling of BrdU$^+$ cardiomyocytes[108]. Overall, the percentage of β-galactosidase$^+$ cardiomyocytes increased from 18%to 26.5% and the number of GFP$^+$ cardiomyocytes decreased from 86% to 73%. Moreover, all BrdU$^+$ cardiomyocytes expressed β-galactosidase without GFP. These researchers then showed that endogenous c-kit$^+$ cells give rise to new cardiomyocytes following isoproterenol injury. Forty percent of endogenous c-kit$^+$ cells were labeled *in vivo* following injection of a *Kit*-driven Cre lentivirus into a YFP Cre-inducible reporter mouse. Despite the low level of labeling of endogenous c-kit$^+$ cells, 43% of all BrdU$^+$ cardiomyocytes were labeled with YFP, with up to 74% of BrdU$^+$ cardiomyocytes in the apex of the heart labeled as well. These studies provided preliminary evidence that endogenous c-kit$^+$ cells could proliferate and differentiate into cardiomyocytes following ischemic and acute adrenergic injury.

To more accurately address the role of residential c-kit$^+$ cells in endogenous cardiac regeneration, the van Berlo lab generated a tamoxifen-inducible, lineage-tracing mouse model driven by the endogenous *Kit* promoter. With this mouse model, it was shown that c-kit$^+$ cells give rise to 0.016% of cardiomyocytes following MI and 0.007% following acute isoproterenol injury. Most of these lineage-traced cardiomyocytes arose from fusion events.

Subsequent studies published by other groups who had generated multiple lineage-tracing strategies corroborated these findings that endogenous c-kit$^+$ cells give rise to a very small number of cardiomyocytes following cardiac injury. Some researchers had concerns that targeting the *Kit* locus in these studies altered the behavior of c-kit$^+$ cells; however, a follow-up study published by the van Berlo lab used single-cell RNA sequencing to show that c-kit$^+$ cells isolated from wild-type mice and knock-in lineage-tracing models were indistinguishable with clustering analysis[110,111]. Others questioned whether a small percentage of cardiomyocytes could express *Kit.* A study published last year reported the use of a dual recombinase system to show that endogenous c-kit$^+$ cells fuse with pre-existing cardiomyocytes at a very low rate that was not quantified, but do not significantly differentiate into cardiomyocytes[112]. This data fits with the original lineage-tracing mouse model published by the van Berlo lab.

Sca-1$^+$ Cells.

Stem cell antigen-1 (Sca-1) has been used in conjunction with other markers to identify HSCs[113]. Because of this, different groups began to study the properties of Sca-1$^+$ cells isolated from the adult murine heart[114,115]. Sca-1$^+$ cells make up about 70% of noncardiomyocytes and can be found in close approximation to the basal lamina of cardiomyocytes[114,116]. One study even suggested that Sca-1$^+$ cells are located under the basal lamina of adult cardiomyocytes analogous to the location of satellite cells under the basal lamina

of skeletal muscle[117]. Cardiac Sca-1$^+$ do not express c-kit, hematopoietic or bone marrow lineage markers (CD4, CD8, B220, Gr-1, Mac-1, Ter119, CD45, CD34), and most endothelial markers (Flt-1, Flk-1, VE-Cadherin, vWF) at the mRNA or protein level[114,118–120]. The majority of Sca-1$^+$ cells express CD31; however, it is the CD31$^-$ subpopulation that has been extensively studied and shown to possess cardiac progenitor cell properties.

Multiple strategies have highlighted the self-renewal and clonal properties of cardiac Sca-1$^+$ cells. Cell lysates of freshly isolated Sca-1$^+$ cells had comparable telomerase activity to neonatal heart lysate. No telomerase activity was observed in Sca-1$^-$ cell lysate[114]. This group also showed that clones derived from single noncardiomyocytes expressed Sca-1 and highly expressed telomerase reverse transcriptase (TERT) with telomerase activity comparable to HeLa cells[118]. Contrary to this finding, another group found that clones derived from single noncardiomyocytes varied widely in their expressing of Sca-1, but all clones analyzed still expressed TERT[120]. Additionally, cultured Sca-1$^+$ CD31$^-$ cells form cardiospheres, and the cells that grow out of these cardiospheres can be propagated for over 30 passages while retaining expression of the same cell surface markers[121]. Using an unbiased approach, this group also identified Sca-1$^+$ cells as a self-renewing population in the adult murine heart.[121] Long-term label-retaining cells isolated from the bone marrow have been shown to be enriched for self-renewing HSCs[122]. This group used a similar approach to identify and characterize long-term label-retaining cells in the heart. They

performed BrdU pulse-chase experiments in adult mice and developed a mathematical model to identify long-term label-retaining noncardiomyocytes. They found that approximately 90% of these cells expressed Sca-1 but not c-kit[121].

Cardiac Sca-1$^+$ cells also differentiate into cardiomyocytes *in vitro* and after transplantation following cardiac injury. Freshly isolated Sca-1$^+$ cells express key cardiac transcription factors (GATA4, MEF-2C, TEF-1) but do not express structural cardiac proteins[114]. After being cultured in media containing 5-azacytidine, an inhibitor of DNA methyltransferase 1, or oxytocin, cardiac Sca-1$^+$ cells express Nkx2.5, α-MHC, β-MHC, MLC-2a, MLC-2v and cardiac α-actin and significantly upregulate expression of GATA4[114,115]. Moreover, about 1% of Sca-1$^+$ cells cultured in oxytocin spontaneously beat with cytosolic calcium transients that increased beating frequency in response to isoproterenol[115]. Spontaneous beating in 5-azacytidine treated Sca-1$^+$ cells was not observed. Other culturing cocktails were also used to induce cardiomyogenic differentiation of Sca-1$^+$ CD31$^-$ cells; however, these cells did not spontaneously beat[123]. Following ischemia/reperfusion injury, Sca-1$^+$ cells injected into the systemic circulation engrafted in injured and surrounding myocardium accounting for about 3% of nuclei in these regions. Interestingly, a little over half of these cardiomyocytes appeared to arise from direct differentiation of transplanted Sca-1+ cells, while the other half arose from fusion of transplanted Sca-1$^+$ cells and pre-existing cardiomyocytes from the recipient mice[114].

Cardiac Sca-1$^+$ cells and their derivatives are multipotent and can differentiate into endothelial, osteogenic, chondrogenic and adipogenic lineages. Sca-1$^+$ CD31$^-$ cells form branched tubular networks of cells when they are cultured on matrigel and begin to express CD31, Flt-1, and vWF when they are cultured in VEGF-containing media[123]. When Sca-1$^+$ cells are cultured with ascorbic acid, dexamethasone and b-glycerolphosphate, they begin to express alkaline phosphatase and osteocalcin[115]. Sca-1$^+$ CD31$^-$ cells and Sca-1$^+$ clones can also differentiate into chondrogenic cells visualized with alcian blue and von Kossa staining.[115,120] Under various culturing conditions, Sca-1$^+$ cells, Sca-1$^+$ CD31$^-$ cells and Sca-1$^+$ clones can differentiate into adipose cells that contain lipid droplets within their cytoplasm[115,120,121].

Transplantation of cardiac Sca-1$^+$ cells has been shown to improve cardiac function after MI through direct differentiation into cardiomyocytes and endothelial cells as well as secretion of paracrine factors. Two separate groups demonstrated that the percent of Sca-1$^+$ CD31$^-$ cells increased a week after permanent ligation of the left coronary artery (LCA) before returning to baseline levels two weeks later[123,124]. This finding suggested the Sca-1$^+$ CD31$^-$ cells survive and expand in response to cardiac injury[123]. Intramyocardial injection of Sca-1$^+$ CD31$^-$ cells improved ventricular systolic and diastolic dimensions, ejection fraction and cardiac bioenergetics following permanent ligation of the left LCA. It was suggested that this improvement arose from increased angiogenesis and differentiation of transplanted Sca-1$^+$ CD31$^-$ cells into endothelial cells and

cardiomyocytes, although fusion of transplanted cells was not assessed. Of note, ejection fraction, but not ventricular systolic and diastolic dimensions, improved following transplantation of Sca-1$^-$ CD31$^-$ cells[123]. Intramyocardial injection of Sca-1$^+$ clones also improved ejection fraction following permanent ligation of the left LCA by differentiation of transplanted cells into endothelial cells and cardiomyocytes[118,120]. This improvement was shown to be dependent on the expression of Sca-1[118]. There is some evidence that the beneficial effects of transplanting cultured Sca-1$^+$ cells following myocardial damage arise from secreted paracrine factors. In a Langendorff isolated heart model of ischemia-reperfusion injury, retrograde aortic infusion of Sca-1$^+$ conditioned media resulted in the recovery of contractility and relaxation during the reperfusion stage comparable to the improvement seen with infusion of cultured Sca-1$^+$ cells[119].

Since the self-renewal and cardiomyogenic properties of cardiac Sca-1$^+$ cells were primarily studied in cell culture or after transplantation, a group generated a doxycycline-inducible, lineage-tracing mouse model to investigate the role of Sca-1$^+$ cells in endogenous cardiac regeneration in vivo. With this model, they showed that lineage-traced Sca-1$^+$ cells give rise to 4.5% of cardiomyocytes over 13 months during the normal aging process. This percentage is much higher than would be expected. One month after MI or transverse aortic constriction, cardiomyocyte labeling increased 41% and 235%, respectively. In these studies, they did not carefully assess whether lineage-

traced cardiomyocytes were newly formed or whether they arose from fusion with Sca-1$^+$ cells.

One of the significant issues that has prevented the translation of cardiac Sca-1$^+$ cells to human studies is the absence of a human homolog for Sca-1[113]. Despite this, groups have used Sca-1 antibodies, which bind to an unknown epitope in humans, to isolate a population of cells from myocardial surgical waste that they could expand in cell culture and differentiate into cardiomyocytes using a complex protocol with 5-azacytidine, TGF-β1, and vitamin C stimulation[125].

Cardiac Sca-1$^+$ cells have also been extensively studied along with the side population phenotype. In the initial study that characterized Sca-1$^+$ cells, the authors found that Sca-1$^+$ cells are enriched for cSPCs 100-fold compared to all noncardiomyocytes (3.6% cSPCs in Sca-1$^+$ cells compared to 0.03% cSPCs in all noncardiomyocytes). However, it is important to note that the percent of cSPCs from total noncardiomyocytes identified in this study was much lower than has been identified by other research groups (0.8%- 2%) and no negative control was used to ensure accurate side population gating. Other studies of side population cells and Sca-1 expression will be discussed in further detail in the cSPC section below.

Cardiac Side Population cells (cSPCs)

The side population phenotype was an incidental finding first described in 1996[126]. When researchers stained isolated bone marrow cells with Hoechst

33342 to identify live HSCs undergoing cell division, they noticed that a small number of cells did not stain as intensely as most of the other bone marrow cells. When they plotted the red and blue fluorescence of Hoechst 33342 against each other on a linear scale, these low-staining cells could easily be identified coming off to the *side* of the rest of the bone marrow cells. These cells were aptly called side population cells. They found that side population cells stained less intensely with Hoechst 33342 because they were actively extruding Hoechst 33342 out of their cytoplasm since Hoechst 33342 enters all cell through passive diffusion[126,127].

Analysis of bone marrow SPCs showed that they were enriched for hematopoietic stem cells (HSCs) with greater potential for long-term bone marrow reconstitution[126,128]. In the original study describing SPCs, HSCs were identified as Sca-1^+ Lineage$^-$ cells[126]. While HSCs made up 1% of whole bone marrow, they accounted for 75% – 90% of SPCs. Moreover, 10% of HSCs fell within the side population gate while only 0.1% of whole bone marrow cells were within the side population gate. To determine the bone marrow reconstitution potential of SPCs, researchers transplanted SPCs into lethally irradiated mice. Transplantation of as little as 500 SPCs rescued 70% of mice after lethal irradiation[126]. Moreover, when Lineage$^-$ Sca-1^+ c-kit^+ cells (LSK) cells from within the side population gate were compared to LSK cells from outside the side population gate, LSK SPC cells reconstituted the bone marrow niche more efficiently than LSK non-SPC cells[128]. Even when six times more LSK non-SPC

cells were transplanted into irradiated mice, they could not reconstitute the bone marrow niche as effectively as LSK SPC cells. Although there was some debate about the staining pattern of CD34 in bone marrow SPCs, it was found that almost all SPCs are CD34$^{-/low}$ [128–130]. These studies provided convincing evidence that the side population phenotype enriches for LSK cells that are more potent long-term reconstituting HSCs (LT-HSCs)[128].

This was not the first time that low-staining Hoechst 33342 cells were reported to enrich for HSCs[131]. An earlier study in 1993 used the blue fluorescence of Hoechst 33342 in conjunction with the green fluorescence of rhodamine 123, a fluorescent mitochondrial dye, to identify cells that were low-staining for both dyes which they showed to be enriched for HSCs[131]. The study by Goodell et al. was the first to plot the blue and red fluorescence of Hoechst 33342 against each other, thereby using a single marker to enrich for HSCs[126].

Bone marrow SPCs can be categorized into lower and upper SPCs based on their relative abilities to efflux Hoechst 33342 with lower SPCs having a greater ability to extrude Hoechst 33342 from their cytoplasm than upper SPCs[128,132,133]. Both groups of SPCs can reconstitute the bone marrow niche; however, they vary in duration of reconstitution and the proportion of different bone marrow lineages they give rise to[128,133]. In competitive bone marrow reconstitution experiments, lower SPCS have more significant long-term engraftment potential with 2.5-fold higher reconstitution capacity than upper SPCs 4 months after transplantation[128,133]. Lower and upper SPCs are both able

to give rise to all lineages; however, the lower SPCs give rise to a higher percentage of myeloid lineages while the upper SPCs give rise to more lymphoid lineages[133].

The side population phenotype also enriches for subpopulations of HSCs that are excluded when using cell surface marker panels to identify LT-HSCs[132,133]. LT-HSCs are commonly identified as LSK $CD34^-$ $Flt3^-$ $CD150^+$ $CD48^-$ cells[134]. CD150, a member of the SLAM surface receptor family, is used to identify LT-HSCs. When the bone marrow reconstitution potential of $CD150^+$ and $CD150^-$ cells isolated from whole bone marrow was compared to each other, it was reported that LT-HSCs are only identifiable in $CD150^+$ cells[135]. Unlike whole bone marrow, $CD150^+$ and $CD150^-$ subpopulations of LSK SP cells both represent LT-HSCs; however, $CD150^-$ LSK SP cells are more proliferative than $CD150^+$ LSK SP cells[132]. This study provides evidence that, while the use of cell surface markers has allowed for the careful identification of LT-HSCs, such a strategy exclude populations of LT-HSCs that can be readily identified with the side population phenotype.

After the side population phenotype was reported in whole bone marrow, many researchers used this phenotype to enrich for stem and progenitor cells in tissues throughout the body[126,127,136–141]. The necessary steps for isolating side population cells are the same regardless of the source. First, the tissue being studied is carefully dissociated to generate a single-cell suspension, which is then stained with Hoechst 33342. The exact concentration of cells to Hoechst

33342 varies between tissues which is why accurate quantification of the number of cells is essential. Most protocols incubate cells with Hoechst 33342 for 90 minutes in a 37^{o}C water bath to allow time for Hoechst 33342 to diffuse into all cells and then be extruded from side population cells. Other dyes that do not require a flow cytometer equipped with a UV laser have been used to identify side population cells but are not commonly used[142,143]. To ensure that side population cells are accurately identified, an aliquot of the single-cell suspension is incubated with Hoechst 33342 and Verapamil, which acts as broad-spectrum ABC transporter inhibitor to block the side population phenotype. The ability of Verapamil to block the side population phenotype is not dependent on its calcium channel blocking properties because it still inhibits the side population phenotype in the presence of the calcium chelator, EDTA. Other chemicals that inhibit the ABC superfamily of transporters, like fumitremorgin C and reserpine, have also been used to block the side population phenotype[144,145].

Cardiac side population cells (cSPCs) were first isolated from the heart in 2002 and were shown to represent a distinct population of cells from bone marrow SPCs and c-kit^{+} cardiac progenitor cells[146–148]. While almost all bone marrow SPCs express CD45, CD44, and c-kit, less than 1% of cSPCs express these markers. Moreover, when cSPCs are maintained in monoculture, they have increased expression of cardiac transcription factors and sarcomeric proteins; while bone marrow SPCS cultured under the same monoculture conditions did not express any of these markers[147]. CSPCs are also residential

cardiac cells that do not originate from the bone marrow in the postnatal mammalian heart. In adult wild-type mice that had been transplanted with bone marrow from transgenic GFP mice at birth, less than 1% of cSPCs expressed GFP providing evidence that cSPCs do not originate from the bone marrow compartment like bone marrow SPCs[149]. CSPCs also represent a distinct population of cells from c-kit$^+$ cardiac progenitor cells. CSPCs do not express c-kit and have a distinct mRNA expression profile from c-kit$^+$ cardiac progenitor cells[146,147].

CSPCs compose 0.8 – 2% of noncardiomyocytes in the adult mammalian heart; however, the percentage of cSPCs changes over an organism's lifetime[137,138,147,148,150,151]. In rats, the percentage of cSPCs gradually decreases from fetal life through adulthood. CSPCs account for 4%, 2% and 1.2% of noncardiomyocytes in fetal, neonatal and adult rat hearts, respectively[150]. This decrease in the percent of cSPCs from fetal to adult life was also observed in humans where cSPCs account for 2.2% and 1.1% of noncardiomyocytes in fetal and adult human hearts[152,153]. This declining trend in the percent of cSPCs appears to reverse in aged hearts. There was a 2.3-fold higher percentage of cSPCs normalized to heart mass in 24-32 month-old mice compared to 6-10-month-old mice[154].

Since their identification, isolated cSPCs have been found to clonally expand to self-renew their population. CSPCs formed colonies when cultured in methylcellulose media with or without neonatal rat cardiomyocytes[137,138,147,148,155–

[157]. Moreover, Sca-1$^+$cSPCs formed colonies in methylcellulose media at ten times the rate of Sca-1$^+$ cells from the main population of cells[147]. The ability of cSPCs to undergo clonal expansion was first convincingly demonstrated when primary and secondary clones derived from Sca-1$^+$ cSPCs could be maintained in cell culture for over ten months and retained Sca-1 expression and the side population phenotype[148].

CSPCs can differentiate into different cardiac cell types. Freshly isolated cSPCs express the cardiomyocyte transcription factors, Nkx2.5 and GATA4, highlighting their cardiomyogenic potential[147,157]. When Sca-1$^+$ CD31$^-$ cSPCs or Cdh5$^-$ cSPCs are cultured with rat neonatal or adult ventricular cardiomyocytes, they differentiate into functional cardiomyocytes that have organized sarcomeres, as well as similar contractility and cytosolic calcium handling properties to adult rat ventricular cardiomyocytes[147,158]. In addition to differentiating into cardiomyocytes when co-cultured with cardiomyocytes, cSPCs can be stimulated to differentiate into cardiomyocytes with chemical induction. Treatment of cSPCs with trichostatin A and oxytocin increased expression of Nkx2.5 and GATA4 and induced expression of cardiac transcription factors MEF2C and sarcomeric proteins β-myosin heavy chain and MLC-2V[150]. Three weeks after trichostatin A or oxytocin treatment, cSPCs developed organized sarcomeric structures and a small percentage began to beat spontaneously[150]. When cSPCs are also cultured for two weeks in media containing dexamethasone, they began to express cardiac troponin T and connexin-43. Four percent of cSPCs cultured

with dexamethasone began to beat spontaneously as well. Interestingly, cSPCs did not differentiate into cardiomyocyte when culture with 5-azacytidine, which stimulates cardiomyocyte differentiation of c-kit+ and Sca-1+ cells[150]. cSPCs can also differentiate into noncardiomyocytes lineages, like endothelial cells and smooth muscle cells *in vitro*. Freshly isolated cSPCs express Tie2 and smooth muscle actin (SMA) which indicates that cSPCs have the potential to differentiate into endothelial and smooth muscle cells *in vivo*. When cSPCs are cultured in media containing VEGF, they can begin to express vWF and angiopoietin2 and increased expression of angiopoietin1, CD31, and VEGF demonstrating an increased commitment to the endothelial lineage. Culturing cSPCs in media with VEGF also increased expression of SMA suggesting increased differentiation into smooth muscle cells.

CSPCs can also differentiate into non-cardiac cell types *in vitro*. When cSPCs are cultured in media containing BMP or β-glycerolphosphate, dexamethasone, and ascorbic acid-2 phosphate; they express alkaline phosphatase at both the mRNA and protein levels, which is a marker of osteoblasts[150,158]. CSPCs cultured in different types of adipogenic media begin to form lipid droplets that can be visualized with Oil Red O staining[150,158]. When cSPCs are cultured in methylcellulose media, they form colonies that stain for granulocyte and monocyte/macrophage markers, Gr-1 and Mac-1, respectively[137].

Transplanted cSPCs or clones derived from cSPCs differentiate into the four main cardiac lineages and improve cardiac function and remodeling following cardiac injury in the adult mammalian heart[148,150,151]. In the first study that evaluated the properties of transplanted cSPCs, 300,000 cSPCs isolated from neonatal transgenic rats that ubiquitously expressed GFP were injected systemically into wild-type adult rats immediately following cryoinjury[150]. Four weeks later, there were approximately eleven times more GFP-labeled cells identified in cryoinjured hearts compared to uninjured hearts (0.15% versus 0.013%). There were also more GFP-labeled cells located in the border zone compared to the infarct and remote regions. Of these GFP-labeled cells identified in the cryoinjured heart, 33% were fibroblasts, 29% were smooth muscle cells, 6.7% were endothelial cells, and 4.5% were cardiomyocytes. Although some GFP-labeled cells were identified in the uninjured controlled hearts four weeks after transplantation, none of them expressed cardiac troponin T. The findings of this study indicated that the cryoinjured heart creates a unique environment that significantly increases homing of cSPCs and promotes their differentiation to cardiomyocytes. A follow-up study evaluated the differentiation potential of Sca-1^+ $CD31^-$ cSPCs labeled with a red fluorescent membrane dye, PKH26, that were injected directly into the border zone immediately after permanent ligation of the left coronary artery. Two weeks later, researchers found that a little less than 4% of the PKH26-labeled cells expressed cardiomyocyte markers similar to the previously described study. This study also evaluated the potential of

transplanted PKH26-labeled Sca-1$^+$ CD31$^-$ cSPCs to migrate from areas of uninjured myocardium to the site of injury[151]. Researchers injected labeled Sca-1$^+$ CD31$^-$ cSPCs into the right ventricular epicardium following permanent ligation of the left coronary artery[151]. Three days later, they found PKH26-labeled cells in the ischemic region of the heart. Neither of these studies evaluated the effect of cSPC transplantation on cardiac function or remodeling[150,151]. In a more recent study, 250,000 mOrange-expressing clones derived from cSPCs were injected into the border zone immediately following ligation of the left coronary artery[148]. In this study, there was no difference in engraftment and cardiomyocyte differentiation between sham and MI hearts at two or twelve weeks after transplantation. The percent of mOrange-labeled cardiomyocytes in both sham and MI hearts increased over time. More importantly, transplantation of cSPC clones decreased infarct size and increased ejection fraction twelve weeks later compared to uninjected controls[148].

While these studies established the cardiac progenitor properties of isolated cSPCs *in vitro* and after transplantation into the heart, further studies have also demonstrated the ability of endogenous cSPCs to respond to cardiac injury. Following cryoinjury in mice, the number of cSPCs increases three-fold and slowly decreases over the next two weeks to levels that are still elevated compared to baseline numbers. The increase in cSPCs was attributed to proliferation of residential cSPCs with no contribution from the bone marrow compartment. In another model of cardiac injury, permanent ligation of the left

coronary artery resulted in a significant decrease in the number of cSPCs one day after MI with subsequent recovery of cSPC number primarily attributed to proliferation of residential cSPCs with a small number coming from the bone marrow. In a human study, cSPCs were quantified histologically by identifying $Abcg2^{+}$ $CD31^{-}$ cells in samples from non-failing ischemic heart disease, dilated cardiomyopathy, and valvular disease patients[159]. They found that the number of $Abcg2^{+}$ $CD31^{-}$ cells were higher in ischemic heart disease patients compared to other heart disease patients suggesting that the cardiac environment in non-failing, ischemic heart disease stimulates cSPC proliferation like the environment of the cryoinjured heart[159].

There may be specific factors in the injured heart that activate cSPCs. Following ischemic injury, cardiac remodeling can alter the stiffness of the myocardium. Substrate elasticity has been shown to affect the self-renewal and regenerative capacity of skeletal muscle satellite cells[160]. To see whether substrate elasticity alters the progenitor properties of cSPCs, isolated cSPCs were cultured on a “soft” matrix to simulate healthy myocardium and a “stiff” matrix to stimulate scarred myocardium[161]. Culturing cSPCs on the “stiff” matrix enhanced symmetrical cSPC proliferation, accelerated cellular aging and inhibiting cardiomyogenic differentiation when co-cultured with neonatal rat ventricular myocytes. Other factors that are released in response to cardiac injury also negatively impacted cSPCs. The levels of circulating Urotensin II increases in heart failure and hypertension. cSPCs express the receptor for Urotensin II at

the mRNA and protein levels suggesting that they may be responsive to changes in circulating levels of Urotensin II[162]. In cell culture, Urotensin II inhibits the proliferation of isolated cSPCs without altering their cardiomyocyte, endothelial cell or smooth muscle cell differentiation potential[162]. Despite this, the percent of cSPCs increased in mice that had undergone transverse aortic constriction (TAC), which results in a ten-fold higher level of circulating Urotensin II compared to sham. This increased percentage of cSPCs was further enhanced when TAC-operated mice were treated with Urantide, a Urotensin II antagonist. The authors hypothesized that other factors, like mechanical stretch, activate cSPCs but that circulating Urotensin II blocks this beneficial effects[163]. Whether Urantide treatment improved cardiac function was not determined in this study; however, it provides more evidence that the environment in the injured heart inhibits the progenitor cell properties of cSPCs.

THESIS STATEMENT

One of the main problems that prevents clinicians from effectively treating heart failure is the progressive loss of functional cardiomyocytes[12,164]. Since current therapies do not directly address this issue, different strategies are being developed to generate new cardiomyocytes in the failing heart[165,166]. Initially, isolation of *Kit*-expressing progenitor cells from the adult heart created a lot of excitement in the field of cardiac regeneration; however, subsequent studies demonstrating negligible differentiation of transplanted and endogenous c-kit^{+}

cells caused many researchers to turn their attention away from cardiac progenitor cells as a direct source of new cardiomyocytes[77,167–171]. Currently, the growing consensus is that proliferation of pre-existing cardiomyocytes gives rise to new cardiomyocytes; however, it is still not clear if this is the only source of new cardiomyocytes[102,172].

By definition, cardiac progenitor cells can give rise to both cardiomyocytes and noncardiomyocytes, which provides them with a unique advantage over proliferating cardiomyocytes as a target for regenerative therapies[173,174]. To determine whether there is a cardiac progenitor cell population in the heart that could contribute to endogenous cardiac regeneration, we utilized the side population phenotype. The side population phenotype is the ability of a small number of cells to extrude Hoechst 33342, a fluorescent DNA intercalator, out of their cytoplasm[126]. It has been shown that cells in many organs and forms of cancer that possess the side population phenotype are enriched for stem and progenitor cells [127,140]. These side population cells (SPCs) were first identified in the bone marrow in 1996 as a way to enrich for hematopoietic stem cells that can reconstitute the bone marrow compartment of lethally irradiated mice[126]. Since the identification of SPCs in the bone marrow, SPCs have been isolated from many different organs, including the heart[137,138,140].

Isolated cardiac side population cells (cSPCs) are enriched for progenitor cells that are self-renewing and multipotent in cell culture and after transplantation; however, it is unclear if the side population phenotype can be

used to enrich for endogenous cardiac progenitor cells [140,148,150,175]. Clones derived from single cSPCs can be propagated in cell culture for over ten months with preservation of their expression profile and without undergoing replicative senescence [148]. cSPCs and clones derived from cSPCs also have the ability to differentiated into cardiomyocytes, endothelial cells, smooth muscle cells and fibroblasts in cell culture or after transplantation into the injured adult heart [148,150,175,176]. Importantly, cSPCs represent a unique population of proposed progenitor cells from *Kit*-expressing cardiac progenitor cells. cSPCs do not express Kit at the mRNA or protein level, and microarray analysis demonstrated a stark contrast in expression profile between cSPCs and from *Kit*-expressing cardiac progenitor cells[146–148]. While the progenitor cell properties of isolated cSPCs are well-established, it is not known whether the side population phenotype can be used to enrich for cardiac progenitor cells in the adult heart that are involved in cardiac homeostasis and regeneration after injury.

Two ABC superfamily transporters, p-glycoprotein and ABCG2, are important for conferring the side population phenotype. They were originally studied in cancer cells because of their ability to efflux drugs extracellularly thereby conferring chemoresistance[177,178]. They have also been shown to extrude xenobiotics, hormones, and cellular metabolites out of many tissues throughout the body[179–181]. While ABCG2 is the sole regulator of the side population phenotype in bone marrow cells, both ABCG2 and p-glycoprotein contribute to the side population phenotype in cSPCs[145,182–184]. ABCG2-

expression is sufficient to confer the side population phenotype in HEK-293, Soas-2 and C2C12 cells[138,145,182,183]. Although ABCG2 and p-glycoprotein work together to confer the side population phenotype in cSPCs, their relative contributions change with age[144].

To determine whether the side population phenotype can be used to enrich for progenitor cells involved in endogenous cardiac regeneration, we generated a tamoxifen-inducible lineage-tracing mouse model driven by *Abcg2*. Bone marrow SPCs are the most well studied and have been convincingly shown to be enriched for HSCs in transplantation studies[126]. We first demonstrated that, in our mouse model, there was extensive labeling of endogenous bone marrow SPCs that gave rise to differentiated bone marrow lineages. Intestinal SPCs are not as well characterized and have only been shown to form enteroids in cell culture[139,185,186]. In our mouse model, we found there was efficient lineage-tracing of intestinal stem cells that give rise to all cell types in the intestine long-term. In the heart, we found that cSPCs were extensively labeled and enriched for a progenitor cell population that gives rise to cardiomyocytes and endothelial cells during cardiac homeostasis and in response to cardiac injury. Importantly, we found that lineage-traced progenitor cells enriched for by the side population phenotype give rise to 21% of all newly-formed cardiomyocytes in the adult heart. Our mouse model shows that the side population phenotype, identified by Abcg2 expression, can be used to enrich for endogenous stem cells in the bone marrow, intestine, and heart. More importantly, it provides evidence that an

endogenous cardiac progenitor cell population exists in the heart that is responsive to cardiac injury and can be targeted by new heart failure therapies.

Materials and Methods

Experimental Mouse Models

All animal procedures used in these studies conformed to NIH guidelines for the use laboratory animals and were approved by the University of Minnesota Institutional Animal Care and Use Committee (Protocol #: 1603-33606A). Both males and female mice were used in all experiments.

The Abcg2-driven, tamoxifen-inducible Cre ($Abcg2^{MCM/+}$) mice were newly generated for these studies. The following primers were used to genotype experimental mice for MerCreMer: wild-type forward: 5'-tcaaagtgctggtatctgtgttga-3', wild-type reverse: 5'-catgaattgaagtatccacagcaa-3', MerCreMer forward: 5'-ggcgttttctgagcatacct-3', MerCreMer reverse: 5'-ctacaccagagacggaaatcc-3'.

We generated experimental mice by cross-breeding $Abcg2^{MCM/MCM}$ mice to previously modified FVB.Cg-Gt(ROSA)26Sortm1(CAG-lacZ,EGFP)Glh/J ($R26^{GFP/GFP}$) reporter mice[169], B6.129(Cg)-Gt(ROSA)26Sortm4(ACTB-tdTomato,-EGFP)Luo/J ($R26^{mTmG/mTmG}$) reporter mice purchased from the Jackson laboratory, or B6.Cg-*Gt(ROSA)26Sortm14(CAG-tdTomato)Hze*/J ($R26^{Tom/Tom}$) reporter mice purchased from the Jackson Laboratory.

A previously published BAC transgenic Cdh5 CreERT2 mouse line was cross-bred to $R26^{GFP/GFP}$ mice[187]. Previously published Myosin Heavy Chain 7-Cre mice was cross-bred to $R26^{Tom/Tom}$ reporter mice[188]. Previously published Abcg2 knockout ($Abcg2^{-/-}$) mice were used to verify ABCG2 antibody specificity[182].

Chemical Injections

Tamoxifen: To induce Cre-mediated recombination in all tamoxifen-inducible mouse models, a Jackson Laboratory protocol was followed ("Intraperitoneal Injection of tamoxifen for Inducible Cre-Driver Lines", https://www.jax.org/research-and-faculty/tools/cre-repository/tamoxifen). Briefly, a 20 mg/ml Tamoxifen solution was prepared by dissolving tamoxifen (Sigma-Aldrich T5648) in corn oil (Sigma-Aldrich C8267) overnight at 37°C with gentle rotation. Tamoxifen solutions were stored at 4˚C and heated up for 10 minutes in a 37°C water bath prior to injections. To induce Cre-mediated recombination, mice were either given a single intraperitoneal injection of 2mgs of tamoxifen (100 µL of 20 mg/ml tamoxifen solution) or five daily intraperitoneal injections of 2mgs of tamoxifen (100 µL of 20 mg/ml tamoxifen solution).

Isoproterenol: A 50 mg/ml isoproterenol solution was prepared by dissolving isoproterenol hydrochloride (Sigma-Aldrich I5627) in 0.9% sodium chloride (Patterson Dental 07-3662632) with gentle vortexing. The freshly prepared isoproterenol solution was stored in 1 ml aliquots at -20°C. Fifteen minutes prior to isoproterenol injections, aliquots were thawed out on ice. For five consecutive days, mice were weighed and given daily 100 mg/kg injections into the subcutaneous tissue overlying their scapulae starting 72 hours after the fifth tamoxifen injection was given (Figure 15A). For vehicle controls, the same volume of 0.9% sodium chloride as isoproterenol solution they would have been given based on their weight was injected subcutaneously.

5-Ethynyl-2'-deoxyuridine (EdU): A 12.5 mg/ml EdU solution was freshly prepared for each experiment by dissolving EdU (Carbosynth NE8701) in 0.9% sodium chloride (Patterson Dental 07-3662632) with vigorous vortexing. EdU solutions were stored at 4˚C and heated up for 30 minutes in a 37°C water bath prior to injections. For the co-injection EdU strategy, 8-week-old mice $Abcg2^{MCM/+}$ $R26^{GFP/+}$ mice were given seven consecutive daily intraperitoneal injections of 2.5 mgs of EdU (200 µL of 12.5 mg/ml EdU solution) starting on the same day as the first tamoxifen injection (Figure 18A). For the sequential EdU injection strategy, 9-week old mice were given seven consecutive daily intraperitoneal injections of 2.5 mgs of EdU starting 72 hours after the fifth tamoxifen injection (Figure 19A).

Myocardial Ischemia Surgery

To induce myocardial ischemic injury in our mouse model, a previously described method for permanently ligating the left coronary artery was followed.[189] Sham or MI surgeries were performed 72 hours after the fifth tamoxifen injection was given (Figure 13A). First, mice were anesthetized with 3% isofluorane, endotracheally intubated and switched to 2.5% isofluorane, which they were maintained on for the remainder of the surgery. To expose the heart, a thoracotomy was performed through the 2^{nd}, 3^{rd} and 4^{th} left ribs. The left coronary artery (LCA) was permanently sutured closed as close as possible to the left atrial appendage using a 7-0 silk suture (Ethicon K809H). Successful ligation of the LCA was confirmed by visualizing blanching of the myocardium

distal to the suture. Finally, the musculature and overlying skin were sutured closed in sequential layers. Mice recovered in new cages warmed with heating pads. For sham operations, all the same steps were followed except for suturing of the LCA. For pain management, mice were given subcutaneous buprenorphine SR-LAB (Zoopharm) injections 15 minutes prior to the start of surgery. Throughout all surgeries, aseptic technique was followed.

Isolation and Flow Cytometric Analysis of Bone Marrow Side Population cells (bmSPCs) and Differentiated Lineages

A previously published protocol for bmSPC and lineage marker analysis was used.[190] A suspension of bone marrow cells was created from bone marrow flushed out of bilateral femora and tibiae of each mouse. For side population analysis, an aliquot of the bone marrow suspension was incubated with 5 μg/ml Hoechst 33342 (Thermo Fisher Scientific H1399) for 90 minutes at 37°C. As a negative control, another aliquot was incubated with both 5 μg/ml Hoechst 33342 and 50 μM verapamil (a non-specific ABC transporter inhibitor, Sigma Aldrich V4629) for 90 minutes at 37°C. For LSK analysis, Hoechst 33342-stained cells were then stained with biotinylated bone marrow lineage antibody panel (BD Pharmingen 559971) followed by staining with streptavidin conjugated to Alexa Fluor™ 647 (Invitrogen S21374), α-Sca-1 PE antibody (BD Biosciences 553108) and α-Kit APC antibody (BD Biosciences 553356). For bone marrow lineage analysis, aliquots of bone marrow suspension were stained with either α-CD3ε

biotin, α-CD11b biotin, α-CD45R biotin, α-Ly6G and Ly6C biotin or α-Ter119 biotinylated antibodies (BD Pharmingen 559971) followed by staining with streptavidin conjugated to Alexa Fluor™ 647 (Invitrogen S21374). For live cell/dead cell discrimination, all samples were stained with propidium iodide (Sigma Aldrich P4170) at a final 2 µg/ml concentration. BmSPCs and differentiated bone marrow lineage data were acquired with the MoFlo XDP flow cytometer cell sorter (Beckman Coulter Life Sciences) and analyzed with the accompanying Summit™ software (Beckman Coulter Life Sciences).

Bone Marrow Transplantation

To generate bone marrow chimera mice, irradiated Myh7-Cre $R26^{Tom/+}$ mice were transplanted with hematopoietic stem cells (HSCs) isolated from $Abcg2^{MCM/+}$ $R26^{GFP/+}$ mice. Myh7-Cre $R26^{Tom/+}$ mice were conditioned with 11.0 Gy total body irradiation one day prior to HSC transplantation. HSCs were isolated from bone marrow harvested from $Abcg2^{MCM/+}$ $R26^{GFP/+}$ mice that had not been previously injected with tamoxifen using a commercial kit (Stem Cell Technologies 19756A), $1x10^6$ HSCs were injected (via tail vein) into the systemic circulation of irradiated Myh7-Cre $R26^{Tom/+}$ mice. After ten weeks, bone marrow chimeric mice injected with tamoxifen to induce Cre-mediated recombination (Figure 11A). Bone marrow and all organs were harvested four weeks after the fifth tamoxifen injection for bmSPC, differentiation bone marrow lineages, and histological analysis.

Isolation and Flow Cytometric Analysis of cSPCs and Noncardiomyocyte Lineages

A previously published protocol for cSPC and noncardiomyocyte analysis was used.[191] Excised hearts were flushed with 10 mls of ice-cold PBS, minced with razor blades into a slurry and digested in a 2.4 U/ml Dispase II (Roche 04942078001), 0.1% Collagenase B (Roche 11088815001) and 2.5 mM calcium chloride solution for 30 minutes at 37°C. Next, the digestion solution was triturated and strained through a 40 μm cell strainer to generate a single cell suspension of noncardiomyocytes. For side population analysis, an aliquot of noncardiomyocytes was incubated with 1.5 μg/ml Hoechst 33342 (Thermo Fisher Scientific H1399) for 90 minutes at 37°C. As a negative control, another aliquot was incubated with both 5 μg/ml Hoechst 33342 and 50 μM verapamil (Sigma Aldrich V4629) for 90 minutes at 37°C. Next, Hoechst 33342-stained cells were then stained with α-CD31 APC (BD Biosciences 551262) and α-Sca1 PE (BD Biosciences 553108) antibodies. For noncardiomyocyte analysis, aliquots of noncardiomyocytes were stained with either α-CD90 APC (BD Biosciences 553007), α-CD45 PE (Biolegend 103106) or α-CD31 APC (BD Biosciences 551262). For live cell/dead cell discrimination, all samples were stained with propidium iodide (Sigma Aldrich P4170) at a final 2 μg/ml concentration. cSPC data was acquired with the MoFlo XDP flow cytometer cell sorter (Beckman Coulter Life Sciences) and analyzed with the accompanying Summit™ software

(Beckman Coulter Life Sciences). Noncardiomyocyte lineage analysis was carried out using the BD FACSAria II flow cytometer cell sorter (BD Biosciences) and analyzed with the FlowJo v10 software application.

Histological Tissue Processing

Harvested tissues are washed in PBS and fixed in 4% paraformaldehyde (Electron Microscopy Sciences C993M31) diluted v/v in PBS for 3 hours at room temperature with gentle rocking. After another wash in PBS, fixed tissues were incubated in 30% sucrose (w/v in PBS) overnight at 4°C. The next day, tissues were trimmed and embedded in O.C.T. (Thermo Fisher Scientific 14-373-65). Hearts were cut and embedded in a four-chamber orientation allowing visualization of outflow tracts and all four chambers of the heart. O.C.T. blocks were frozen using a slurry of dry ice and Isopentane and cut into 5 µm-thick sections that were mounted on Fisherbrand Superfrost Plus Microscope slides (Fischer Scientific 12-550-15). All samples were stored at -80˚C.

Histological Stains, Image Acquisition and Analysis

Cardiac cryosections were stained with antibodies outlined in Supplementary Table 1. Air-dried slides were rehydrated and permeabilized with 0.1% Triton X-100 (v/v in PBS), blocked in antibody-specific blocking solution for an hour at room temperature, and stained with primary antibody solutions overnight at 4°C. The next day, slides were washed in PBS, stained with

secondary antibodies and washed again in PBS. Coverslips were mounted on slides with Vectashield mounting medium (Vector Laboratories H-1400). A commercially available kit was used to stain nuclei for EdU incorporation (Click-iT Plus EdU Alexa Fluor Imaging Kit, Thermo Fisher Scientific C10638). GFP-labeling of cardiomyocytes was quantified using histological sections stained with Wheat Germ Agglutinin conjugated to Texas Red-X (Life Technologies W21405). Ten 200X images were taken throughout the left ventricle with the Zeiss Axio Imager M1 Upright Microscope and GFP-labeling of cardiomyocytes was quantified as the percent of GFP^+ cardiomyocytes as a percentage over total cardiomyocytes using FIJI image processing software.[192] Nuclei in all Cryosections were counterstained with DAPI (Thermo Fisher Scientific D3571, 50 ng/ml). All fluorescent images, except $Abcg2^{MCM/+}$ $R26^{mTmG/+}$ images, were taken with the Zeiss Axio Imager M1 Upright Microscope. Fluorescent images of $Abcg2^{MCM/+}$ $R26^{mTmG/+}$ sections stained with DAPI were obtained using the Nikon C2 and Nikon A1 confocal microscopes at the University Imaging Centers, University of Minnesota.

Cryosections of MI and sham-operated hearts were stained with Sirius Red Fast Green. Air-dried cryosections were fixed with Bouin's fixative (Sigma Aldrich HT10132) at 55°C for 1 hour, stained with 0.4% Fast Green (Sigma Aldrich F7252, v/v in picric acid) for 10 min at room temperature and then 0.1% Sirius Red (Sigma Aldrich 365548, v/v in picric acid) for 30 minutes at room temperature. After each step, cryosections were washed with water to remove

excess dye. Coverslips were mounted onto slides with Permount Mounting Medium (Fischer Scientific SP15-500). Whole cryosections were imaged using the Huron Technologies TISSUEscope LE brightfield slide scanner at the University Imaging Center at the University of Minnesota. Images were viewed using the free HuronViewer software (Huron Digital Pathology, http://www.hurondigitalpathology.com/resource/download-huronviewer/).

Isolation, Imaging, and Quantification of Adult Cardiomyocytes

A previously described protocol was used to isolate adult cardiomyocytes.[193] First, the heart is excised for the chest cavity and cannulated through the aorta on a Langendorff perfusion setup that is gravity dependent. The heart is perfused with a digestion buffer with 2.4 mg/ml Collagenase type 2 (Worthington LS004176) for approximately 9 minutes, removed from the Langendorff setup, cut into ten to twelve pieces with a razor blade and gently pipetted up and down to release single cardiomyocytes. Cardiomyocytes are then pelleted out of solution by centrifugation at 19 g for 5 min. One individual counted the total number of rod-shaped cardiomyocytes, which are the live, healthy cardiomyocytes, using a Fuchs-Rosenthal counting chamber (Electron Microscopy Sciences 63512-10) for each heart. Another individual blinded to the experimental source of the isolated cardiomyocytes, counted the number of GFP-labelled rod-shaped cardiomyocytes using a Zeiss Axio Observer Z1 Inverted

Microscope. Quantification of GFP-labeled cardiomyocytes was calculated as the percent of total rod-shaped cardiomyocytes that are labeled with GFP.

To stain adult cardiomyocytes for Troponin T and EdU incorporation, isolated adult cardiomyocytes were fixed with 4% paraformaldehyde diluted in PBS (Electron Microscopy Sciences C993M31, v/v) for 5 minutes. For Troponin T staining, fixed cardiomyocytes were washed in PBS, permeabilized with 0.1% Triton X-100 diluted in PBS (v/v) for 10 minutes at room temperature, blocked in 5% normal goat serum (Vector Laboratories S-1000, v/v in PBS) for an hour at room temperature, incubated with a troponin T antibody overnight at 4^{o}C washed in PBS the next day, and incubated with Donkey a-mouse antibody Alexa Fluor 568 (Invitrogen A10037, Supplementary Table 2 For EdU staining, a commercially available kit was used (Click-iT Plus EdU Alexa Fluor Imaging Kit, Thermo Fisher Scientific C10638). EdU-stained cardiomyocytes were then stained for GFP using the same protocol described above for Troponin T staining (Supplementary Table 2), Nuclei of all fixed isolated cardiomyocytes were counterstained with DAPI. All images of stained cardiomyocytes were acquired using both the Zeiss Axio Observer Z1 Inverted Microscope and the Zeiss Axio Imager M1 Upright Microscope.

Adult Cardiomyocyte Cytosolic Calcium ($_{c}Ca^{2+}$) Transient Recordings

A previously described protocol was used to record $_{c}Ca^{2+}$ transients in Tom+ and Tom- cardiomyocytes with and without isoproterenol stimulation.[194]

Isolated adult cardiomyocytes were incubated with 1 μM Fluo-4 AM (Invitrogen F14201) in a sealed 37°C chamber mounted on a Zeiss Axio Observer Z1 Inverted Microscope equipped with Sutter DG4 plus: excitation and Sutter Lambda 10-2: emission illumination systems, physiological Tyrode's solution with 2 mM $CaCl_2$ was perfused through the chamber, and cardiomyocytes were paced at 1 Hz. $_cCa^{2+}$ transients were recorded using the Photometrics Evolve Delta EMCCD camera and pCLAMP 10 software (Molecular Devices) was used to analyze the data collected. After two minutes of continuous recording, the physiological Tyrode's solution with containing 2 mM $CaCl_2$ was changed to a 100 nM isoproterenol physiological Tyrode's solution with 2 mM $CaCl_2$. Background fluorescence was subtracted from $_cCa^{2+}$ fluorescence measurements. Normalized fluorescence (F/F0) was used to evaluate changes in cytoplasmic calcium concentrations. F is the maximal peak fluorescence and F0 is unstimulated fluorescence averaged over 50 ms prior to pacing stimuli.

Statistics

All results are reported as mean ± standard deviation except for adult cardiomyocyte $_cCa^{2+}$ transient data, which are reported as mean ± standard error of the mean. For comparison of two groups, student's t-tests were performed. For comparisons among multiple groups, 2-way ANOVA was used. A *p*-value less than 0.05 was considered statistically significant. Statistical analysis was carried out using excel and prism.

Results

Lineage-tracing strategy efficiently labels Abcg2-expressing cells throughout the body.

We evaluated the ability of our tamoxifen-inducible, lineage-tracing mouse model to label *Abcg2*-expressing cells in the kidney, intestines, and liver. ABCG2 is expressed at the apical membranes of renal proximal tubule epithelium, at the brush border of ileal epithelium, and at the canalicular membranes of hepatocytes[195–197]. To confirm this reported ABCG2-expression pattern, we stained renal, ileal and hepatic cryosections from Abcg2$^{+/+}$ and Abcg2$^{-/-}$ mice using three different ABCG2 antibodies: BXP-53, BXP-9 and a polyclonal anti-ABCG2 antibody. We found that the BXP-53 monoclonal antibody consistently and specifically stained cells known to express ABCG2 in renal, ileal and hepatic sections from Abcg2$^{+/+}$ mice but not from Abcg2$^{-/-}$ mice (Figure 1A). In our hands, the BXP-9 monoclonal antibody and a rabbit polyclonal anti-ABCG2 antibody did not specifically or consistently stain ABCG2-expressing cells (data not shown). To determine the specificity of our tamoxifen-inducible, lineage-tracing mouse model, we evaluated labeling of ABCG2-expressing cells in tamoxifen-injected Abcg2$^{MCM/+}$ R26$^{GFP/+}$ mice. We imaged the native fluorescence of GFP in renal, ileal, and hepatic cryosections and observed labeling of cells known to express ABCG2 (Figure 1B). There was no GFP fluorescence in cryosections from vehicle-injected Abcg2$^{MCM/+}$ R26$^{GFP/+}$ mice (Figure 1B).

The side population phenotype enriches for endogenous hematopoietic

stem cells that give rise to differentiated bone marrow lineages.

The side population phenotype was first identified in the bone marrow where it was shown to enrich HSCs without using cell surface markers[126]. The stem cell properties of bone marrow side population cells are the most well characterized of any side population cell type in cell culture and after transplantation. However, whether the side population phenotype can be used to identify endogenous stem cells in the bone marrow is unclear. We evaluated labeling of endogenous side population cells in the bone marrow of tamoxifen-injected Abcg2$^{MCM/+}$ R26$^{GFP/+}$ mice (Figure 2A). Negative control samples incubated with Verapamil, which blocks ABC-transporter efflux, were used to ensure accurate identification of bone marrow side population cells (Figure 2B). Sixty-six percent of bone marrow side population cells were labeled with GFP (Figure 2C). Since LSK cells within the side population gate represent a more potent subpopulation of LT-HSCs, we wondered whether LSK cells within the side population gate would be differentially labeled compared to all LSK cells. Interestingly, we found that a higher percentage of LSK cells within the side population gate were labeled compared to all LSK cells, indicating an enrichment for GFP labeled LSK cells by the side population phenotype (Figure 2D - F).

To assess whether the side population phenotype enriches for hematopoietic stem cells in the bone marrow, we pulsed Abcg2$^{MCM/+}$ R26$^{GFP/+}$ mice with tamoxifen and then evaluated GFP-labeling of differentiated bone marrow lineages before and after a four-week chase period (Figure 3A). We

found that Ter119^{+} erythroid cells were extensively labeled with GFP before and after the four-week chase period with 91.2 ± 3.1% and 71.5 ± 5.4% labeled with GFP at Week 9 and Week 13, respectively (Figure 3B and 3C). This high level of labeling was not surprising since it has been shown that Ter119^{+} erythroid cells do express *Abcg2.* For monocytes/macrophages, granulocytes, T cells and B cells that do not express *Abcg2*, there was a significant increase in GFP-labeling over the four-week chase period (Figure 3B and 3C). We found a three-fold increase in labeling of granulocytes from 23.1 ± 5.6% to 69.1 ± 5.2%, of monocytes/macrophages from 20.8 ± 6.2% to 68.7 ± 5.7%, and of B cells from 16.3 ± 7.3% to 50.7 ± 5.7%. Labeling of T cells increased almost 2-fold from 15.8 ± 4.1% to 26.2 ± 6.4% over the four-week chase period. No bone marrow lineages were labeled in vehicle-injected Abcg2$^{MCM/+}$ R26$^{GFP/+}$ mice indicating no aberrant nuclear translocation of MerCreMer fusion proteins in the absence of tamoxifen (Figure 3B). Taken together, the bone marrow labeling data provides evidence that the side population phenotype enriches for endogenous HSCs that contribute to bone marrow homeostasis.

The side population phenotype enriches for endogenous, long-term intestinal stem cells that give rise to differentiated intestinal lineages.

Side population cells have been isolated from the small intestine; however, their stem cell properties have not been well established[139,185,186]. Small intestine side population cells can differentiate into enteroid bodies in cell culture

that contain four differentiated intestinal lineages[185]. Because of the limited characterization of side population cells in the intestine, we wanted to see whether our side population lineage-tracing model could identify an endogenous stem cell population in the murine ileum. We performed a short-term lineage tracing experiment by evaluating GFP-labeling in $Abcg2^{MCM/+}$ $R26^{GFP/+}$ mice 72 hours and four weeks after a single injection of tamoxifen (Figure 4A). At the 72-hour time point, the intestinal epithelium was extensively labeled with sparse labeling at the bottom of the intestinal crypts (Figure 4B). Four weeks later, there was labeling of the villi in a striated manner extending from the bottom of crypts to the tips of willi (Figure 4C). We also performed long-term lineage-tracing experiments (Figure 5A). After a five-month chase period, we still observed labeling in a classic stem cell pattern extending from the base of the intestinal crypt to the tips of villi (Figure 5B). Since the intestinal epithelium turns over every 2 – 4 days in the ileum, these two experiments highlight the role of endogenous intestinal stem cells labeled in our lineage-tracing mouse model[198,199].

The side population phenotype enriches for endogenous progenitor cells that give rise to endothelial cells and cardiomyocytes in the adult heart.

Next, we assessed whether side population cells isolated from the heart were labeled in our lineage-tracing mouse model. This was an important step because, unlike bone marrow side population cells where it has been shown that

Abcg2 is solely responsible for the side population phenotype, both Abcg2 and p-glycoprotein are responsible for the side population phenotype in the adult heart. In tamoxifen-injected $Abcg2^{MCM/+}$ $R26^{GFP/+}$ mice, cSPCs accounted for 1.5 ± 0.87% of isolated non-cardiomyocytes in line with previously published studies (Figure 6A). We also ensured accurate identification of cSPCs using negative control samples incubated with Verapamil (Figure 6B). Of the cSPCs identified, 73.2 ± 9.8% were labeled with GFP (Figure 6C).

To assess whether the side population phenotype enriches for an endogenous cardiac progenitor cells population that gives rise to non-cardiomyocytes in the adult heart, we pulsed $Abcg2^{MCM/+}$ $R26^{GFP/+}$ mice with tamoxifen and then evaluated GFP-labeling of non-cardiomyocytes before and after a four-week chase period (Figure 7A). Lineage-tracing of endothelial cells was assessed using immunofluorescent staining and flow cytometric analysis for $CD31^{+}$ cells from tamoxifen-injected $Abcg2^{MCM/+}$ $R26^{GFP/+}$ mice (Figure 7B and 7C). Cardiac endothelial cells are known to express Abcg2, so we were not surprised to find extensive GFP-labeling of endothelial cells at Week 9[200]. Interestingly, over the four-week chase period, we found a significant increase in GFP-labeling of endothelial cells from 85.2 ± 3.0% (n=4) to 92.6 ± 2.0% (Figure 7D). Immunofluorescent staining and flow cytometric analysis for fibroblasts with Vimentin and CD90.2 did not show any significant change in GFP-labeling with 15.9 ± 2.7% of fibroblasts labeled at Week 9 and 20.0 ± 3.3% labeled at Week 13 (Figure 7E – 7G). Similarly, the percent of labeled $CD45^{+}$ cells did not change

significantly over the four-week chase period from 2.4 ± 1.5% labeled at Week 9 to 5.0 ± 3.1% labeled at Week 13 (Figure 7H – 7J). Smooth muscle cells, pericytes, and lymphatic vessels were occasionally labeled with no measurable increase in labeling over time (Figure 7K – 7M).

To assess whether the side population phenotype enriches for an endogenous cardiac progenitor cells population that gives rise to cardiomyocytes in the adult heart, we pulsed Abcg2$^{MCM/+}$ R26$^{GFP/+}$ mice with tamoxifen and then evaluated GFP-labeling of isolated adult cardiomyocytes before and after a four-week chase period (Figure 8A). In cardiac sections and isolated adult cardiomyocytes stained with Troponin, we were surprised to find labeling of a small number of cardiomyocytes (Figure 8B and 8C). When we measured GFP-labeling of cardiomyocytes before and after the four-week chase period, we measured close to a five-fold increase in GFP-labeling from 0.17 ± 0.1% to 0.84 ± 0.2% (Figure 8D and 8E).

Since we observed GFP-labeling of cardiomyocytes at Week 9, we were concerned that cardiomyocyte labeling arose from active *Abcg2* expression in adult cardiomyocytes. First, we verified that adult cardiomyocytes do not express ABCG2 with immunohistochemical staining of cardiac sections with the BXP-53 monoclonal antibody. We observed specific labeling of cardiac endothelial cells with no labeling of cardiomyocytes (Figure 9A and 9B). To more rigorously assess whether cardiomyocyte labeling arises from *Abcg2*-expression in cardiomyocytes, we measured cardiomyocyte labeling in histological sections

from Abcg2$^{MCM/+}$ R26$^{GFP/+}$ mice 72 hours and four weeks after a single, 2mg injection of tamoxifen (Figure 9C). In this experiment, only 0.03% ± 0.03% of cardiomyocytes were labeled with GFP at the 72-hour time point with a substantial increase to 0.74 ± 0.36% four weeks later (Figure 9D).

To assess how lineage-traced cardiomyocytes function compared to unlabeled cardiomyocytes, we compared cytoplasmic calcium ($_cCa^{2+}$) dynamics of isolated adult cardiomyocytes at rest and in response to isoproterenol stimulation in tamoxifen-injected Abcg2$^{MCM/+}$ R26$^{Tom/+}$ mice (Figure 9A). There was no significant difference in $_cCa^{2+}$ dynamics between labeled and unlabeled cardiomyocytes indicating that lineage-traced cardiomyocytes function normally and respond appropriately to adrenergic stimulation (Figure 9B – 9G).

Because our mouse model also lineage-traces HSCs, we evaluated the contribution of labeled bone marrow cells to cardiomyocyte labeling. Some studies have demonstrated the ability of endogenous bone marrow cells to give rise to cardiomyocytes very infrequently through fusion of bone marrow cells with pre-existing cardiomyocytes instead of direct differentiation of bone marrow cells into cardiomyocytes[100,201]. We generated chimeric Myh7$^{Cre/+}$ R26$^{Tom/+}$ mice with Abcg2$^{MCM/+}$ R26$^{GFP/+}$ bone marrow mice by transplanting LSK cells isolated from Abcg2$^{MCM/+}$ R26$^{GFP/+}$ mice into irradiated Myh7$^{Cre/+}$ R26$^{Tom/+}$ mice. After waiting ten weeks for reconstitution of the bone marrow niche, we injected chimeric mice with tamoxifen and evaluated bone marrow and cardiomyocyte labeling after a four-week chase period (Figure 11A). Bone marrow labeling in tamoxifen-injected

chimeric mice was comparable to bone marrow labeling in Abcg2$^{MCM/+}$ R26$^{GFP/+}$ mice at Week 13, confirming bone marrow reconstitution and lineage-tracing of endogenous bmSPCs (Table 1). Histological analysis of ventricular cardiomyocyte labeling revealed that 0.02 ± 0.03% of cardiomyocytes were labeled with GFP. These GFP-labeled cardiomyocytes also expressed tdTomato indicating that they arose from fusion of GFP-labeled bone marrow cells with pre-existing tdTomato-labeled cardiomyocytes (Figure 11B and 11C). Notably, one GFP-only cardiomyocyte was found in the atrium of one out of five tamoxifen-injected bone marrow chimeric mice (Figure 11D). This transplantation study demonstrates that lineage-tracing of bone marrow cells rarely contribute to cardiomyocyte labeling consistent with previously published studies[100,201].

Cell culture and *in vivo* lineage-tracing studies have demonstrated the ability of cardiac endothelial cells to give rise to cardiomyocytes through fusion and dedifferentiation into a progenitor-like cell before redifferentiating into cardiomyocytes [202,203]. To assess whether GFP-labeled cardiac endothelial cells contribute to cardiomyocyte-labeling with the lineage-tracing strategy we used, we injected BAC-Cdh5$^{CreER/+}$ R26$^{GFP/+}$ mice, tamoxifen-inducible endothelial cell lineage-tracing mouse model, with tamoxifen and evaluated endothelial cell and cardiomyocyte labeling four weeks later (Figure 12A) [187]. Flow cytometric analysis revealed that 91.8 ± 5.1% of CD31^{+} cells were labeled with GFP (Figure 12B). There was also minimal labeling of bone marrow side population cells, LSK cells and differentiated lineages (Table 2). Despite efficient labeling of cardiac

endothelial cells, no GFP-labeled cardiomyocytes could be identified with histological analysis of cardiac sections stained for Troponin (Figure 12C).

Taken together, our findings in these studies demonstrate that the side population phenotype enriches for an endogenous progenitor cell population that gives rise to functional cardiomyocytes in the adult heart. Importantly, these progenitor cells do not originate from the bone marrow niche or from endothelial cells.

Cardiac injury enhances the contribution of endogenous cardiac side population cells to cardiomyocytes.

Endogenous cardiac regeneration is activated following myocardial ischemic injury[88,102,140,175]. To assess how the endogenous cardiac progenitor cells lineage-traced in our model respond to MI injury, we permanently ligated the left coronary artery in tamoxifen-injected Abcg2$^{MCM/+}$ R26$^{GFP/+}$ mice and analyzed GFP-labeling of cardiomyocytes and noncardiomyocytes four weeks later (Figure 13A - 13C). We measured a three-fold higher level of cardiomyocyte labeling in MI-operated mice compared to sham-operated mice (Figure 13D and 13E). There was no significant difference in cardiomyocyte labeling between the border zones and remote regions (Figure 13C). We also assessed GFP labeling of noncardiomyocytes following MI injury and found widespread labeling of cardiac endothelial cells and sparse labeling of fibroblasts and hematopoietic cells (Figure 14A – 14C).

Next, we assess the effect of acute adrenergic injury on the endogenous cardiac progenitor cells lineage-traced in our model. We modified a previously described protocol that had been shown to cause transient cardiomyocyte damage without stimulating endogenous cardiac regeneration[107,204,205]. We gave five daily 100mg/kg isoproterenol injections in tamoxifen-injected Abcg2$^{MCM/+}$ R26$^{GFP/+}$ mice. There was a more moderate increase in cardiomyocyte labeling with a 60% higher level of labeling in isoproterenol-injected mice compared to their saline-injected controls (Figure 15). These data show that the endogenous cardiac progenitor cells lineage-traced in our model are responsive to different forms of cardiac injury.

Endogenous cardiac progenitor cells identified by the side population phenotype give rise to newly-formed cardiomyocytes.

In the cardiac regeneration literature, there are examples of cardiomyocyte differentiation and fusion occurring with different cell types. To determine the contribution of each of these cellular mechanisms to lineage-traced cardiomyocytes, we cross-bred the R26$^{mTom\text{-}mGFP/mTom\text{-}mGFP}$ reporter mouse line to our Abcg2-driven lineage-tracing mouse model to generate Abcg2$^{MCM/+}$ R26$^{mTom\text{-}mGFP/+}$ mice. In these mice, we can identify cardiomyocytes that arise from fusion from those that arise from differentiation of an endogenous progenitor cell population. In these mice, membrane-bound tdTomato (mTom) is expressed until cre-mediated recombination excises the mTom DNA resulting in the

expression of membrane-bound GFP. If cardiomyocytes arise from direct differentiation of Abcg2-expressing cells, these cardiomyocytes will only express GFP. If cardiomyocytes arise from fusion of Abcg2-expressing cells with pre-existing $mTom^{+}$ cardiomyocytes, then these cardiomyocytes will express both mTom and mGFP. We performed the same baseline tamoxifen pulse-chase experiments as previously used in $Abcg2^{MCM/+}$ $R26^{GFP/+}$ mice and evaluated the portion of cardiomyocytes that expressed mGFP alone and mGFP with mTom at Week 9 and Week 13 (Figure 16A). At Week 9, all cardiomyocytes expressed both mTom and mGFP; however, at Week 13, 85.3 ± 3.1% of mGFP+ cardiomyocytes also expressed mTom while 14.6 ± 3.1% of mGFP+ cardiomyocytes did not (Figure 16B and 16C). This indicated to us, that while the majority of lineage-traced cardiomyocytes arose from fusion of Abcg2-expressing cells with pre-existing cardiomyocytes; there was a portion of them that may have originated from an endogenous progenitor cell population.

To accurately identify newly formed cells that arise from lineage-traced cells, we injected (5-Ethynyl-2'-deoxyuridine) EdU and tamoxifen into $Abcg2^{MCM/+}$ $R26^{GFP/+}$ mice and evaluated EdU incorporation in cardiomyocytes and non-cardiomyocytes four weeks later (Figure 17A). EdU is a thymidine analog that is incorporated into newly synthesized DNA. We identified EdU incorporation in GFP-labeled noncardiomyocytes and cardiomyocytes on histological sections (Figure 17B and 17C). There were some cells with EdU incorporation that were not labeled with GFP as well (Figure 17C). To more accurately identify

cardiomyocytes with EdU incorporation, we isolated cardiomyocytes and stained with EdU and DAPI. We found that 25% of mononucleated EdU^+ cardiomyocytes are GFP-labeled while only 6.3% of binucleated EdU^+ cardiomyocytes were labeled with GFP (Supplemental Figure 2). There was no difference in nucleation of GFP-labeled and unlabeled cardiomyocytes (Figure 18).

We also used a sequential EdU strategy, where we started EdU injections in $Abcg2^{MCM/+}$ $R26^{GFP/+}$ mice 72 hours after the last tamoxifen injection (Figure 19A). Three weeks after the last EdU injection, we isolated adult cardiomyocytes and evaluated nucleation and EdU incorporation. We measured EdU incorporation of 0.00123% of all adult cardiomyocytes. This comes out to an annual cardiomyocyte renewal rate of about 0.77% in line with previous publications that used N14 thymidine incorporation to approximate a yearly cardiomyocyte renewal rate of about 0.76% in adult mice. Similar to the co-injection strategy, there was an enrichment of GFP-labeled cardiomyocytes in EdU^+ cardiomyocytes. Overall GFP-labeled cardiomyocytes accounted for 21% of EdU+ cardiomyocytes and only 0.7% of all cardiomyocytes (Figure 19B - 19F). We found that 30% of mononucleated EdU+ cardiomyocytes were GFP-labeled while 16.7% of binucleated EdU+ cardiomyocytes were GFP-labeled. Additionally, the percent of mononucleated GFP+ cardiomyocytes that had EdU incorporation was higher than the percent of GFP- cardiomyocytes that had EdU incorporation (Figure 19C). The same trend was found with binucleated cardiomyocytes (Figure 19E). If we take all the data together, it demonstrated

that lineage-traced cardiomyocytes account for 21% of newly-formed cardiomyocytes in the adult heart.

ACKNOWLEDGEMENTS AND CONTRIBUTIONS

We would like to thank the following people for their specific contributions:

Yi Ren for setting-up and optimizing bone marrow and cardiac side population analysis. These studies could not have been done without all his time and effort.

Ron T. McElmurry and **Jakub Tolar** for generating the bone marrow chimeric mice for our bone marrow transplantation studies.

Jonathan P. Lambert, Sadia Mohsin, Steven R. Houser and **John Elrod** for performing and analyzing the cytosolic calcium transient studies in isolated adult cardiomyocytes.

We would also like to thank **Natsumi Nemoto, Chetana Guthikonda, Jessica Shaklee, Wuqiang Zhu, Ingrid Bender** and **John Calvert** for their assistance throughout these studies.

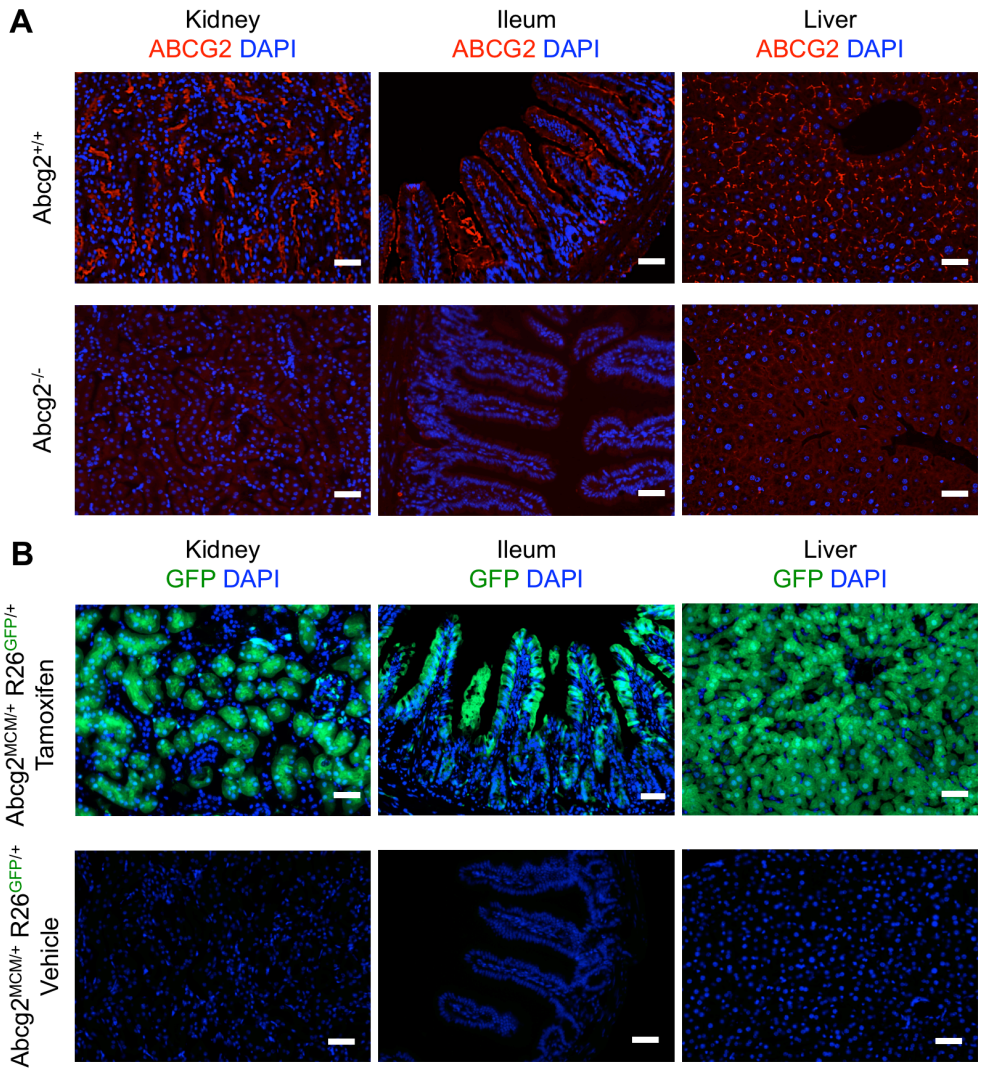

Figure 1. Efficient labeling of ABCG2-expressing cells in tamoxifen-injected Abcg2$^{MCM/+}$ R26$^{GFP/+}$ mice. (A) Representative fluorescent images of immunofluorescence staining for ABCG2 in renal, ileal, and hepatic sections from Abcg2$^{+/+}$ mice (top row) and Abcg2$^{-/-}$ mice (bottom row). **(B).** Representative fluorescent images of the native GFP fluorescence in renal, ileal, and hepatic sections from tamoxifen-injected Abcg2$^{MCM/+}$ R26$^{GFP/+}$ mice (top row) and vehicle-

injected Abcg2$^{MCM/+}$ R26$^{GFP/+}$ mice (bottom row). Nuclei are counterstained with DAPI in all images. Scale Bars: 50 μm.

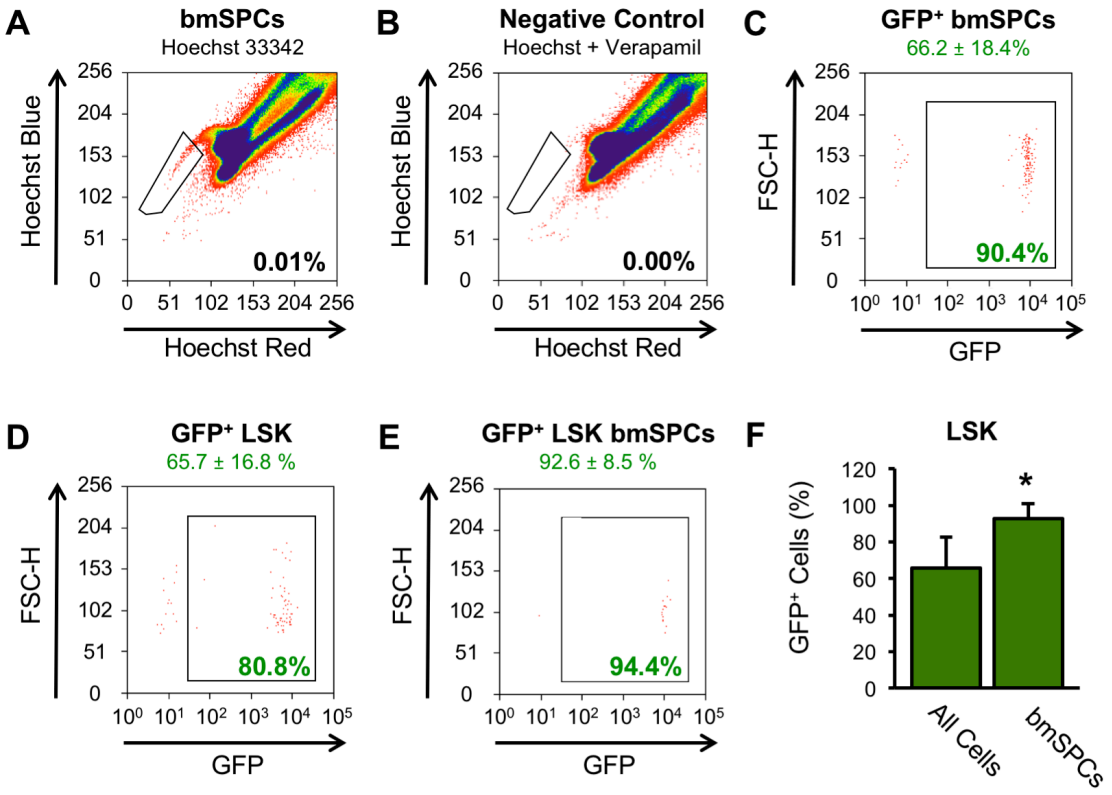

Figure 2. BmSPCs and LSK cells are extensively labeled in tamoxifen-injected Abcg2$^{MCM/+}$ R26$^{GFP/+}$ mice. (A) Representative flow cytometry plot of bmSPCs (cells inside black side population gate) identified from bone marrow of tamoxifen-injected Abcg2$^{MCM/+}$ R26$^{GFP/+}$ mice. **(B)** Corresponding flow cytometry plot of verapamil-stained, negative control for bmSPCs. **(C)** Corresponding flow cytometry plot of GFP-labeling of bmSPCs (n=6). **(D)**. Representative flow cytometry plot of GFP-labeling of all LSK cells from bone marrow of tamoxifen-injected Abcg2$^{MCM/+}$ R26$^{GFP/+}$ mice (n=5). **(E)**. Representative flow cytometry plot of GFP-labeling of LSK cells identified within the side population gate from bone marrow of tamoxifen-injected Abcg2$^{MCM/+}$ R26$^{GFP/+}$ mice (n=3) **(F)** Quantification

of GFP-labeling of LSK cells from all bone marrow cells or from bmSPCs. * $P < 0.05$, mean ± SD.

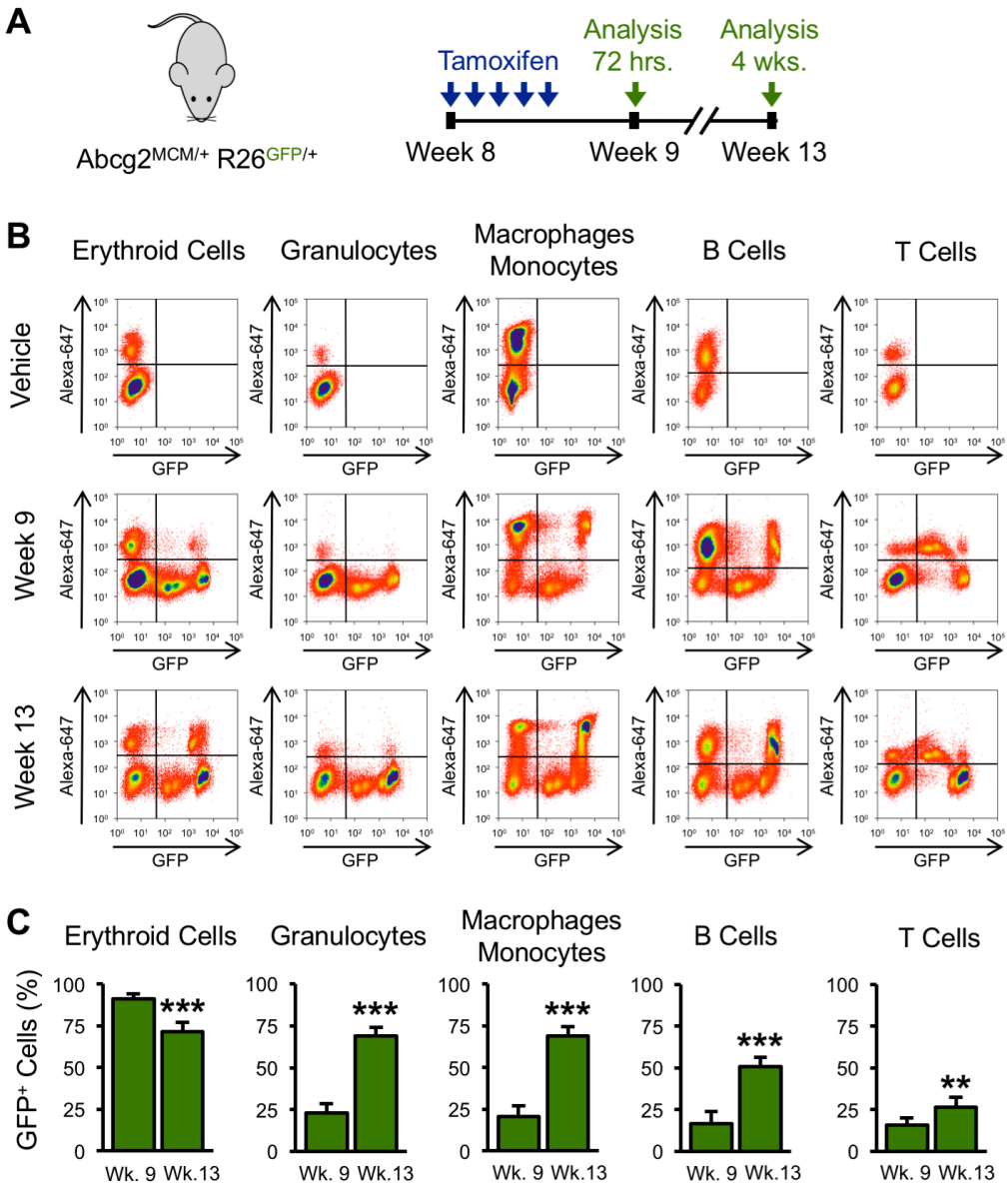

Figure 3. Endogenous, lineage-traced bmSPCs give rise to differentiated bone marrow cells *in vivo.* (A) Diagram illustrating pulse-chase timeline used to study the role of endogenous bmSPCs in Abcg2$^{MCM/+}$ R26$^{GFP/+}$ mice. The blue arrows represent single, 2-mg tamoxifen injections. The green arrows represent time points when GFP-labeling in the ileum was assessed, 72 hours and 4 weeks

after the fifth 2mg tamoxifen injection. **(B)** Representative flow cytometry plots of GFP-labeling of differentiated bone marrow lineages in vehicle-injected Abcg2$^{MCM/+}$ R26$^{GFP/+}$ mice (top row), tamoxifen-injected Abcg2$^{MCM/+}$ R26$^{GFP/+}$ mice at Week 9 (middle row) tamoxifen-injected Abcg2$^{MCM/+}$ R26$^{GFP/+}$ mice at Week 13 (bottom row). **(C)**. Analysis of GFP-labeled differentiated bone marrow lineages from tamoxifen-injected Abcg2$^{MCM/+}$ R26$^{GFP/+}$ at Week 9 and Week 13 (n=6). ** $P < 0.01$, *** $P < 0.001$, mean ± SD.

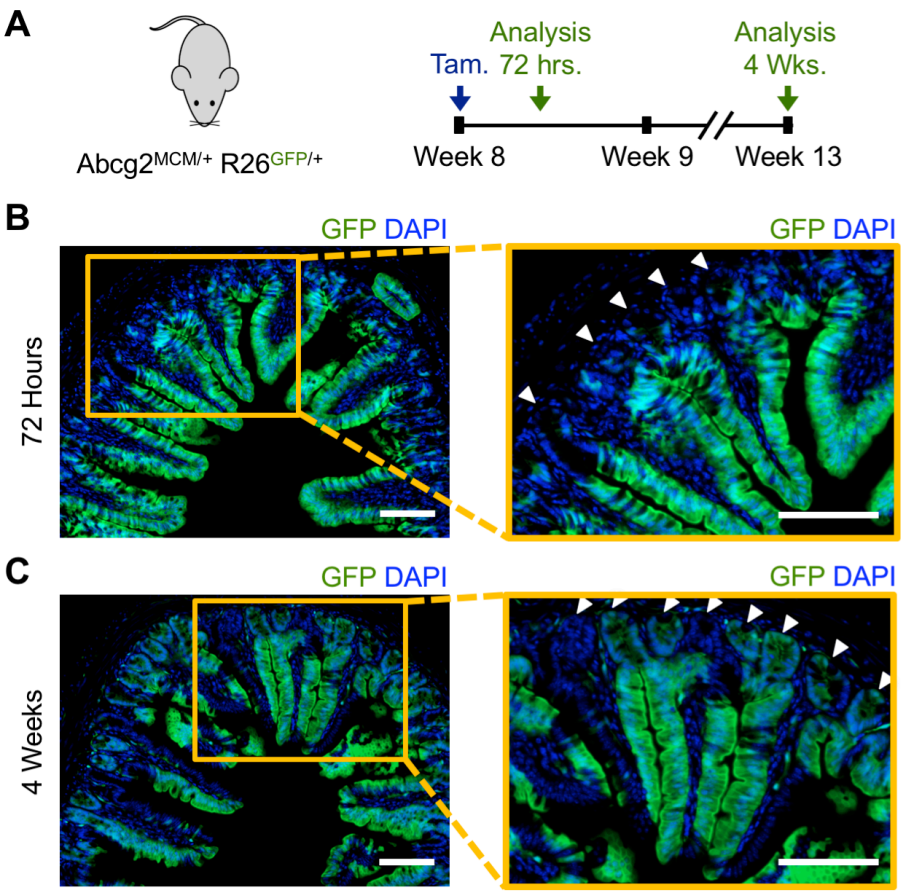

Figure 4. Short-term lineage-tracing of endogenous intestinal stem cells give rise to differentiated intestinal cells *in vivo.* (A) Diagram illustrating pulse-chase timeline used to study the role of intestinal stem cells in Abcg2$^{MCM/+}$ R26$^{GFP/+}$ mice. The blue arrow represents a single, 2-mg tamoxifen injection. The green arrows represent time points when GFP-labeling in the ileum was assessed, 72 hours and 4 weeks after a single, 2mg injection of tamoxifen. **(B)** Representative fluorescent images of the ileum harvested at the 72-hour timepoint showing the native fluorescence of GFP. The higher magnification

image to the right highlights GFP-labeling observed in ileal crypts (white arrow head). **(C)** Representative fluorescent images of the ileum harvested at the 4-week timepoint showing the native fluorescence of GFP. The higher magnification image to the right highlights GFP-labeling observed in ileal crypts (white arrow head). In all images, nuclei are counterstained with DAPI. Scale Bars: 100 μm.

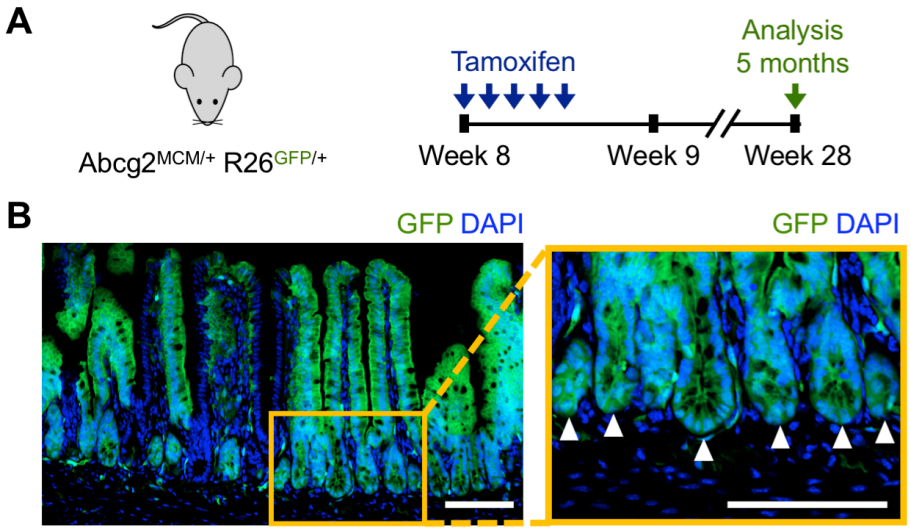

Figure 5. Long-term lineage-tracing of endogenous intestinal stem cells give rise to differentiated intestinal cells *in vivo.* (A) Diagram illustrating pulse-chase timeline used to study the long-term role of intestinal stem cells in Abcg2$^{MCM/+}$ R26$^{GFP/+}$ mice. **(B)** Representative fluorescent images of the ileum harvested at the 5-month timepoint showing the native fluorescence of GFP. The higher magnification image to the right highlights GFP-labeling observed in ileal crypts (white arrow head). In all images, nuclei are counterstained with DAPI. Scale Bars: 100 μm.

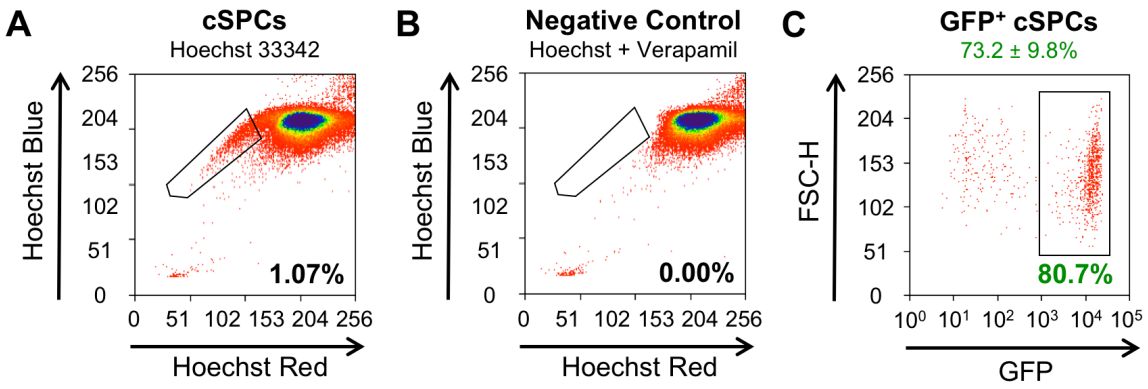

Figure 6. cSPCs are extensively labeled in tamoxifen-injected Abcg2$^{MCM/+}$ R26$^{GFP/+}$ mice. (A) Representative flow cytometry plot of cSPCs (cells inside black side population gate) identified from non-cardiomyocytes isolated from tamoxifen-injected Abcg2$^{MCM/+}$ R26$^{GFP/+}$ mice. **(B)** Corresponding flow cytometry plot of verapamil-stained, negative control for cSPCs within black side population gate. **(C)** Corresponding flow cytometry plot of GFP-labeling of cSPCs (n=7).

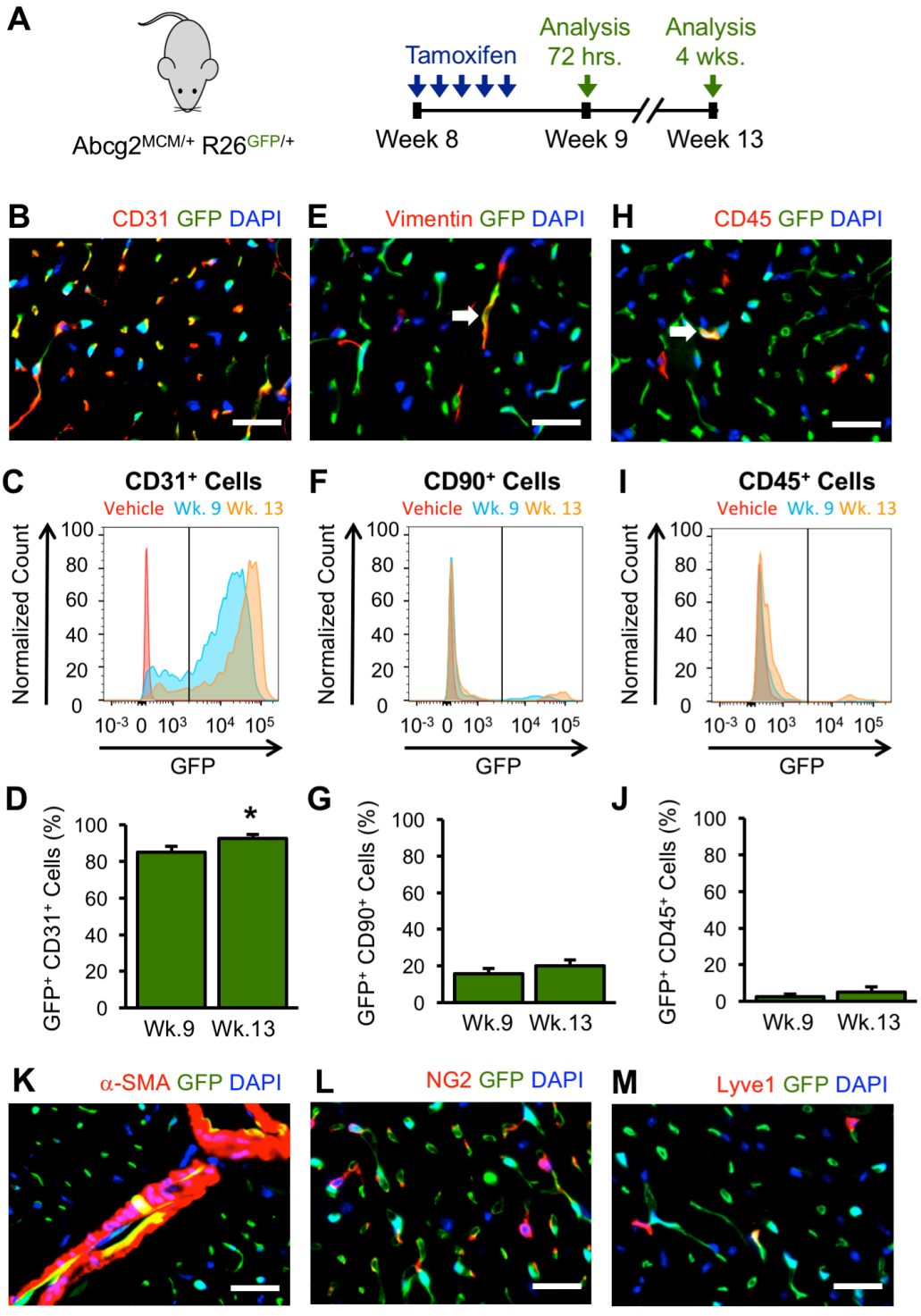
A
Abcg2MCM/+ R26GFP/+
Tamoxifen
Analysis 72 hrs.
Analysis 4 wks.
Week 8
Week 9
Week 13
B
CD31 GFP DAPI
E
Vimentin GFP DAPI
H
CD45 GFP DAPI
C
CD31+ Cells
Vehicle Wk. 9 Wk. 13
Normalized Count
GFP
F
CD90+ Cells
Vehicle Wk. 9 Wk. 13
Normalized Count
GFP
I
CD45+ Cells
Vehicle Wk. 9 Wk. 13
Normalized Count
GFP
D
GFP+ CD31+ Cells (%)
Wk.9
Wk.13
G
GFP+ CD90+ Cells (%)
Wk.9
Wk.13
J
GFP+ CD45+ Cells (%)
Wk.9
Wk.13
K
α-SMA GFP DAPI
L
NG2 GFP DAPI
M
Lyve1 GFP DAPI

Figure 7. Endogenous, lineage-traced cSPCs give rise to cardiac endothelial cells. (A) Diagram illustrating pulse-chase timeline used to study the contribution of endogenous cSPCs to noncardiomyocytes in Abcg2$^{MCM/+}$ R26$^{GFP/+}$ mice. The blue arrows represent single, 2-mg tamoxifen injections. The green arrows represent time points when GFP-labeling in the ileum was assessed, 72 hours and 4 weeks after the fifth 2mg tamoxifen injection. **(B)** Representative image of CD31 immunofluorescence staining on cardiac sections from tamoxifen-injected Abcg2$^{MCM/+}$ R26$^{GFP/+}$ mice. **(C)** Histogram overlay of GFP-expression in CD31^{+} noncardiomyocytes isolated from vehicle-injected Abcg2$^{MCM/+}$ R26$^{GFP/+}$ mice (red), tamoxifen-injected Abcg2$^{MCM/+}$ R26$^{GFP/+}$ mice at Week 9 (cyan) tamoxifen-injected Abcg2$^{MCM/+}$ R26$^{GFP/+}$ mice at Week 13 (orange). **(D)** Analysis of GFP-labeled CD31^{+}noncardiomyocytes from tamoxifen-injected Abcg2$^{MCM/+}$ R26$^{GFP/+}$ mice at Week 9 and Week 13 (n=4). **(E)** Representative image of Vimentin immunofluorescence staining on cardiac sections from tamoxifen-injected Abcg2$^{MCM/+}$ R26$^{GFP/+}$ mice. **(F)** Histogram overlay of GFP-expression in CD90^{+} noncardiomyocytes isolated from vehicle-injected Abcg2$^{MCM/+}$ R26$^{GFP/+}$ mice (red), tamoxifen-injected Abcg2$^{MCM/+}$ R26$^{GFP/+}$ mice at Week 9 (cyan) tamoxifen-injected Abcg2$^{MCM/+}$ R26$^{GFP/+}$ mice at Week 13 (orange). **(G)** Analysis of GFP-labeled CD90^{+} noncardiomyocytes from tamoxifen-injected Abcg2$^{MCM/+}$ R26$^{GFP/+}$ mice at Week 9 and Week 13 (n=4). **(H)** Representative image of CD45^{+} immunofluorescence staining on cardiac sections from tamoxifen-injected Abcg2$^{MCM/+}$ R26$^{GFP/+}$ mice. **(I)** Histogram overlay of GFP-expression in CD45^{+}

noncardiomyocytes isolated from vehicle-injected Abcg2$^{MCM/+}$ R26$^{GFP/+}$ mice (red), tamoxifen-injected Abcg2$^{MCM/+}$ R26$^{GFP/+}$ mice at Week 9 (cyan) tamoxifen-injected Abcg2$^{MCM/+}$ R26$^{GFP/+}$ mice at Week 13 (orange). **(J)** Analysis of GFP-labeled CD90^{+} noncardiomyocytes from tamoxifen-injected Abcg2$^{MCM/+}$ R26$^{GFP/+}$ mice at Week 9 and Week 13 (n=4). **(K)** Representative image of α-SMA immunofluorescence staining on cardiac sections from tamoxifen-injected Abcg2$^{MCM/+}$ R26$^{GFP/+}$ mice. **(L)** Representative image of NG2 chondroitin sulfate proteoglycan immunofluorescence staining on cardiac sections from tamoxifen-injected Abcg2$^{MCM/+}$ R26$^{GFP/+}$ mice. **(M)** Representative image of LYVE1 immunofluorescence staining on cardiac sections from tamoxifen-injected Abcg2$^{MCM/+}$ R26$^{GFP/+}$ mice. * $P < 0.05$, mean $\pm$ SD. In all images, nuclei are counterstained with DAPI. Scale Bars: 50 μm.

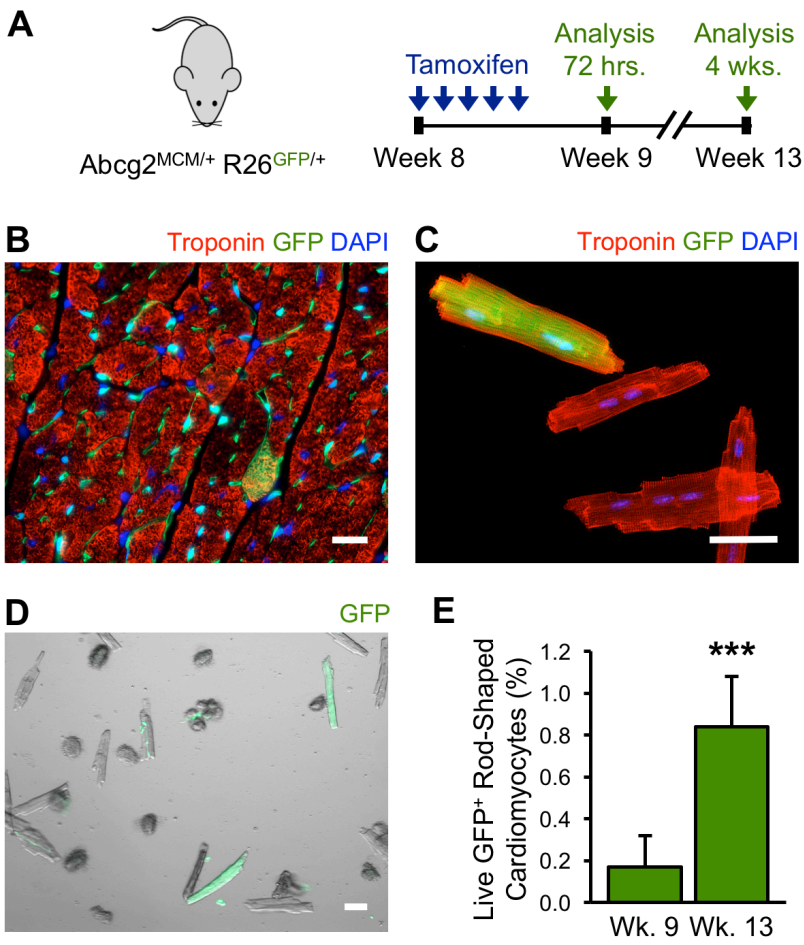

Figure 8. Endogenous, lineage-traced cSPCs give rise to cardiomyocytes. **(A)** Diagram illustrating pulse-chase timeline used to study the contribution of endogenous cSPCs to cardiomyocytes in Abcg2$^{MCM/+}$ R26$^{GFP/+}$ mice. The blue arrows represent single, 2-mg tamoxifen injections. The green arrows represent time points when GFP-labeling in the ileum was assessed, 72 hours and 4 weeks after the fifth 2mg tamoxifen injection. **(B)** Representative image of troponin immunofluorescence staining on cardiac sections from tamoxifen-injected Abcg2$^{MCM/+}$ R26$^{GFP/+}$ mice. **(C)** Representative image of troponin

immunofluorescence staining on isolated adult cardiomyocytes, **(D)** Representative image of native GFP fluorescence of live, isolated adult cardiomyocytes. **(E)** Quantification of the percent of total, rod-shaped cardiomyocytes labeled with GFP from tamoxifen-injected $Abcg2^{MCM/+}$ $R26^{GFP/+}$ mice at Week 9 (n=5) and Week 13 (n=7). *** $P < 0.001$, mean ± SD. In all images, nuclei are counterstained with DAPI. Scale Bars: 25 μm.

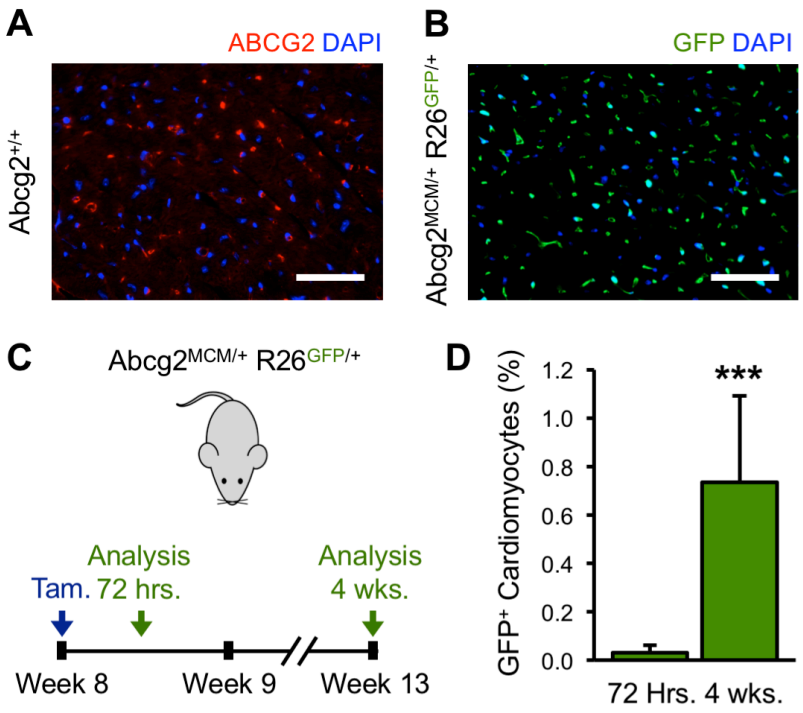

Figure 9. Cardiomyocytes do not express ABCG2. (A) Representative fluorescent images of immunofluorescence staining for ABCG2 in cardiac sections from Abcg2$^{+/+}$ mice. **(B)** Representative fluorescent images of the native GFP fluorescence in cardiac sections from tamoxifen-injected Abcg2$^{MCM/+}$ R26$^{GFP/+}$ mice**. (C)** Diagram illustrating pulse-chase timeline used in Abcg2$^{MCM/+}$ R26$^{GFP/+}$ mice. The blue arrow represents a single, 2-mg tamoxifen injection. The green arrows represent time points when GFP-labeling in cardiomyocytes was assessed, 72 hours and 4 weeks after a single, 2mg injection of tamoxifen. **(D)** Quantification of the percent of cardiomyocytes labeled with GFP in tamoxifen-injected Abcg2$^{MCM/+}$ R26$^{GFP/+}$ mice at 72 hours (n=6) and 4 weeks (n=6) after a

single, 2mg injection of tamoxifen. *** $P < 0.001$, mean ± SD. In all images, nuclei are counterstained with DAPI. Scale Bars: 50 μm.

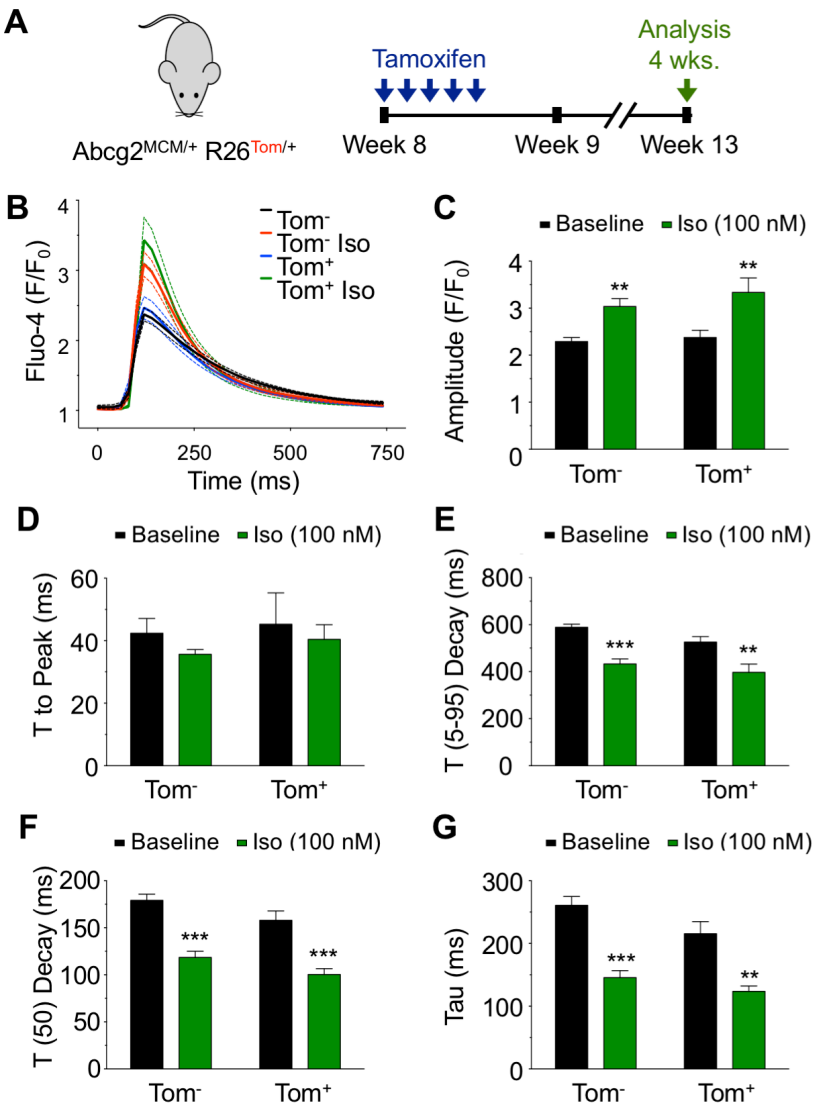

Figure 10. Cytosolic calcium dynamics of lineage-traced cardiomyocytes are comparable to non-lineage- traced cardiomyocytes. (A) Diagram illustrating pulse-chase timeline used in Abcg2$^{MCM/+}$ R26$^{Tom/+}$ mice. The blue arrows represent single, 2-mg tamoxifen injection. The green arrow represents the timepoint when cytosolic calcium dynamics were recorded in isolated cardiomyocytes. **(B)** Calcium dynamic traces in paced Tom^{+} and Tom^{-}

cardiomyocytes with or without isoproterenol stimulation. The solid lines represent the mean and the dashed lines represent the SEM. **(C)** Analysis of peak amplitude of calcium transients. **(D)** Analysis of the time to peak amplitude. **(E)** Analysis of the time between 5% and 95% decay of peak amplitude. **(F)** Analysis of the time from peak amplitude to 50% decay of peak amplitude. **(G)** Analysis of the time constant of calcium transient decay (Tau). ** $P < 0.01$, *** $P < 0.001$, mean ± SEM.

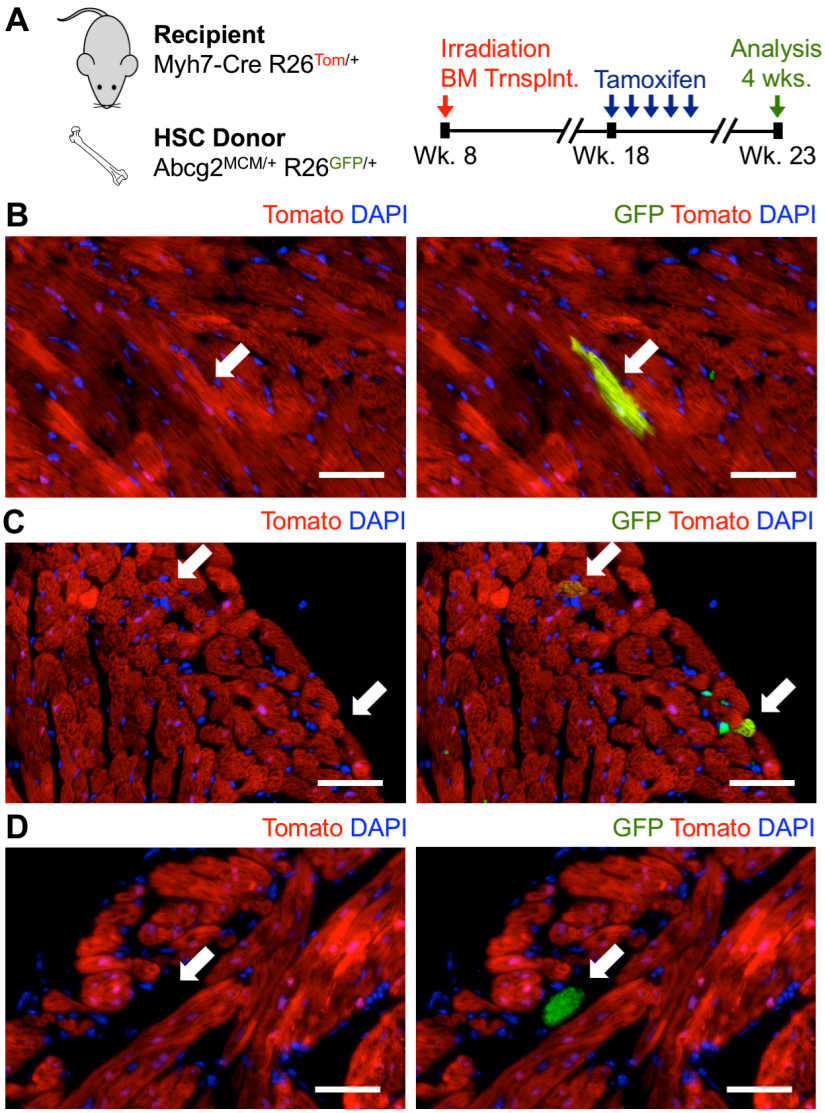

Figure 11. Lineage-traced bone marrow cells do not significantly contribute to lineage-traced cardiomyocytes. (A) Diagram illustrating timeline used to generate bone marrow chimera mice (Myh7-Cre R26$^{Tom/+}$ mice with Abcg2$^{MCM/+}$ R26$^{GFP/+}$ bone marrow) and the pulse-chase used with these mice. The blue arrows represent single, 2-mg tamoxifen injection. The green arrow represents the timepoint when labeling of cardiomyocytes was assessed. **(B)** Representative

fluorescence image of Tom^+ and GFP^+ cardiomyocyte. All GFP^+ ventricular cardiomyocytes identified were also Tom^+ (n=5). **(C)** Representative fluorescence image of Tom^+ GFP^+ cardiomyocytes and Tom^- GFP^+ noncardiomyocytes. **(D)** Image of the single Tom^- GFP^+ cardiomyocyte identified in the atria of one mouse. In all images, nuclei are counterstained with DAPI. Scale Bars: 50 μm.

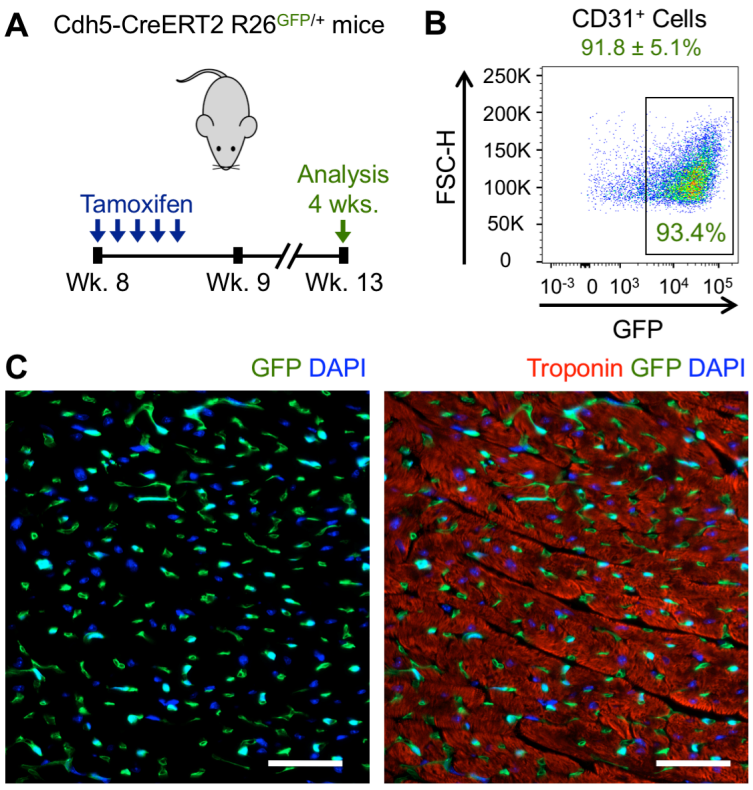

Figure 12. Labeled endothelial cells do not contribute to lineage trace-cardiomyocytes. (A) Diagram illustrating pulse-chase timeline used to study the contribution of labeled endothelial cells to cardiomyocytes in Cdh5-CreERT2 R26$^{GFP/+}$ mice. The blue arrows represent single, 2-mg tamoxifen injection. The green arrow represents the timepoint when labeling of cardiomyocytes was assessed. **(B)** Representative flow cytometry plot of GFP-expression in CD31+ noncardiomyocytes isolated from tamoxifen-injected Cdh5-CreERT2 R26$^{GFP/+}$ mice. **(C)** Representative image of troponin immunofluorescence staining on cardiac sections from tamoxifen-injected Cdh5-CreERT2 R26$^{GFP/+}$ mice. In all images, nuclei are counterstained with DAPI. Scale Bars: 50 μm.

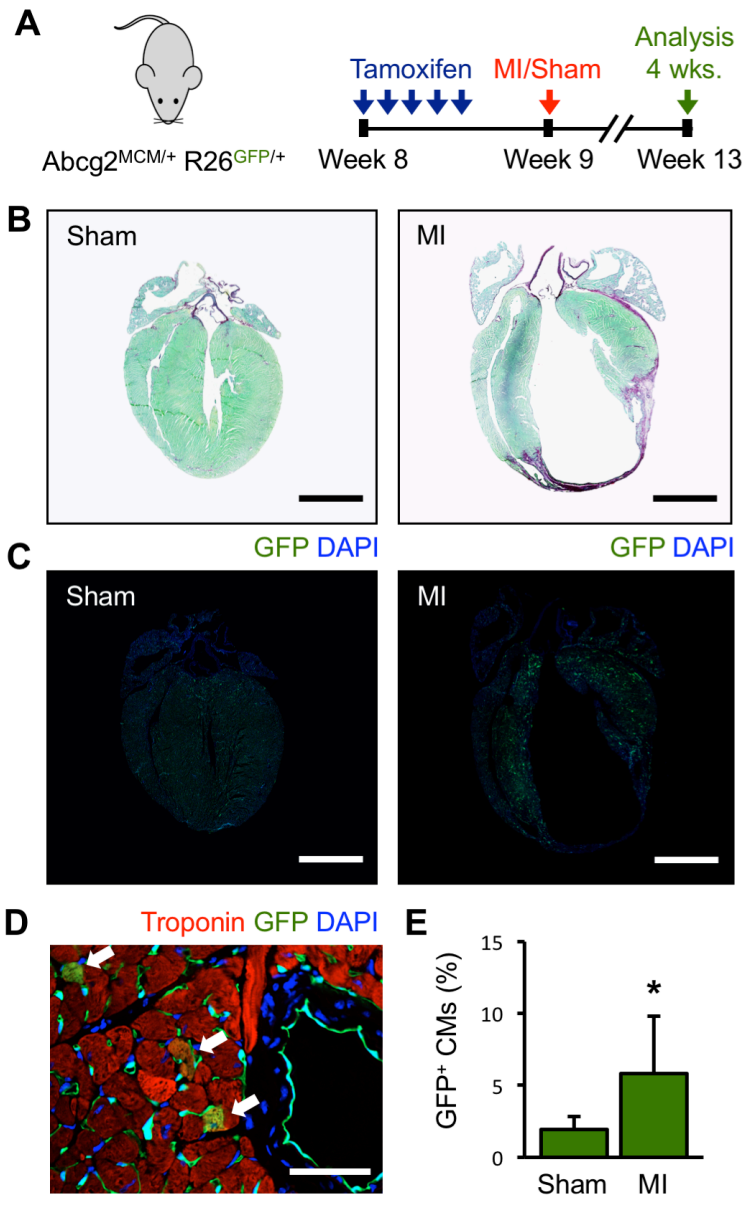

Figure 13. CSPC contribution to cardiomyocytes increases following MI. (A) Diagram illustrating pulse-chase timeline used to study the contribution of endogenous cSPCs to cardiomyocytes following MI n Abcg2$^{MCM/+}$ R26$^{GFP/+}$ mice. The blue arrows represent single, 2-mg tamoxifen injections. The red arrow represents either MI or sham surgeries. The green arrow represents the

timepoint when GFP-labeling of cardiomyocytes was assessed 4 weeks MI or sham surgery. **(B)** Representative brightfield images of cardiac sections from sham and MI-operated Abcg2$^{MCM/+}$ R26$^{GFP/+}$ mice stained with Sirius Red Fast Green **(C)** Representative fluorescent images of the native GFP fluorescence from sham and MI-operated Abcg2$^{MCM/+}$ R26$^{GFP/+}$ mice. **(D)** Representative image of troponin immunofluorescence staining on cardiac sections from MI-operated Abcg2$^{MCM/+}$ R26$^{GFP/+}$ mice. **(E)** Quantification of the percent of cardiomyocytes labeled with GFP in tamoxifen-injected Abcg2$^{MCM/+}$ R26$^{GFP/+}$ mice following sham operation (n=7) and MI operation (n=7). * $P < 0.05$, mean ± SD. In all images, nuclei are counterstained with DAPI. Scale Bars: 2mm (B and C) and 50 μm (D).

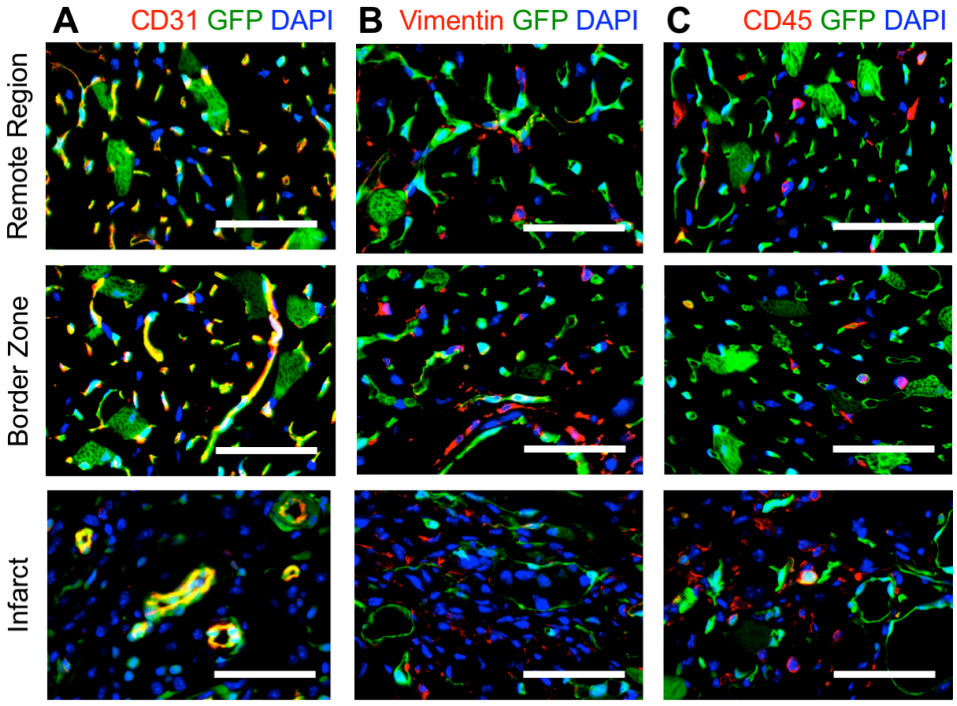

Figure 14. Noncardiomyocyte labeling in the remote region, border zone and infarct following MI. (A) Representative image of CD31 immunofluorescence staining in the remote region, border zone and infarct of hearts harvested from tamoxifen-injected, MI-operated Abcg2$^{MCM/+}$ R26$^{GFP/+}$ mice. **(B)** Representative image of Vimentin immunofluorescence staining in the remote region, border zone and infarct of hearts harvested from tamoxifen-injected, MI-operated Abcg2$^{MCM/+}$ R26$^{GFP/+}$ mice. **(C)** Representative image of CD45 immunofluorescence staining in the remote region, border zone and infarct of hearts harvested from tamoxifen-injected, MI-operated Abcg2$^{MCM/+}$ R26$^{GFP/+}$ mice. In all images, nuclei are counterstained with DAPI. Scale Bars: 50 μm.

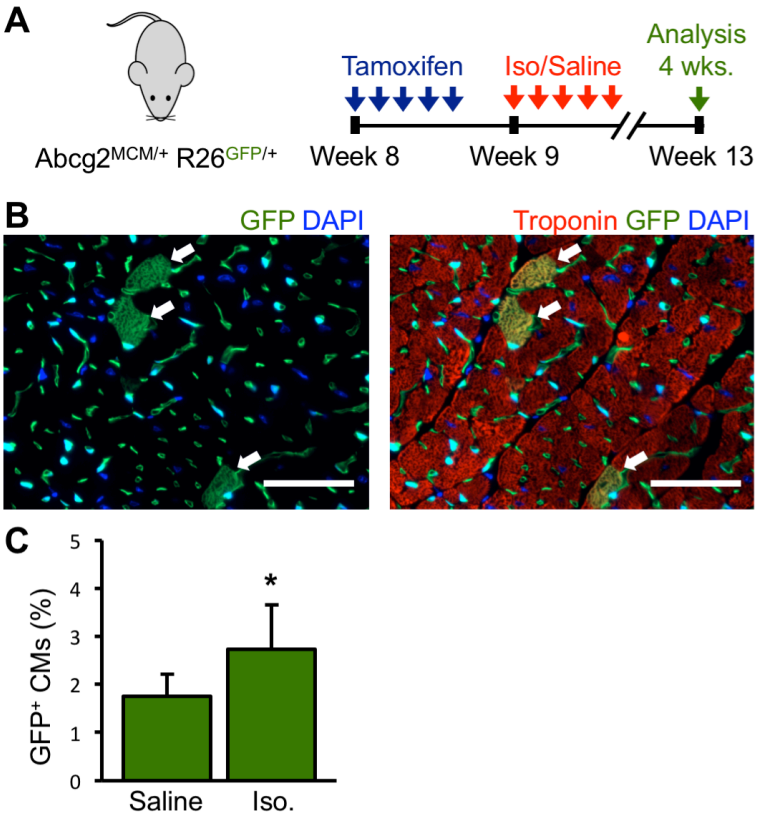

Figure 15. CSPC contribution to cardiomyocytes increases following acute adrenergic cardiac injury. (A) Diagram illustrating pulse-chase timeline used to study the contribution of endogenous cSPCs to cardiomyocytes following acute adrenergic injury in Abcg2$^{MCM/+}$ R26$^{GFP/+}$ mice. The blue arrows represent single, 2-mg tamoxifen injections. The red arrows represent subcutaneous saline or isoproterenol (100 mg/kg) injections. The green arrow represents the timepoint when GFP-labeling of cardiomyocytes was assessed 4 weeks after the initiation of saline or isoproterenol injections. **(B)** Representative image of troponin immunofluorescence staining on cardiac sections from isoproterenol-injected Abcg2$^{MCM/+}$ R26$^{GFP/+}$ mice. **(C)** Quantification of the percent of cardiomyocytes

labeled with GFP in tamoxifen-injected Abcg2$^{MCM/+}$ R26$^{GFP/+}$ mice following saline (n=8) and isoproterenol injections (n=10). * $P < 0.05$, mean ± SD. In all images, nuclei are counterstained with DAPI. Scale Bars: 50 μm.

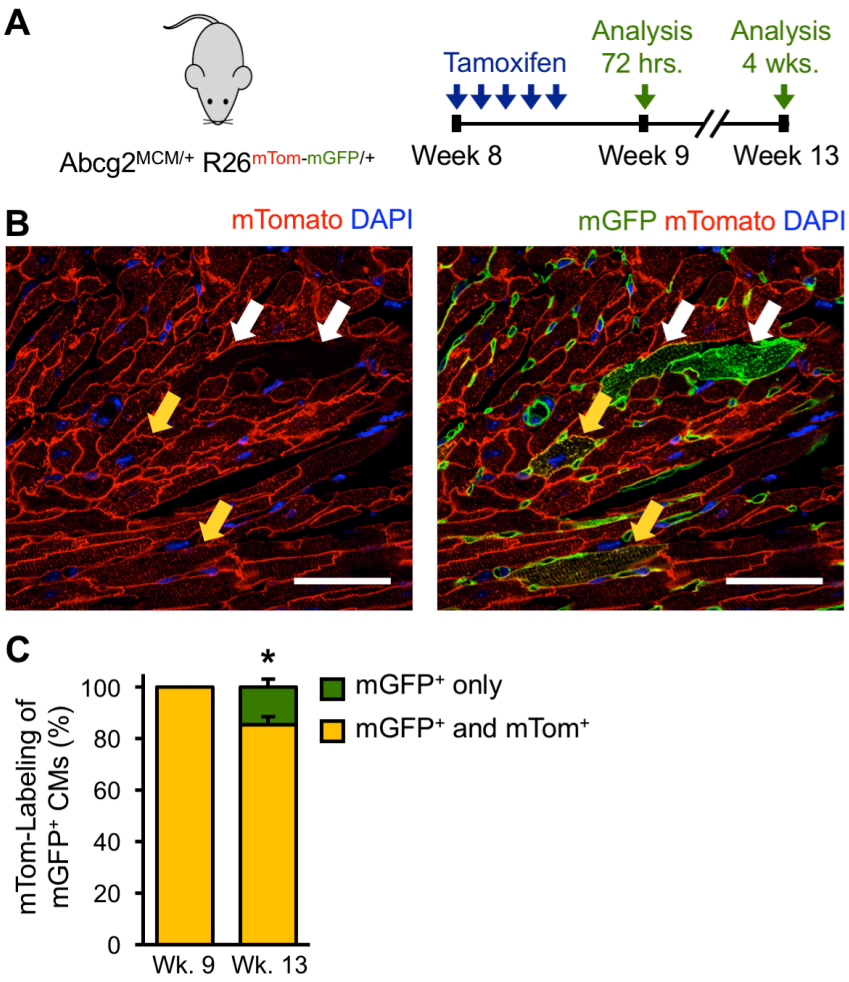

Figure 16. CSPCs give rise to cardiomyocyte through fusion and differentiation into cardiomyocytes. (A) Diagram illustrating pulse-chase timeline used to study the contribution of endogenous cSPCs to cardiomyocytes in Abcg2$^{MCM/+}$ R26$^{mTom\text{-}mGFP/+}$ mice. The blue arrows represent single, 2-mg tamoxifen injections. The green arrows represent time points when GFP-labeling in the ileum was assessed, 72 hours and 4 weeks after the fifth 2mg tamoxifen injection. **(B)** Representative confocal image of mTom^{+} mGFP^{+} cardiomyocytes (yellow arrows) and mTom^{-} mGFP^{+} cardiomyocytes (white arrows) from cardiac

sections of tamoxifen-injected Abcg2$^{MCM/+}$ R26$^{mTom\text{-}mGFP/+}$ mice. **(C)** Quantification of the percent of mGFP^{+} cardiomyocytes that are mTom^{-} or mTom^{+} at Week 9 and Week 13. * $P < 0.05$, mean ± SD. In all images, nuclei are counterstained with DAPI. Scale Bars: 50 μm.

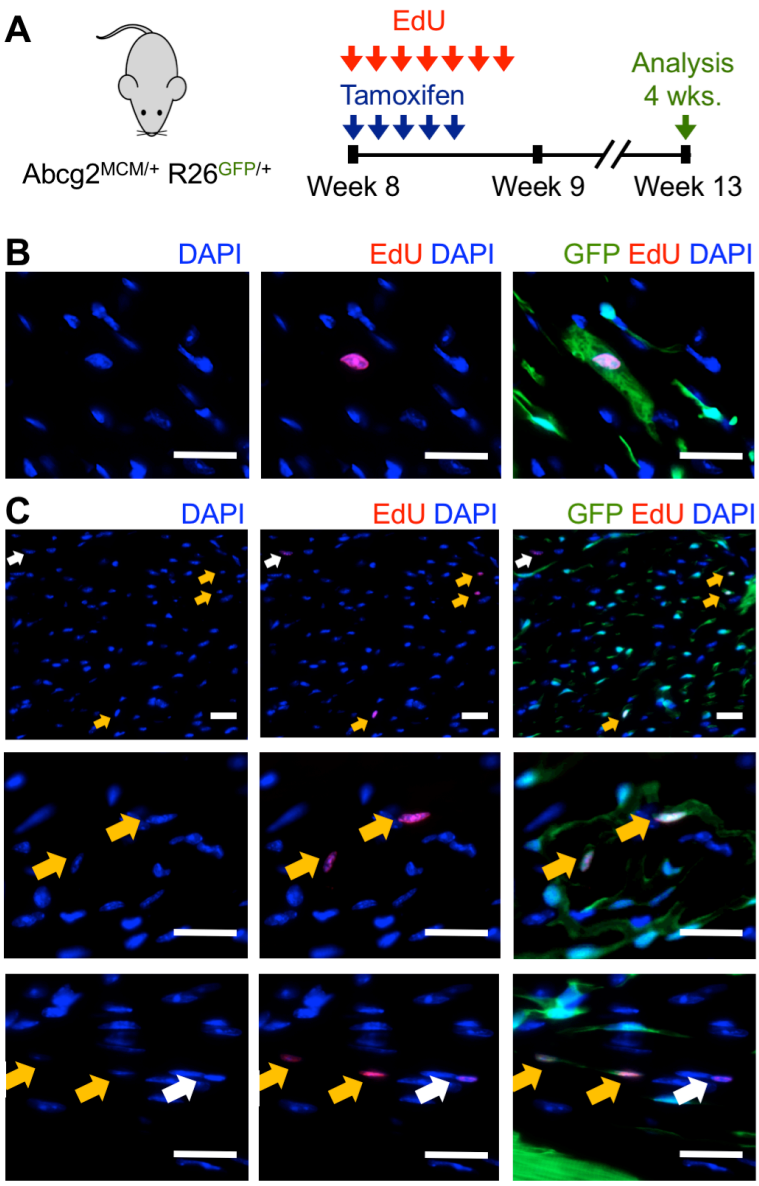

Figure 17. CSPCs give rise to newly-formed noncardiomyocytes and cardiomyocytes. (A) Diagram illustrating co-injection EdU timeline used to study the contribution of cSPCs to newly formed cells in the adult heart. The blue arrows represent single, 2-mg tamoxifen injections. The red arrows represent single, 2.5mg EdU injections. The green arrow represents the timepoint when

EdU incorporation and GFP-labeling was assessed 4 weeks after the last EdU injection. **(B)** Representative fluorescent image of an EdU^+ GFP^+ cardiomyocyte. **(C)** Representative fluorescent images of an EdU^+ GFP^+ noncardiomyocytes. The top row is a lower magnification image that 4 EdU+ noncardiomyocytes, three of which are GFP^+ and one which is GFP^-. The middle and bottom row show higher magnification images of EdU^+ GFP^+ and EdU+ GFP^- noncardiomyocytes. In all images, nuclei are counterstained with DAPI. Scale Bars: 25 μm.

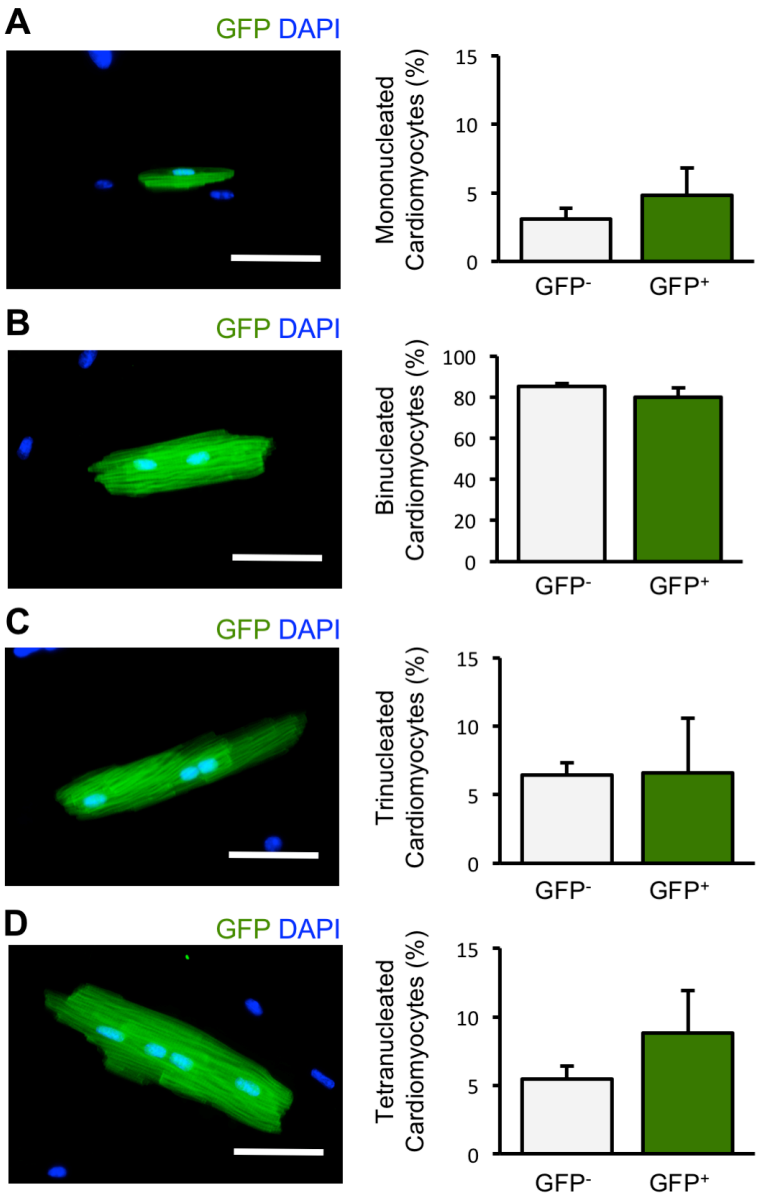

Figure 18. Nucleation of lineage-traced and non-lineage-traced cardiomyocytes is the same. (A) Representative image of the native fluorescence of a mononucleated GFP$^+$ cardiomyocytes and quantification of the percent of GFP$^-$ or GFP$^+$ cardiomyocytes that are mononucleated. **(B)** Representative image of the native fluorescence of a binucleated GFP$^+$ cardiomyocytes and quantification of the percent of GFP$^-$ or GFP$^+$

cardiomyocytes that are binucleated. **(C)** Representative image of the native fluorescence of a trinucleated GFP^+ cardiomyocytes and quantification of the percent of GFP^- or GFP^+ cardiomyocytes that are trinucleated. **(D)** Representative image of the native fluorescence of a tetranucleated GFP^+ cardiomyocytes and quantification of the percent of GFP^- or GFP^+ cardiomyocytes that are tetranucleated. In all images, nuclei are counterstained with DAPI. Scale Bars: 50 μm.

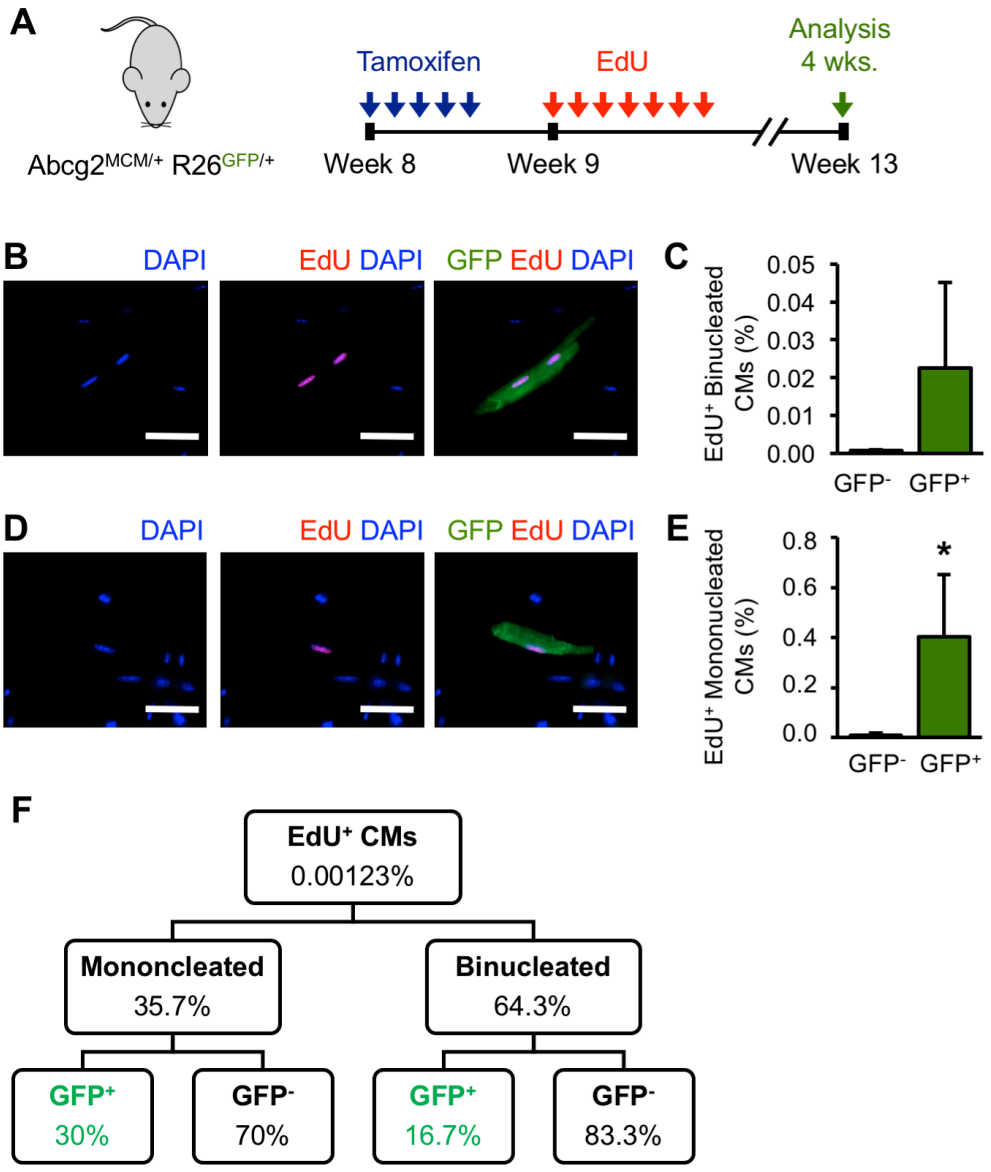

Figure 19. Lineage-traced cSPCs give rise to 21% of newly-formed cardiomyocytes in the adult heart. (A) Diagram illustrating sequential EdU timeline used to study the contribution of cSPCs to newly formed cells in the adult heart. The blue arrows represent single, 2-mg tamoxifen injections. The red arrows represent single, 2.5mg EdU injections. The green arrow represents the

timepoint when EdU incorporation and GFP-labeling was assessed 4 weeks after the last EdU injection. **(B)** Representative fluorescent image of a binucleated EdU^+ GFP^+ cardiomyocyte. **(C)** Quantification of the percent of GFP^+ and GFP^- cardiomyocytes that are EdU^+ and binucleated. **(D)** Representative fluorescent image of a mononucleated EdU^+ GFP^+ cardiomyocyte. **(E)** Quantification of the percent of GFP^+ and GFP^- cardiomyocytes that are EdU^+ and mononucleated. **(F)** Web diagram illustrating the breakdown of Edu^+ cardiomyocytes into mononucleated versus binucleated and then GFP^+ versus GFP^-. * $P < 0.05$, mean ± SD. In all images, nuclei are counterstained with DAPI. Scale Bars: 50 μm.

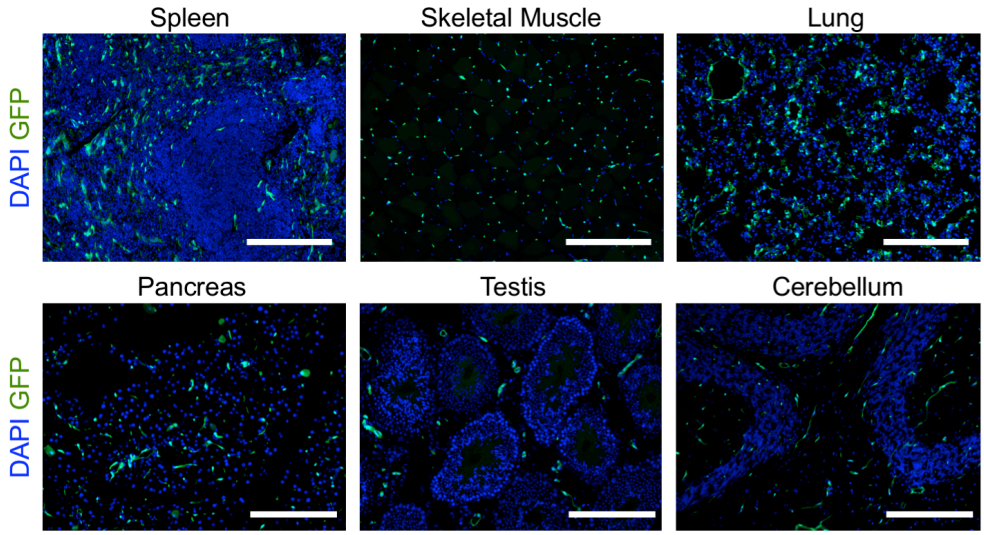

Supplementary Figure 1. Labeling in other organs in Abcg2$^{MCM/+}$ R26$^{GFP/+}$ mice. Representative fluorescent images of the native GFP fluorescence in sections from tamoxifen-injected Abcg2$^{MCM/+}$ R26$^{GFP/+}$ mice. In all images, nuclei are counterstained with DAPI. Scale Bars: 200 μm.

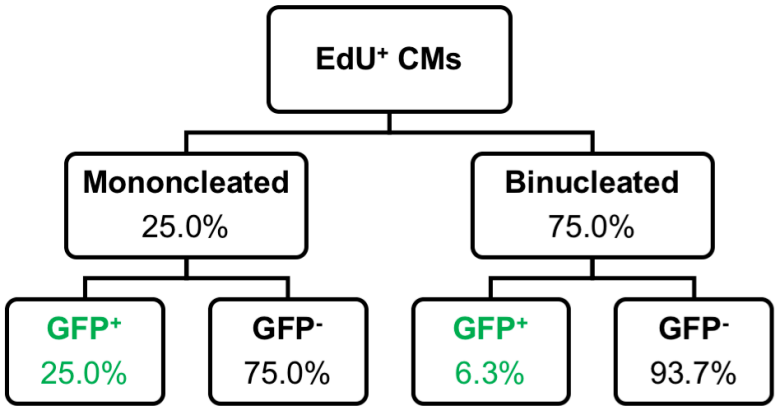

Supplementary Figure 2. Quantification of newly-formed cardiomyocytes using the EdU and Tamoxifen co-injection strategy.

Bone Marrow Cell Type	GFP^+ Cells (%)
bmSPCs	40.5 ± 9.30
LSK (Lin^- $Sca\text{-}1^+$ Kit^+)	56.9 ± 7.31
Granulocytes	56.9 ± 7.23
Monocytes/Macrophages	58.0 ± 7.50
Erythroid Cells	50.4 ± 6.80
B Cells	40.1 ± 6.30
T Cells	14.0 ± 3.00

Table 1. GFP-labeling of bmSPCs, LSK and bone marrow lineages in Mhy7-CreER $R26^{Tom/+}$ $Abcg2^{MCM/+}$ $R26^{GFP/+}$ bone marrow chimeric mice.

Bone Marrow Cell Type	GFP^+ Cells (%)
bmSPCs	1.6 ± 0.2
LSK (Lin^- $Sca\text{-}1^+$ Kit^+)	4.8 ± 0.2
Granulocytes	1.5 ± 0.11
Monocytes/Macrophages	1.3 ± 0.2
Erythroid Cells	3.0 ± 0.4
B Cells	1.6 ± 0.3
T Cells	11.0 ± 4.1

Table 2. GFP-labeling of bmSPCs, LSK and bone marrow lineages in VE-Cadherin-CreERT2 $R26^{GFP/+}$ mice.

Cellular Target	Blocking Solution	Primary Antibody	Secondary Antibody
Abcg2+ Cells	0.1% Triton 5% Normal Goat Serum (NGS) diluted in PBS *1 hour, Room Temperature (RT)*	**α-Abcg2** **Santa Cruz Biotechnology sc-58224** Rat Monoclonal Antibody (BXP-53) 1:400 in Blocking Solution *Overnight, 4°C*	**Goat α-rat antibody Alexa Fluor™ 568** **Invitrogen A-11077** 1:400 in Blocking Solution *1 hour, RT*
Endothelial Cells	0.1% Triton and 5% NGS diluted in PBS *1 hour, RT*	**α-CD31** **LifeSpan BioSciences LS-B4737** Rabbit Polyclonal Antibody 1:20 in Blocking Solution *Overnight, 4°C*	**Donkey α-rabbit antibody Alexa Fluor™ 568** **Invitrogen A10042** 1:400 in Blocking Solution *1 hour, RT*
Fibroblasts	0.1% Triton and 5% NGS diluted in PBS *1 hour, RT*	**α-Vimentin** **Abcam ab45939** Rabbit Polyclonal Antibody 1:50 in Blocking Solution *Overnight, 4°C*	**Donkey α-rabbit antibody Alexa Fluor™ 568** **Invitrogen A10042** 1:400 in Blocking Solution *1 hour, RT*
Hematopoietic Cells	0.1% Triton and 3% BSA diluted in PBS *1 hour, RT*	**α-CD45** **R&D Systems AF114** Goat Polyclonal Antibody 1:20 in Blocking Solution *Overnight, 4°C*	**Donkey α-goat antibody Alexa Fluor™ 568** **Invitrogen A-11057** 1:400 in Blocking Solution *1 hour, RT*
Smooth Muscle Cells	0.1% Triton and 5% NGS diluted in PBS *1 hour, RT*	**a-Smooth Muscle Actin** **Abcam ab5694** Rabbit Polyclonal Antibody 1:150 in Blocking Solution *Overnight, 4°C*	**Donkey α-rabbit antibody Alexa Fluor™ 568** **Invitrogen A10042** 1:400 in Blocking Solution *1 hour, RT*
Lymphatic Vessels	0.1% Triton and 5% NGS diluted in PBS *1 hour, RT*	**α- Lyve1** **Abcam ab14917** Rabbit Polyclonal Antibody 1:250 in Blocking Solution *Overnight, 4°C*	**Donkey α-rabbit antibody Alexa Fluor™ 568** **Invitrogen A10042** 1:400 in Blocking Solution *1 hour, RT*
Pericytes	0.1% Triton and 5% NGS diluted in PBS *1 hour, RT*	**α-NG2 Chondroitin Sulfate Proteoglycan** **EMD Millipore AB5320** Rabbit Polyclonal Antibody 1:150 in Blocking Solution *Overnight, 4°C*	**Donkey α-rabbit antibody Alexa Fluor™ 568** **Invitrogen A10042** 1:400 in Blocking Solution *1 hour, RT*
Sca1⁺ Cells	0.1% Triton and 5% NGS diluted in PBS *1 hour, RT*	**α-Sca1** **Abcam ab51317** Rat Monoclonal Antibody (E13 161-7) 1:100 in Blocking Solution *Overnight, 4°C*	**Goat α-rat antibody Alexa Fluor™ 568** **Invitrogen A-11077** 1:400 in Blocking Solution *1 hour, RT*
Cardiomyocytes	0.1% Triton 5% Normal Goat Serum (NGS) diluted in PBS *1 hour, Room Temperature (RT)*	**α-cardiac Troponin I** **Abcam ab47003** Rabbit Polyclonal Antibody 1:100 in Blocking Solution *Overnight, 4°C*	**Donkey α-rabbit antibody Alexa Fluor™ 568** **Invitrogen A10042** 1:400 in Blocking Solution *1 hour, RT*

Supplementary Table 1. Antibody details for immunofluorescence staining of histological sections.

Protein Target	Blocking Solution	Primary Antibody	Secondary Antibody
Troponin T	0.1% Triton 5% Normal Goat Serum (NGS) diluted in PBS *1 hour, Room Temperature (RT)*	**α-Troponin T, clone 13-11** **Thermo Fisher Scientific MS295PABX** Mouse Monoclonal Antibody 1:100 in Blocking Solution *Overnight, 4°C*	**Donkey α-mouse antibody Alexa Fluor™ 568** **Invitrogen A10037** 1:400 in Blocking Solution *1 hour, RT*
GFP	0.1% Triton and 5% NGS diluted in PBS *1 hour, RT*	**α-GFP** **Abcam ab290** Rabbit Polyclonal Antibody 1:100 in Blocking Solution *Overnight, 4°C*	**Donkey α-rabbit antibody Alexa Fluor™ 488** **Invitrogen A-21206** 1:400 in Blocking Solution *1 hour, RT*

Supplementary Table 2. Antibody details for immunofluorescence staining of fixed, isolated adult cardiomyocytes.

Discussion and Future Directions

In the past, the mammalian heart was thought to be a post-mitotic organ with no new cardiomyocytes formed after birth; however, in recent years, evidence that endogenous cardiac regeneration exists in postnatal mouse and human hearts opened up the exciting possibility of regenerating cardiomyocytes lost during the progression of heart failure[88,93,94,102]. Unfortunately, the low annual rate of cardiomyocyte generation cannot compensate for the cardiomyocyte death that occurs during the progression of heart failure. If we can develop new therapies that enhance endogenous cardiac regeneration sufficiently, we can treat this crucial problem in heart failure patients.

There are several different approaches being developed to enhance endogenous cardiac regeneration[172,174,206]. Initially, there was a lot of interest in utilizing cardiac progenitor cells to regenerate the heart but, as more recent studies have highlighted the limited contribution of *Kit*-expressing cardiac progenitor cells, the attention has turned towards stimulating proliferation of pre-existing cardiomyocytes[77,85,112,168–171,207,208]. While this approach has a lot of potential, it is limited in its ability to give rise to only cardiomyocytes. Unlike proliferating cardiomyocytes, cardiac progenitor cells can give rise to cardiomyocytes and noncardiomyocytes that are required for normal cardiac function[173,174]. For this reason, it is important that we carefully identify and evaluate the contribution of other endogenous cardiac progenitor cells that are unique from *Kit*-expressing cardiac progenitor cells. To do this, we used the side population phenotype, which enriches for stem and progenitor cells in many

organs and forms of cancer. Isolated cSPCs do not express the *Kit* gene and their expression profile is distinct from *Kit*-expressing cardiac progenitor cells[146,148,149].

In these studies, we used an *Abcg2*-driven lineage-tracing mouse model to determine whether the side population phenotype can enrich for endogenous cardiac progenitor cells in the adult heart. We choose the *Abcg2* gene to lineage-trace side population cells because the ABCG2 transporter confers the side population phenotype in SPCs from different tissues and forms of cancer. In the bone marrow, ABCG2 is solely responsible for the side population phenotype. In *Abcg2* knockout mice, side population cells are no longer identifiable with flow cytometry; however, hematopoiesis occurs normally indicating that ABCG2 is not essential for the stem cell and differentiation properties of bone marrow side population cells [182]. In the adult heart, ABCG2 and p-glycoprotein both contribute to the side population phenotype of cSPCs at varying levels throughout the aging process [144,209]. Because *Abcg2* plays a role in the side population phenotype without effecting *in vivo* self-renewal and differentiation of tissue stem cells, we thought that an *Abcg2*-driven lineage-tracing mouse model would be the most effective way to study endogenous side population cells in tissues throughout the body.

Using this mouse model, we first found that the side population phenotype enriches for endogenous stem cells in organs where there is relatively high, continuous turnover of cells under normal homeostatic conditions. In the bone

marrow, the side population phenotype enriches well-characterized HSCs. We found that endogenous side population cells give rise to differentiated bone marrow lineages and confirmed the ability of our model to lineage-trace side population cells in an organ system with continuous cellular turnover and where the stem cell properties of side population cells are well-established. Then we moved to the small intestines, where side population cells have been identified but their self-renewal and differentiation properties are not very well established. With both short-term and long-term studies, we showed that endogenous intestinal stem cells are labeled and give rise to terminally differentiated cells during normal homeostatic conditions. These results showed that our *Abcg2*-driven approach could be used to successfully lineage-trace endogenous stem cells in organs with continuous cellular turnover.

In the heart, where regeneration occurs to a much lower extent than in the bone marrow and intestines; we found that the side population phenotype enriched from endogenous cardiac progenitor cells that give rise to cardiomyocytes and endothelial cells during cardiac homeostasis and in response to two different forms of cardiac injury. Importantly, we showed that our lineage-traced cSPCs account for 21% of all newly-formed cardiomyocytes. This finding shows the lineage-traced progenitor cells contribute to a portion of newly-formed cardiomyocytes indicating there are other sources like pre-existing cardiomyocytes. We may also be underestimating the contribution of endogenous cardiac progenitor cells because we do not know whether we are

labeling all progenitor cells since the side population phenotype has just been shown to enrich for stem and progenitor cells.

We ruled out the contribution of other cells types that are labeled in our mouse model. We used a bone marrow chimeric mouse models to rule out the contribution of labeled bone marrow cells. Our findings fit with previous studies that showed that cSPCs do not originate from the bone marrow compartment and bone marrow cells do not transdifferentiate into cardiomyocytes under homeostatic conditions[100,149]. We also showed that labeled endothelial cells do not contribute to the labeling of cardiomyocyte we observe in our lineage-tracing mouse model. There was a recently published study that provided some evidence that endothelial cells dedifferentiate into a progenitor-like state before differentiating into cardiomyocytes[202]. With our lineage-tracing mouse model and tamoxifen strategy, we did not observe any cardiomyocyte labeling indicating that the cellular process described in that paper did not occur in the mouse model that we used. Careful analysis of GFP-labeled side population will need to be done to identify the endogenous cardiac progenitor cells enriched for by the side population phenotype.

In addition to enriching for cardiac progenitor cells, the side population phenotype appeared to enrich for cells that fuse with pre-existing cardiomyocytes. Fusion and proliferation are often discussed as discrete cellular processes; however, there is growing evidence that these two processes may be tied together. Recent studies have shown that in cell culture and *in vivo*

cardiomyocyte fusion with non-cardiomyocytes or other cardiomyocytes, causes cardiomyocytes to re-enter the cell cycle and begin to proliferate[203,210]. These studies suggest that an alternative interpretation of the data presented here is that cSPCs fuse with pre-existing cardiomyocytes causing the cardiomyocytes to proliferate.

Another interpretation of our data is that a small number of proliferative cardiomyocytes express *Abcg2*; however, we performed experiments to carefully rule out ABCG2 expression in cardiomyocytes. Two studies evaluated *Abcg2*-expression in diseased human samples both noting an overall increase in *Abcg2*-expression in heart failure samples; however, most of the measurements evaluated mRNA and protein from a mixture of cells from the heart and did not use controls to verify the specificity of their techniques[211,212]. In our studies, we first identified an ABCG2-specific antibody with consistent staining on $Abcg2^{+/+}$ mouse samples and no staining on $Abcg2^{-/-}$ mouse samples. Of the three antibodies we carefully studied, only one had specific and consistent staining for ABCG2 on cells known to express *Abcg2*. We used this antibody to confirm a previous study that showed that ABCG2 is expressed by the microvasculature in the heart but not by cardiomyocytes; however, we cannot conclusively say that there are no cardiomyocytes that express *Abcg2* [200]. Next, we performed a single tamoxifen injection pulse-chase experiment and observed labeling of a very small number of cardiomyocytes 72-hours after a single injection with a significant increase in cardiomyocyte labeling over the following four weeks.

In the field of cardiac regeneration, the ongoing quest to understand which cells participate in endogenous regeneration in the adult mammalian heart has been challenging but exciting. With many different progenitor cells studied in cell culture and after transplantation, we sought to use the side population phenotype to identify endogenous cardiac progenitor cells in an unbiased manner. To do this, we generated an inducible, lineage-tracing mouse model that allowed us to trace stem and progenitor cells enriched by the side population *phenotype in vivo*. Using our mouse model, we identified an endogenous cardiac progenitor cell population that gives rise to 21% of newly-formed cardiomyocytes in the adult heart. When we consider our findings along with those published by Senyo et al., where they reported that pre-existing cardiomyocytes give rise to 77% of newly-formed cardiomyocytes under homeostatic conditions; it would suggest that our approach labels and lineage-traces all endogenous cardiac progenitor cells in the adult heart[93].

Next, we are working to further characterize the cardiac side population cells labeled in our mouse model. To do this, we have chosen to use single-cell RNA sequencing to further characterize three populations of noncardiomyocytes in our mouse model: GFP+ CD31- cSPCs, GFP-CD31- cSPCs and GFP+ main population cells. Because we found no cardiomyocyte labeling in our endothelial cell lineage-tracing experiments, we decided to exclude CD31+ cells from our analysis. We can perform clustering analysis to study subpopulations of cells and evaluate differential expression of specific gene sets in these clusters[204]. With the

data obtained through these experiments, we may be able to identify unique expression profiles that characterize the endogenous cardiac progenitor cells we have identified. More importantly, if we can identify pathways that regulate the proliferation and differentiation of endogenous cSPCs, then we may be able to develop strategies to target these cells in vivo.

Another important aspect of our work that needs to be studied further is the role of Abcg2 in the endogenous progenitor cells we have lineage-traced. Abcg2 is essential for the side population phenotype and the function of cSPCs in vitro[129,135,173]. In cell culture, knockout of Abcg2 alters proliferation, cell survival and differentiation of cSPCs. CSPCs isolated from Abcg2-/- mice are less proliferative, more susceptible to damage caused by oxidative stress and undergo apoptosis and necrosis at higher rates under normal culturing conditions[135,200]. Interestingly, knockout of Abcg2 does not affect the cardiomyogenic potential of cSPCs, but overexpression of Abcg2 inhibits cardiomyocyte differentiation of cultured cSPCs[135,200]. To determine whether Abcg2 plays as important a role in the function of endogenous cSPCs, we have knocked out Abcg2 in our lineage-tracing mouse model and will evaluate labeling of newly-formed cardiomyocytes during cardiac homeostasis and following cardiac injury.

In our mouse model, we also found that we had labeled a group of cells that appear to fuse with cardiomyocytes. In cardiovascular research, few studies specifically study cardiomyocyte fusion, but there are many reports of fusion

occurring between cardiomyocytes and other endogenous or exogenous cells types. It is unclear whether these observed fusion events are physiologically relevant or are just incidental occurrences. What makes studying fusion in vivo even more difficult, is that the outcomes of fusion can be very different. For example, in a recent publication, it was shown that fusion between cardiomyocytes in zebrafish occurs through transient membrane fusion without complete cell fusion. They found that this transient membrane fusion enhanced cardiomyocytes proliferation[201]. An older study that co-cultured neonatal rat ventricular myocytes reported that cardiomyocytes fuse entirely with other cell types like endothelial cells and fibroblasts. Fused cells more closely resembled cardiomyocytes and were more proliferative than other surrounding cardiomyocytes[194]. In our mouse model, we found a similar finding to the zebrafish study where nucleation status of cardiomyocytes was not different between lineage-traced cardiomyocytes and non-lineage-traced cardiomyocytes even though 85% of them had undergone some form of fusion. While the physiological importance of cardiomyocyte fusion is still unclear, when jamb3b, a gene encoding an adhesion junction protein that is important for skeletal muscle fusion, is knocked out; transient cardiomyocyte membrane fusion is decreased, and cardiac function is significantly depressed[201]. The level of cardiomyocyte fusion we observed in our study would also suggest that cardiomyocyte fusion may be physiologically relevant; however, more studies will have to be done to study this phenomenon in our mouse model further.

As the demographics of heart failure in the US shift, it will be important to understand how endogenous cSPCs would behave in the context of HFpEF. The reason for this is because aging is thought to be a significant factor in HFpEF and cSPCs have been shown to be increased in the aged heart without undergoing replicative senescence[145]. This increase in cSPCs with age was also observed in humans[150]. The problem is that they appear to lose their ability to differentiate into cardiomyocytes during the aging process[145]. If we can understand how cSPCs respond to HFpEF and develop methods to enhance their cardiomyogenic potential within this context, we may be able to develop therapies that improve clinical outcomes for HFpEF, which are much needed. At the moment, there is no good mouse model for HFpEF, but many labs are working to develop them[213,214].

Taken together, the studies described here offer preliminary findings that an endogenous cardiac progenitor cell population exists in the adult heart that contributes to newly-formed cardiomyocytes either through fusion or direct differentiation and could serve as a potential target for new heart failure therapies. More work will have to be done to further characterize these cells and develop methods of targeting them in vivo.

REFERENCES

1. Ponikowski, P. *et al.* 2016 ESC Guidelines for the diagnosis and treatment of acute and chronic heart failure The Task Force for the diagnosis and treatment of acute and chronic heart failure of the European Society of Cardiology (ESC) Developed with the special contribution of. *Eur. Heart J.* **18,** 891–975 (2016).
2. Yancy, C. W. *et al.* 2013 ACCF/AHA guideline for the management of heart failure: Executive summary: A report of the American college of cardiology foundation/American Heart Association task force on practice guidelines. *Circulation* **128,** 1810–1852 (2013).
3. Butler, J. *et al.* Developing therapies for heart failure with preserved ejection fraction: current state and future directions. *JACC. Heart Fail.* **2,** 97–112 (2014).
4. Roger, V. L. *et al.* Trends in heart failure incidence and survival in a community-based population. *J. Am. Med. Assoc.* **292,** 344–350 (2004).
5. Owan, T. E. *et al.* Trends in Prevalence and Outcome of Heart Failure with Preserved Ejection Fraction. *N. Engl. J. Med.* **355,** 251–259 (2006).
6. Gerber, Y. *et al.* A contemporary appraisal of the heart failure epidemic in Olmsted County, Minnesota, 2000 to 2010. *JAMA Intern. Med.* **175,** 996–1004 (2015).
7. Heidenreich, P. A. *et al.* Forecasting the impact of heart failure in the united states a policy statement from the American Heart Association. *Circ. Hear. Fail.* **6,** 606–619 (2013).
8. Cook, C., Cole, G., Asaria, P., Jabbour, R. & Francis, D. P. The annual global economic burden of heart failure. *Int. J. Cardiol.* **171,** 368–376 (2014).
9. Lymperopoulos, A., Rengo, G. & Koch, W. J. Adrenergic Nervous System in Heart Failure Pathophysiology and Therapy. *Circ. Res.* **113,** 739–753 (2018).
10. Wang, W., Zhu, G.-Q., Gao, L., Tan, W. & Qian, Z.-M. Baroreceptor reflex in heart failure. *Acta Physiol. Sin.* **56,** 269–281 (2004).
11. Anand, I. S. *et al.* Changes in brain natriuretic peptide and norepinephrine over time and mortality and morbidity in the Valsartan Heart Failure Trial (Val-HeFT). *Circulation* **107,** 1278–1283 (2003).
12. van Empel, V. P. M. *et al.* Myocyte apoptosis in heart failure. *Cardiovasc. Res.* **67,** 21–29 (2005).
13. Narula, J. *et al.* Apoptosis in myocytes in end-stage heart failure. *N. Engl. J. Med.* **335,** 1182–1189 (1996).
14. Olivetti, G. *et al.* Apoptosis in the failing human heart. *N. Engl. J. Med.* **336,** 1131–1141 (1997).
15. Saraste, A. *et al.* Cardiomyocyte apoptosis and progression of heart failure to transplantation. *Eur. J. Clin. Invest.* **29,** 380–386 (1999).
16. Guerra, S. *et al.* Myocyte death in the failing human heart is gender dependent. *Circ. Res.* **85,** 856–866 (1999).

17. Rayment, N. B. *et al.* Myocyte loss in chronic heart failure. *J. Pathol.* **188,** 213–219 (1999).
18. Whelan, R. S., Kaplinskiy, V. & Kitsis, R. N. Cell Death in the Pathogenesis of Heart Disease : Mechanisms and Significance. *Annu. Rev. Physiol.* **72,** 19–44 (2010).
19. Wencker, D. *et al.* A mechanistic role for cardiac myocyte apoptosis in heart failure. *J. Clin. Invest.* **111,** 1497–1504 (2003).
20. Communal, C., Singh, K., Pimentel, D. R. & Colucci, W. S. Norepinephrine Stimulates Apoptosis in Adult Rat Ventricular Myocytes by Activation of the. *Circulation* **98,** 1329–1334 (1998).
21. Sabbah, H. N. *et al.* Chronic therapy with metoprolol attenuates cardiomyocyte apoptosis in dogs with heart failure. *J. Am. Coll. Cardiol.* **36,** 1698–1705 (2000).
22. Kajstura, J. *et al.* Angiotensin II induces apoptosis of adult ventricular myocytes in vitro. *J Mol Cell Cardiol* **29,** 859–870 (1997).
23. Orogo, A. M. & Gustafsson, Å. B. Cell Death in the Myocardium : My Heart Won't Go On. *IUBMB Life* **65,** 651–656 (2013).
24. Menasché, P. *et al.* Myoblast transplantation for heart failure. *Lancet* **357,** 279–280 (2001).
25. Kahlon, A., Viadya, G. & Bolli, R. Cell Therapy for Heart Disease : Current Status and Future Directions. *Minerva Cardioangiol.* (2018). doi:10.23736/S0026-4725.18.04596-6
26. Koh, G. Y., Klug, M. G., Soonpaa, M. H. & Field, L. J. Differentiation and long-term survival of C2C12 myoblast grafts in heart. *J. Clin. Invest.* **92,** 1548–1554 (1993).
27. Robinson, S. W. *et al.* Arterial delivery of genetically labelled skeletal myoblasts to the murine heart: long-term survival and phenotypic modification of implanted myoblasts. *Cell Transplant.* **5,** 77–91 (1996).
28. Khan, M. *et al.* Skeletal myoblasts transplanted in the ischemic myocardium enhance in situ oxygenation and recovery of contractile function. *Am. J. Physiol. - Hear. Circ. Physiol.* **293,** 2129–2139 (2007).
29. Scorsin, M. *et al.* Comparison of the effects of fetal cardiomyocyte and skeletal myoblast transplantation on postinfarction left ventricular function. *J. Thorac. Cardiovasc. Surg.* **119,** 1169–1175 (2000).
30. Murry, C. E., Wiseman, R. W., Schartz, S. M. & Hauschka, S. D. Skeletal myoblast transplantation for repair of myocardial necrosis. *J. Clin. Invest.* **98,** 2512–2523 (1996).
31. Taylor, D. A. *et al.* Regenerating functional myocardium: improved performance after skeletal myoblast transplantation. *Nat. Med.* **4,** 929–933 (1998).
32. Gavira, J. J. *et al.* A comparison between percutaneous and surgical transplantation of autologous skeletal myoblasts in a swine model of chronic myocardial infarction. *Cardiovasc. Res.* **71,** 744–753 (2006).
33. Gavira, J. J. *et al.* Repeated implantation of skeletal myoblast in a swine

model of chronic myocardial infarction. *Eur. Heart J.* **31,** 1013–1021 (2010).
34. Souza, G. *et al.* Long-Term Efficacy of Myoblast Transplantation on Regional Structure and Function After. *Circualtion* **106,** 131–136 (2002).
35. Pagani, F. D. *et al.* Autologous Skeletal Myoblasts Transplanted to Ischemia-Damaged Myocardium in Humans. Histological Analysis of Cell Survival and Differentiation. *J. Am. Coll. Cardiol.* **41,** 879–888 (2003).
36. Menasché, P. *et al.* Autologous Skeletal Myoblast Transplantation for Severe Postinfarction Left Ventricular Dysfunction. *J. Am. Coll. Cardiol.* **41,** 1078–1083 (2003).
37. Dib, N. *et al.* One-Year Follow-Up of Feasibility and Safety of the First U . S ., Randomized , Controlled Study Using 3-Dimensional Guided Catheter-Based Delivery of Autologous Skeletal Myoblasts for Ischemic Cardiomyopathy (CAuSMIC Study). *J. Am. Coll. Cardiol.* **2,** 9–16 (2009).
38. Menasché, P. *et al.* The Myoblast Autologous Grafting in Ischemic Cardiomyopathy (MAGIC) trial: first randomized placebo-controlled study of myoblast transplantation. *Circulation* **117,** 1189–1200 (2008).
39. Durrani, S., Konoplyannikov, M., Ashraf, M., Haider, K. H. & S, D. Skeletal myoblasts for cardiac repair. *J. Mol. Cell. Cardiol.* **5,** 919–932 (2008).
40. Tomita, S. *et al.* Autologous Transplantation of Bone Marrow Cells Improves Damaged Heart Function. *Circulation* **100,** 247–256 (1999).
41. Orlic, D. *et al.* Bone marrow cells regenerate infarcted myocardium. *Nature* **410,** 701–705 (2001).
42. Orlic, D. *et al.* Transplanted adult bone marrow cells repair myocardial infarcts in mice. *Ann. N. Y. Acad. Sci.* **938,** 221–229 (2001).
43. Nygren, J. M. *et al.* Bone marrow-derived hematopoietic cells generate cardiomyocytes at a low frequency through cell fusion, but not transdifferentiation. *Nat. Med.* **10,** 494–501 (2004).
44. Balsam, L. B. *et al.* Haematopoietic stem cells adopt mature haematopoietic fates in ischaemic myocardium. *Nature* **428,** 668–673 (2004).
45. Murry, C. E. *et al.* Haematopoietic stem cells do not transdifferentiate into cardiac myocytes in myocardial infarcts. *Nature* **428,** 664–668 (2004).
46. Perin, E. C. *et al.* Transendocardial, Autologous Bone Marrow Cell Transplantation for Severe, Chronic ISchemic Heart Failure. *Circulation* **107,** 2294–2303 (2003).
47. Toma, C., Pittenger, M. F., Cahill, K. S., Byrne, B. J. & Kessler, P. D. Human Mesenchymal Stem Cells Differentiate to a Cardiomyocyte Phenotype in the Adult Murine Heart. *Circulation* **105,** 93–98 (2002).
48. Beeres, S. L. M. A. *et al.* Intramyocardial Injection of Autologous Bone Marrow Mononuclear Cells in Patients With Chronic Myocardial Infarction and Severe Left Ventricular Dysfunction. *Am. J. Cardiol.* **100,** 1094–1098 (2007).
49. Perin, E. C. *et al.* A randomized study of transendocardial injection of

autologous bone marrow mononuclear cells and cell function analysis in ischemic heart failure (FOCUS-HF). *Am. Heart J.* **161,** 1078–1087 (2011).
50. Perin, E. C. *et al.* Effect of transendocardial delivery of autologous bone marrow mononuclear cells on functional capacity, left ventricular function, and perfusion in chronic heart failure: the FOCUS-CCTRN trial. *JAMA* **307,** 1717–1726 (2012).
51. Assmus, B. *et al.* Transcoronary Transplantation of Progenitor Cells after Myocardial Infarction. *N. Engl. J. Med.* **355,** 1222–1232 (2006).
52. Assmus, B. *et al.* Transcoronary transplantation of functionally competent BMCs is associated with a decrease in natriuretic peptide serum levels and improved survival of patients with chronic postinfarction heart failure: Results of the TOPCARE-CHD registry. *Circ. Res.* **100,** 1234–1241 (2007).
53. Yao, K. *et al.* Administration of intracoronary bone marrow mononuclear cells on chronic myocardial infarction improves diastolic function. *Heart* **94,** 1147–1153 (2008).
54. Assmus, B. *et al.* Effect of Shock Wave–Facilitated Intracoronary Cell Therapy on LVEF in Patients With Chronic Heart Failure. *JAMA* **309,** 1622–1631 (2013).
55. Seth, S. *et al.* Percutaneous Intracoronary Cellular Cardiomyoplasty for Nonischemic Cardiomyopathy: Clinical and Histopathological Results: The First-in-Man ABCD (Autologous Bone Marrow Cells in Dilated Cardiomyopathy) Trial. *J. Am. Coll. Cardiol.* **48,** 2350–2351 (2006).
56. Seth, S. *et al.* The ABCD (Autologous Bone Marrow Cells in Dilated Cardiomyopathy) Trial. A Long-Term Follow-Up Study. *J. Am. Coll. Cardiol.* **55,** 1643–1644 (2010).
57. Amado, L. C. *et al.* Cardiac repair with intramyocardial injection of allogeneic mesenchymal stem cells after myocardial infarction. *Proc. Natl. Acad. Sci.* **102,** 11474–11479 (2005).
58. Quevedo, H. C. *et al.* Allogeneic mesenchymal stem cells restore cardiac function in chronic ischemic cardiomyopathy via trilineage differentiating capacity. *PNAS* **106,** 14022–14027 (2009).
59. Mathiasen, A. B. *et al.* Rationale and design of the first randomized, double-blind, placebo-controlled trial of intramyocardial injection of autologous bone-marrow derived Mesenchymal Stromal Cells in chronic ischemic Heart Failure (MSC-HF Trial). *Am. Heart J.* **164,** 285–291 (2012).
60. Mathiasen, A. B. *et al.* Bone marrow-derived mesenchymal stromal cell treatment in patients with severe ischaemic heart failure: A randomized placebo-controlled trial (MSC-HF trial). *Eur. Heart J.* **36,** 1744–1753 (2015).
61. Bartunek, J. *et al.* Cardiopoietic stem cell therapy in heart failure: the C-CURE (Cardiopoietic stem Cell therapy in heart failURE) multicenter randomized trial with lineage-specified biologics. *J. Am. Coll. Cardiol.* **61,** 2329–2338 (2013).
62. Hare, J. M. *et al.* Comparison of allogeneic vs autologous bone marrow-

derived mesenchymal stem cells delivered by transendocardial injection in patients with ischemic cardiomyopathy: The POSEIDON randomized trial. *JAMA* **308,** 2369–2379 (2012).
63. Hare, J. M. *et al.* Randomized Comparison of Allogeneic Versus Autologous Mesenchymal Stem Cells for Nonischemic Dilated Cardiomyopathy: POSEIDON-DCM Trial. *J. Am. Coll. Cardiol.* **69,** 526–537 (2017).
64. Williams, A. R. *et al.* Intramyocardial stem cell injection in patients with ischemic cardiomyopathy: Functional recovery and reverse remodeling. *Circ. Res.* **108,** 792–796 (2011).
65. Heldman, A. W. *et al.* Transendocardial Mesenchymal Stem Cells and Mononuclear Bone Marrow Cells for Ischemic Cardiomyopathy. *JAMA* **311,** 62–73 (2014).
66. Fisher, S. A., Doree, C., Mathur, A., Taggart, D. P. & Martin-Rendon, E. Stem cell therapy for chronic ischaemic heart disease and congestive heart failure. *Cochrane Database Syst. Rev.* (2016). doi:10.1002/14651858.CD007888.pub3
67. Messina, E. *et al.* Isolation and expansion of adult cardiac stem cells from human and murine heart. *Circ. Res.* **95,** 911–921 (2004).
68. Smith, R. R. *et al.* Regenerative potential of cardiosphere-derived cells expanded from percutaneous endomyocardial biopsy specimens. *Circulation* **115,** 896–908 (2007).
69. Davis, D. R. *et al.* Validation of the cardiosphere method to culture cardiac progenitor cells from myocardial tissue. *PLoS One* **4,** e7195 (2009).
70. Johnston, P. V. *et al.* Engraftment, differentiation, and functional benefits of autologous cardiosphere-derived cells in porcine ischemic cardiomyopathy. *Circulation* **120,** 1075–1083 (2009).
71. Carr, C. A. *et al.* Cardiosphere-derived cells improve function in the infarcted rat heart for at least 16 weeks - an mri study. *PLoS One* **6,** e25669 (2011).
72. Li, T. S. *et al.* Cardiospheres recapitulate a niche-like microenvironment rich in stemness and cell-matrix interactions, rationalizing their enhanced functional potency for myocardial repair. *Stem Cells* **28,** 2088–2098 (2010).
73. Li, T. S. *et al.* Direct comparison of different stem cell types and subpopulations reveals superior paracrine potency and myocardial repair efficacy with cardiosphere-derived cells. *J. Am. Coll. Cardiol.* **59,** 942–953 (2012).
74. Makkar, R. R. *et al.* Intracoronary cardiosphere-derived cells for heart regeneration after myocardial infarction (CADUCEUS): A prospective, randomised phase 1 trial. *Lancet* **379,** 895–904 (2012).
75. Malliaras, K. *et al.* Intracoronary cardiosphere-derived cells after myocardial infarction: Evidence of therapeutic regeneration in the final 1-year results of the CADUCEUS trial (CArdiosphere-derived aUtologous stem CElls to reverse ventricular dysfunction). *J. Am. Coll. Cardiol.* **63,**

110–122 (2014).
76. Quaini, F. *et al.* Chimerism of the transplanted heart. *N. Engl. J. Med.* **346,** 5–15 (2002).
77. Beltrami, A. P. *et al.* Adult Cardiac Stem Cells Are Multipotent and Support Myocardial Regeneration. *Cell* **114,** 763–776 (2003).
78. Linke, A. *et al.* Stem cells in the dog heart are self-renewing , clonogenic , and multipotent and regenerate infarcted myocardium , improving cardiac function. *Proc. Natl. Acad. Sci. U. S. A.* **102,** 8966–8971 (2005).
79. Dawn, B. *et al.* Cardiac stem cells delivered intravascularly traverse the vessel barrier, regenerate infarcted myocardium, and improve cardiac function. *Proc. Natl. Acad. Sci.* **102,** 3766–3771 (2005).
80. Tang, X. L. *et al.* Intracoronary administration of cardiac progenitor cells alleviates left ventricular dysfunction in rats with a 30-day-old infarction. *Circulation* **121,** 293–305 (2010).
81. Li, Z. *et al.* Imaging Survival and Function of Transplanted Cardiac Resident Stem Cells. *J. Am. Coll. Cardiol.* **53,** 1229–1240 (2009).
82. Zaruba, M.-M., Soonpaa, M., Reuter, S. & Field, L. J. Cardiomyogenic potential of C-kit+-expressing cells derived from neonatal and adult mouse hearts. *Circulation* **121,** 1992–2000 (2010).
83. Bolli, R. *et al.* Cardiac stem cells in patients with ischaemic cardiomyopathy (SCIPIO): Initial results of a randomised phase 1 trial. *Lancet* **378,** 1847–1857 (2011).
84. Chugh, A. R. *et al.* Administration of cardiac stem cells in patients with ischemic cardiomyopathy: The SCIPIO trial: Surgical aspects and interim analysis of myocardial function and viability by magnetic resonance. *Circulation* **126,** S54–S65 (2012).
85. Bolli, R. *et al.* Intracoronary Delivery of Autologous Cardiac Stem Cells Improves Cardiac Function in a Porcine Model of Chronic Ischemic Cardiomyopathy. *Circulation* **128,** 122–131 (2013).
86. Editors, T. L. Expression of concern : the SCIPIO trial. *Lancet* **383,** 1279 (2014).
87. Bolli, R. *et al.* Rationale and Design of the CONCERT-HF (Combination Of meseNchymal and c-kit+ Cardiac stEm cells as Regenerative Therapy for Heart Failure) Trial. *Circ. Res.* (2018). doi:10.1161/CIRCRESAHA.118.312978
88. Hsieh, P. C. H. *et al.* Evidence from a genetic fate-mapping study that stem cells refresh adult mammalian cardiomyocytes after injury. *Nat. Med.* **13,** 970–974 (2007).
89. Loffredo, F. S., Steinhauser, M. L., Gannon, J. & Lee, R. T. Bone Marrow-Derived Cell Therapy Stimulates Endogenous Cardiomyocyte Progenitors and Promotes Cardiac Repair. *Cell Stem Cell* **8,** 389–398 (2011).
90. Malliaras, K. *et al.* Cardiomyocyte proliferation and progenitor cell recruitment underlie therapeutic regeneration after myocardial infarction in the adult mouse heart. *EMBO Mol. Med.* **5,** 191–209 (2013).

91. Hatzistergos, K. E. *et al.* Bone marrow mesenchymal stem cells stimulate cardiac stem cell proliferation and differentiation. *Circ. Res.* **107,** 913–922 (2010).
92. Hatzistergos, K. E. *et al.* Stimulatory Effects of Mesenchymal Stem Cells on cKit+ Cardiac Stem Cells Are Mediated by SDF1/CXCR4 and SCF/cKit Signaling Pathways. *Circ. Res.* **119,** 921–930 (2016).
93. Bergmann, O. *et al.* Evidence for cardiomyocyte renewal in humans. *Science (80-.).* **324,** 98–102 (2009).
94. Bergmann, O. *et al.* Dynamics of cell generation and turnover in the human heart. *Cell* **161,** 1566–1575 (2015).
95. Müller, P. *et al.* Cardiomyocytes of noncardiac origin in myocardial biopsies of human transplanted hearts. *Circulation* **106,** 31–35 (2002).
96. Laflamme, M. A., Myerson, D., Saffitz, J. E. & Murry, C. E. Evidence for cardiomyocyte repopulation by extracardiac progenitors in transplanted human hearts. *Circ. Res.* **90,** 634–640 (2002).
97. Höcht-Zeisberg, E. *et al.* Cellular repopulation of myocardial infarction in patients with sex-mismatched heart transplantation. *Eur. Heart J.* **25,** 749–758 (2004).
98. Wu, J. M. F. *et al.* Circulating Cells Contribute to Cardiomyocyte Regeneration After Injury. *Circ. Res.* **116,** 633–641 (2015).
99. Deb, A. *et al.* Bone marrow-derived cardiomyocytes are present in adult human heart: A study of gender-mismatched bone marrow transplantation patients. *Circulation* **107,** 1247–1249 (2003).
100. Alvarez-Dolado, M. *et al.* Fusion of bone-marrow-derived cells with Purkinje neurons, cardiomyocytes and hepatocytes. *Nature* **425,** 968–973 (2003).
101. Steinhauser, M. L. *et al.* Multi-isotope imaging mass spectrometry quantifies stem cell division and metabolism. *Nature* **481,** 516–519 (2012).
102. Senyo, S. E. *et al.* Mammalian heart renewal by pre-existing cardiomyocytes. *Nature* **493,** 433–436 (2013).
103. Kimura, W. *et al.* Hypoxia fate mapping identifies cycling cardiomyocytes in the adult heart. *Nature* **523,** 226–230 (2015).
104. Patterson, M. *et al.* Frequency of mononuclear diploid cardiomyocytes underlies natural variation in heart regeneration. *Nat. Genet.* **49,** 1346–1353 (2017).
105. Urbanek, K. *et al.* Myocardial regeneration by activation of multipotent cardiac stem cells in ischemic heart failure. *Proc. Natl. Acad. Sci. U. S. A.* **102,** 8692–8697 (2005).
106. Fransioli, J. *et al.* Evolution of the c-kit-Positive Cell Response to Pathological Challenge in the Myocardium. *Stem Cells* **26,** 1315–1324 (2008).
107. Ellison, G. M. *et al.* Acute Beta-adrenergic overload produces myocyte damage through calcium leakage from the ryanodine receptor 2 but spares cardiac stem cells. *J. Biol. Chem.* **282,** 11397–11409 (2007).

108. Ellison, G. M. *et al.* Adult c-kit(pos) cardiac stem cells are necessary and sufficient for functional cardiac regeneration and repair. *Cell* **154,** 827–842 (2013).
109. Angert, D. *et al.* Repair of the Injured Adult Heart Involves New Myocytes Potentially Derived From Resident Cardiac Stem Cells. *Circ. Res.* **108,** 1226–1237 (2011).
110. Chen, Z. *et al.* Pathologic Stimulus Determines Lineage Commitment of Cardiac C-kit+ Cells. *Circulation* **136,** 2359–2372 (2017).
111. Nadal-ginard, B., Ellison, G. M. & Torella, D. Absence of evidence is not evidence of absence: pitfalls of cre knock-ins in the c-Kit locus. *Circ. Res.* **115,** 415–419 (2014).
112. He, L. *et al.* Enhancing the precision of genetic lineage tracing using dual recombinases. *Nat. Med.* **23,** 1488–1498 (2017).
113. Holmes, C. & Stanford, W. L. Concise Review: Stem Cell Antigen-1: Expression, Function, and Enigma. *Stem Cells* **25,** 1339–1347 (2007).
114. Oh, H. *et al.* Cardiac progenitor cells from adult myocardium : Homing , differentiation , and fusion after infarction. *Proc. Natl. Acad. Sci.* **100,** 12313–12318 (2003).
115. Matsuura, K. *et al.* Adult cardiac Sca-1-positive cells differentiate into beating cardiomyocytes. *J. Biol. Chem.* **279,** 11384–11391 (2004).
116. Valente, M., Nascimento, D. S., Cumano, A. & Pinto-do-O, P. Sca-1+ cardiac progenitor cells and heart-making: a critical synopsis. *Stem Cells Dev.* **23,** 2263–2273 (2014).
117. Uchida, S. *et al.* Sca1-Derived Cells Are a Source of Myocardial Renewal in the Murine Adult Heart. *Stem Cell Reports* **1,** 397–410 (2013).
118. Tateishi, K. *et al.* Clonally amplified cardiac stem cells are regulated by Sca-1 signaling for efficient cardiovascular regeneration. *J. Cell Sci.* **120,** 1791–1800 (2007).
119. Huang, C. *et al.* Sca-1+ cardiac stem cells mediate acute cardioprotection via paracrine factor SDF-1 following myocardial ischemia/reperfusion. *PLoS One* **6,** (2011).
120. Takamiya, M., Haider, K. H. & Ashraf, M. Identification and characterization of a novel multipotent sub-population of Sca-1^{+} cardiac progenitor cells for myocardial regeneration. *PLoS One* **6,** (2011).
121. Meinhardt, A. *et al.* Immunohistochemical and flow cytometric analysis of long-term label-retaining cells in the adult heart. *Stem Cells Dev.* **20,** 211–222 (2011).
122. Foudi, A. *et al.* Analysis of histone 2B-GFP retention reveals slowly cycling hematopoietic stem cells. *Nat. Biotechnol.* **27,** 84–90 (2009).
123. Wang, X. *et al.* The role of the Sca-1+/CD31- cardiac progenitor cell population in postinfarction left ventricular remodeling. 1779–1788 (2006). doi:10.1634/stemcells.2005-0386
124. Ryzhov, S. *et al.* Role of A2B adenosine receptors in regulation of paracrine functions of stem cell antigen 1-positive cardiac stromal cells. *J.*

Pharmacol. Exp. Ther. **341,** 764–774 (2012).
125. Smits, A. M. *et al.* Human cardiomyocyte progenitor cells differentiate into functional mature cardiomyocytes: an in vitro model for studying human cardiac physiology and pathophysiology. *Nat. Protoc.* **4,** 232–243 (2009).
126. Goodell, M. A., Brose, K., Paradis, G., Conner, A. S. & Mulligan, R. C. Isolation and Functional Properties of Murine Hematopoietic Stem Cells that are Replicating In Vivo. *J. Exp. Med.* **183,** 1797–1806 (1996).
127. Golebiewska, A., Brons, N. H. C., Bjerkvig, R. & Niclou, S. P. Critical appraisal of the side population assay in stem cell and cancer stem cell research. *Cell Stem Cell* **8,** 136–147 (2011).
128. Camargo, F. D., Chambers, S. M., Drew, E., Mcnagny, K. M. & Goodell, M. A. Hematopoietic stem cells do not engraft with absolute efficiencies. *Blood* **107,** 501–507 (2006).
129. Goodell, M. A. *et al.* Dye efflux studies suggest that hematopoietic stem cells expressing low or undetectable levels of CD34 antigen exist in multiple species. *Nat. Med.* **3,** 1337–1345 (1997).
130. Matsuzaki, Y., Kinjo, K., Mulligan, R. C. & Okano, H. Unexpectedly Efficient Homing Capacity of Purified Murine Hematopoietic Stem Cells. *Immunity* **20,** 87–93 (2004).
131. Wolf, N. S., Kone, A., Priestley, G. V. & Bartelmez, S. H. In vivo and in vitro characterization of long-term repopulating primitive hematopoietic cells isolated by sequential Hoechst 33342-rhodamine 123 FACS selection. *Exp. Hematol.* **21,** 614–622 (1993).
132. Weksberg, D. C., Chambers, S. M., Boles, N. C. & Goodell, M. A. CD150- side population cells represent a functionally distinct population of long-term hematopoietic stem cells. *Blood* **111,** 2444–2451 (2007).
133. Challen, G. A., Boles, N. C., Chambers, S. M. & Goodell, M. A. Distinct Hematopoietic Stem Cell Subtypes Are Differentially Regulated by TGF-β1. *Cell Stem Cell* **6,** 265–278 (2010).
134. Tornack, J. *et al.* Flt3 ligand-eGFP-reporter expression characterizes functionally distinct subpopulations of CD150+ long-term repopulating murine hematopoietic stem cells. *Eur. J. Immunol.* **47,** 1477–1487 (2017).
135. Kiel, M. J. *et al.* SLAM family receptors distinguish hematopoietic stem and progenitor cells and reveal endothelial niches for stem cells. *Cell* **121,** 1109–1121 (2005).
136. Asakura, A., Seale, P., Girgis-Gabardo, A. & Rudnicki, M. A. Myogenic specification of side population cells in skeletal muscle. *J. Cell Biol.* **159,** 123–134 (2002).
137. Hierlihy, A. M., Seale, P., Lobe, C. G., Rudnicki, M. A. & Megeney, L. A. The Post-Natal Heart Contains a Myocardial Stem Cell Population. *FEBS Lett.* **530,** 239–243 (2002).
138. Martin, C. M. *et al.* Persistent Expression of the ATP-Binding Cassette Transporter, Abcg2, Identifies Cardiac SP Cells in the Developing and Adult Heart. *Dev. Biol.* **265,** 262–275 (2004).

139. Dekaney, C. M., Rodriguez, J. M., Graul, M. C. & Henning, S. J. Isolation and Characterization of a Putative Intestinal Stem Cell Fraction from Mouse Jejunum. *Gastroenterology* **129,** 1567–1580 (2005).
140. Unno, K., Jain, M. & Liao, R. Cardiac side population cells: Moving toward the center Stage in cardiac regeneration. *Circ. Res.* **110,** 1355–1363 (2012).
141. Montanaro, F. *et al.* Demystifying SP Cell Purification: Viability, Yield, and Phenotype are Defined by Isolation Parameters. *Exp. Cell Res.* **298,** 144–154 (2004).
142. Telford, W. G. Stem Cell Identification by DyeCycle Violet Side Population Analysis. *Basic Cell Cult. Protoc. Methods Mol. Biol.* **946,** 163–179 (2013).
143. Liu, W., Qian, N., Li, R. & Dou, K. Replacing Hoechst33342 with rhodamine123 in isolation of cancer stem-like cells from the MHCC97 cell line. *Toxicol. Vitr.* **24,** 538–545 (2010).
144. Pfister, O. *et al.* Role of the ATP-Binding Cassette Transporter Abcg2 in the Phenotype and Function of Cardiac Side Population Cells. *Circ. Res.* **103,** 825–835 (2008).
145. Zhou, S. *et al.* The ABC Transporter Bcrp1 / ABCG2 is Expressed in a Wide Variety of Stem Cells and is a Molecular Determinant of the Side-Population Phenotype. *Nat. Med.* **7,** 1028–1034 (2001).
146. Dey, D. *et al.* Dissecting the molecular relationship among various cardiogenic progenitor cells. *Circ. Res.* **112,** 1253–1262 (2013).
147. Pfister, O. *et al.* CD31- but Not CD31+ Cardiac Side Population Cells Exhibit Functional Cardiomyogenic Differentiation. *Circ. Res.* **97,** 52–61 (2005).
148. Noseda, M. *et al.* PDGFRα Demarcates the Cardiogenic Clonogenic Sca1+ Stem/Progenitor Cell in Adult Murine Myocardium. *Nat. Commun.* **6,** 1–16 (2015).
149. Mouquet, F. *et al.* Restoration of cardiac progenitor cells after myocardial infarction by self-proliferation and selective homing of bone marrow-derived stem cells. *Circ. Res.* **97,** 1090–1092 (2005).
150. Oyama, T. *et al.* Cardiac side population cells have a potential to migrate and differentiate into cardiomyocytes in vitro and in vivo. *J. Cell Biol.* **176,** 329–341 (2007).
151. Liang, S. X., Tan, T. Y. L., Gaudry, L. & Chong, B. Differentiation and Migration of Sca1+/CD31- Cardiac Side Population Cells in a Murine Myocardial Ischemic Model. *Int. J. Cardiol.* **138,** 40–49 (2010).
152. Alfakir, M. *et al.* The temporal and spatial expression patterns of ABCG2 in the developing human heart. *Int. J. Cardiol.* **156,** 133–138 (2012).
153. Sandstedt, J. *et al.* Left Atrium of the Human Adult Heart Contains a Population of Side Population Cells. *Basic Res. Cardiol.* **107,** 1–10 (2012).
154. Mulligan, J. D. *et al.* Caloric restriction does not alter effects of aging in cardiac side population cells. *Age (Dordr).* **33,** 351–361 (2011).
155. Asakura, A. & Rudnicki, M. A. Side Population Cells from Diverse Adult

Tissues are Capable of In Vitro Hematopoietic Differentiation. *Exp. Hematol.* **30,** 1339–1345 (2002).
156. Liang, S. X. *et al.* In Vitro and In Vivo Proliferation, Differentiation and Migration of Cardiac Endothelial Progenitor Cells (SCA1 +/CD31 + Side-Population Cells). *J. Thromb. Haemost.* **9,** 1628–1637 (2011).
157. Yoon, J., Choi, S.-C., Park, C. Y., Shim, W.-J. & Lim, D.-S. Cardiac side population cells exhibit endothelial differentiation potential. *Exp. Mol. Med.* **39,** 653–662 (2007).
158. Yamahara, K. *et al.* Heterogeneic Nature of Adult Cardiac Side Population Cells. *Biochem. Biophys. Res. Commun.* **371,** 615–620 (2008).
159. Emmert, M. Y. *et al.* Higher frequencies of BCRP+cardiac resident cells in ischaemic human myocardium. *Eur. Heart J.* **34,** 2830–2838 (2013).
160. Gilbert, P. M. *et al.* Substrate elasticity regulates skeletal muscle stem cell self-renewal in culture. *Science (80-.).* **1078,** 1078–1081 (2010).
161. Qiu, Y. *et al.* A role for matrix stiffness in the regulation of cardiac side population cell function. *Am. J. Physiol. Circ. Physiol.* **308,** H990–H997 (2015).
162. Gong, H. *et al.* Urotensin II inhibits the proliferation but not the differentiation of cardiac side population cells. *Peptides* **32,** 1035–1041 (2011).
163. Chen, Z. *et al.* Urotensin II Inhibited the Proliferation of Cardiac Side Population Cells in Mice during Pressure Overload by JNK-LRP6 Signalling. *J. Cell. Mol. Med.* **18,** 852–862 (2014).
164. Chiong, M. *et al.* Cardiomyocyte death: Mechanisms and translational implications. *Cell Death Dis.* **2,** e244-11 (2011).
165. van Berlo, J. H. & Molkentin, J. D. An Emerging Consensus on Cardiac Regeneration. *Nat. Med.* **20,** 1386–1393 (2014).
166. Tzahor, E. & Poss, K. D. Cardiac regeneration strategies: Staying young at heart. *Science (80-.).* **356,** 1035–1039 (2017).
167. Sanganalmath, S. K. & Bolli, R. Cell therapy for heart failure: A comprehensive overview of experimental and clinical studies, current challenges, and future directions. *Circ. Res.* **113,** 810–834 (2013).
168. Hong, K. U. *et al.* C-Kit+ Cardiac Stem Cells Alleviate Post-Myocardial Infarction Left Ventricular Dysfunction Despite Poor Engraftment and Negligible Retention in the Recipient Heart. *PLoS One* **9,** e98725 (2014).
169. van Berlo, J. H. *et al.* C-Kit+ Cells Minimally Contribute Cardiomyocytes to the Heart. *Nature* **509,** 337–341 (2014).
170. Sultana, N. *et al.* Resident C-Kit(+) Cells in the Heart are not Cardiac Stem Cells. *Nat. Commun.* **6,** 1–10 (2015).
171. Liu, Q. *et al.* Genetic Lineage Tracing Identifies In Situ Kit-expressing Cardiomyocytes. *Cell Res.* **26,** 119–130 (2016).
172. Eschenhagen, T. *et al.* Cardiomyocyte Regeneration: A Consensus Statement. *Circulation* 680–686 (2017). doi:10.1161/CIRCULATIONAHA.117.029343

173. Bollini, S., Smart, N. & Riley, P. R. Resident cardiac progenitor cells : At the heart of regeneration. *J. Mol. Cell. Cardiol.* **50,** 296–303 (2011).
174. Garbern, J. C. & Lee, R. T. Cardiac stem cell therapy and the promise of heart regeneration. *Cell Stem Cell* **12,** 689–698 (2013).
175. Yellamilli, A. & van Berlo, J. H. The Role of Cardiac Side Population Cells in Cardiac Regeneration. *Front. Cell Dev. Biol.* **4,** (2016).
176. Liang, S. X., Tan, T. Y. L., Gaudry, L. & Chong, B. Differentiation and migration of Sca1+/CD31- cardiac side population cells in a murine myocardial ischemic model. *Int. J. Cardiol.* **138,** 40–49 (2010).
177. Juliano, R. L. & Ling, V. A surface glycoprotein modulating drug permeability in Chinese hamster ovary cell mutants. *Biochim. Biophys. Acta* **455,** 152–162 (1976).
178. Doyle, L. A. & Ross, D. D. Multidrug Resistance Mediated by the Breast Cancer Resistance Protein BCRP (ABCG2). *Oncogene* **22,** 7340–7358 (2003).
179. Schinkel, A. H. *et al.* Normal viability and altered pharmacokinetics in mice lacking mdr1-type (drug-transporting) P-glycoproteins. *Proc. Natl. Acad. Sci.* **94,** 4028–4033 (1997).
180. Schinkel, A. H. *et al.* Disruption of the Mouse Mdr1a P-Glycoprotein Gene Leads to a Deficiency in the Blood-Brain Barrier and to Increased Sensitivity to Drugs. *Cell* **77,** 491–502 (1994).
181. Stacy, A. E., Jansson, P. J. & Richardson, D. R. Molecular Pharmacology of ABCG2 and Its Role in Chemoresistance. *Mol. Pharmacol.* **84,** 655–669 (2013).
182. Zhou, S. *et al.* Bcrp1 Gene Expression is Required for Normal Numbers of Side Population Stem Cells in Mice, and Confers Relative Protection to Mitoxantrone in Hematopoietic Cells In Vivo. *Proc. Natl. Acad. Sci. U. S. A.* **99,** 12339–12344 (2002).
183. Scharenberg, C. W., Harkey, M. a & Torok-storb, B. The ABCG2 transporter is an efficient Hoechst 33342 efflux pump and is preferentially expressed by immature human hematopoietic progenitors The ABCG2 transporter is an efficient Hoechst 33342 efflux pump and is preferentially expressed by immature human h. *Blood* **99,** 507–512 (2013).
184. Jonker, J. W. *et al.* Contribution of the ABC transporters Bcrp1 and Mdr1a/1b to the side population phenotype in mammary gland and bone marrow of mice. *Stem Cells* **23,** 1059–1065 (2005).
185. von Furstenberg, R. J. *et al.* Side population sorting separates subfractions of cycling and non-cycling intestinal stem cells. *Stem Cell Res.* **12,** 364–375 (2014).
186. Gulati, A. S., Ochsner, S. A. & Henning, S. J. Molecular properties of side population-sorted cells from mouse small intestine. *Am. J. Physiol. Liver Physiol.* **294,** G286–G294 (2008).
187. Okabe, K. *et al.* Neurons limit angiogenesis by titrating VEGF in retina. *Cell* **159,** 584–596 (2014).

188. Parsons, S. A. *et al.* Genetic loss of calcineurin blocks mechanical overload-induced skeletal muscle fiber type switching but not hypertrophy. *J. Biol. Chem.* **279,** 26192–26200 (2004).
189. Gundewar, S., Calvert, J. W., Elrod, J. W. & Lefer, D. J. Cytoprotective effects of N,N,N-trimethylsphingosine during ischemia- reperfusion injury are lost in the setting of obesity and diabetes. *Am. J. Physiol. - Hear. Circ. Physiol.* **293,** H2462-2471 (2007).
190. Ergen, A. V, Jeong, M., Lin, K. K., Challen, G. A. & Goodell, M. A. Isolation and characterization of mouse side population cells. *Methods Mol. Biol.* **946,** 151–162 (2013).
191. Pfister, O., Oikonomopoulos, A., Sereti, K.-I. & Liao, R. Isolation of resident cardiac progenitor cells by Hoechst 33342 staining. *Methods Mol. Biol. - Stem Cells Myocard. Regen. Methods Protoc.* **660,** 53–63 (2010).
192. Schindelin, J. *et al.* Fiji: An open-source platform for biological-image analysis. *Nat. Methods* **9,** 676–682 (2012).
193. O'Connell, T. D., Rodrigo M C & Simpson, P. C. Isolation and Culture of Adult Mouse Cardiac Myocytes. *Methods Mol. Biol.* **357,** 271–296 (2007).
194. Luongo, T. S. *et al.* The mitochondrial Na+/Ca2+exchanger is essential for Ca2+homeostasis and viability. *Nature* **545,** 93–97 (2017).
195. Stacy, A. E., Jansson, P. J. & Richardson, D. R. Molecular Pharmacology of ABCG2 and Its Role in Chemoresistance. *Mol. Pharmacol.* **84,** 655–669 (2013).
196. Krishnamurthy, P. & Schuetz, J. D. Role of Abcg2/Bcrp in Biology and Medicine. *Annu. Rev. Pharmacol. Toxicol.* **46,** 381–410 (2006).
197. Horsey, A. J., Cox, M. H., Sarwat, S. & Kerr, I. D. The multidrug transporter ABCG2: still more questions than answers. *Biochem. Soc. Trans.* **44,** 824–830 (2016).
198. Darwich, A. S., Aslam, U., Ashcroft, D. M. & Rostami-Hodjegan, A. Meta-analysis of the turnover of intestinal epithelia in preclinical animal species and humans. *Drug Metab. Dispos.* **42,** 2016–2022 (2014).
199. Lipkin, M. Growth and Development of Gastrointestinal Cells. *Annu. Rev. Physiol.* **47,** 175–179 (1985).
200. Higashikuni, Y. *et al.* The ATP-binding cassette transporter BCRP1/ABCG2 plays a pivotal role in cardiac repair after myocardial infarction via modulation of microvascular endothelial cell survival and function. *Arterioscler. Thromb. Vasc. Biol.* **30,** 2128–2135 (2010).
201. Jackson, K. a. *et al.* Regeneration of Ischemic Cardiac Muslce and Vascular Endothelium By Adult Stem Cells. *J. Clin. Invest.* **107,** 1395–1402 (2001).
202. Fioret, B. A., Heimfeld, J. D., Paik, D. T. & Hatzopoulos, A. K. Endothelial cells contribute to generation of adult ventricular myocytes during cardiac homeostasis. *Cell Rep.* **8,** 229–241 (2014).
203. Matsuura, K. *et al.* Cardiomyocytes fuse with surrounding noncardiomyocytes and reenter the cell cycle. *J. Cell Biol.* **167,** 351–363

(2004).
204. Brooks, W. W. & Conrad, C. H. Isoproterenol-induced myocardial injury and diastolic dysfunction in mice: structural and functional correlates. *Comp Med* **59,** 339–343 (2009).
205. Wallner, M. *et al.* Acute Catecholamine Exposure Causes Reversible Myocyte Injury Without Cardiac Regeneration. *Circ. Res.* **119,** 865–879 (2016).
206. Laflamme, M. A. & Murry, C. E. Heart regeneration. *Nature* **473,** 326–35 (2011).
207. Leach, J. P. *et al.* Hippo pathway deficiency reverses systolic heart failure after infarction. *Nature* **550,** 260–264 (2017).
208. Nakada, Y. *et al.* Hypoxia induces heart regeneration in adult mice. *Nature* **541,** 222–227 (2017).
209. Sereti, K.-I. *et al.* ATP-Binding Cassette G-Subfamily Transporter 2 Regulates Cell Cycle Progression and Asymmetric Division in Mouse Cardiac Side Population Progenitor Cells. *Circ. Res.* **112,** 27–34 (2013).
210. Sawamiphak, S., Kontarakis, Z., Filosa, A., Reischauer, S. & Stainier, D. Y. R. Transient cardiomyocyte fusion regulates cardiac development in zebrafish. *Nat. Commun.* **8,** 1525 (2017).
211. Meissner, K. *et al.* The ATP-binding cassette transporter ABCG2 (BCRP), a marker for side population stem cells, is expressed in human heart. *J. Histochem. Cytochem.* **54,** 215–221 (2006).
212. Solbach, T. F. *et al.* ATP-binding cassette transporters in human heart failure. *Naunyn. Schmiedebergs. Arch. Pharmacol.* **377,** 231–243 (2008).
213. Valero-Muñoz, M., Backman, W. & Sam, F. Murine Models of Heart Failure With Preserved Ejection Fraction: A 'Fishing Expedition'. *JACC Basic to Transl. Sci.* **2,** 770–789 (2017).
214. Roh, J., Houstis, N. & Rosenzweig, A. Why Don't We Have Proven Treatments for HFpEF? *Circ. Res.* **120,** 1243–1245 (2017).